

**XeF<sub>2</sub> Gas Phase Micromachining of Silicon:  
Modeling, Equipment Development and Verification**

**George Floarea**

A Thesis

In

The Department

of

Mechanical and Industrial Engineering

Presented in Partial Fulfillment of the Requirements

for the Degree of Master of Applied Science

at

Concordia University,

Montréal, Québec, Canada

August 2007

© George Floarea, 2007



Library and  
Archives Canada

Bibliothèque et  
Archives Canada

Published Heritage  
Branch

Direction du  
Patrimoine de l'édition

395 Wellington Street  
Ottawa ON K1A 0N4  
Canada

395, rue Wellington  
Ottawa ON K1A 0N4  
Canada

*Your file    Votre référence*

*ISBN: 978-0-494-34744-7*

*Our file    Notre référence*

*ISBN: 978-0-494-34744-7*

#### NOTICE:

The author has granted a non-exclusive license allowing Library and Archives Canada to reproduce, publish, archive, preserve, conserve, communicate to the public by telecommunication or on the Internet, loan, distribute and sell theses worldwide, for commercial or non-commercial purposes, in microform, paper, electronic and/or any other formats.

The author retains copyright ownership and moral rights in this thesis. Neither the thesis nor substantial extracts from it may be printed or otherwise reproduced without the author's permission.

#### AVIS:

L'auteur a accordé une licence non exclusive permettant à la Bibliothèque et Archives Canada de reproduire, publier, archiver, sauvegarder, conserver, transmettre au public par télécommunication ou par l'Internet, prêter, distribuer et vendre des thèses partout dans le monde, à des fins commerciales ou autres, sur support microforme, papier, électronique et/ou autres formats.

L'auteur conserve la propriété du droit d'auteur et des droits moraux qui protègent cette thèse. Ni la thèse ni des extraits substantiels de celle-ci ne doivent être imprimés ou autrement reproduits sans son autorisation.

---

In compliance with the Canadian Privacy Act some supporting forms may have been removed from this thesis.

Conformément à la loi canadienne sur la protection de la vie privée, quelques formulaires secondaires ont été enlevés de cette thèse.

While these forms may be included in the document page count, their removal does not represent any loss of content from the thesis.

Bien que ces formulaires aient inclus dans la pagination, il n'y aura aucun contenu manquant.

  
**Canada**

## **ABSTRACT**

### **XeF<sub>2</sub> Gas Phase Micromachining of Silicon: Modeling, Equipment Development and Verification**

**George Floarea**

The rapid progress in Micro-Electro Mechanical Systems necessitated the development of a micromachining technique in order to release micro-mechanical device in integrated chips. In the late 1990's there was a quest for a dry etchant that would not require an expensive setup, and overcome the problems related to wet etching, such as, stiction and etching slowdown due to bubble formation. A good alternative to wet etching would have been plasma etching, but fine tuning of the process parameters to achieve an effective control of the process, combined with the expensiveness of the equipment made plasma etching a less affordable etching method for many small labs. In gaseous phase, xenon difluoride was found to etch silicon isotropically and the required process setup is quite simple compared to other isotropic etching equipment for silicon.

In the present work, a new and computer-controlled xenon difluoride etching equipment for silicon was designed and installed. A model for the XeF<sub>2</sub> isotropic etching of silicon based on an atomic approach and fine tuned through pressure increase in the reaction chamber due to formation of the reaction products is presented. The shape of the etch features is predicted by a Matlab<sup>®</sup> code, based on the developed model.

The etch depth and lateral under-etch can be calculated for a given feature and the chamber loading. The effect of concave corners is ignored in the model although the experimental results indicated a slow down etch rate at such locations.

Using the designed and fully in house built etching equipment, experiments were carried on silicon samples with square and circular mask openings in order to validate the proposed etching model. The pressure in the etching chamber was monitored during experimental work and the values were used to be used later in the Matlab<sup>®</sup> script for verification purpose. The experimental values were compared with the theoretical ones and were found to be in good agreement.

The equipment, as designed and built, has embedded safety features required by toxic gas handling equipment codes.



*Dedicated to my parents*

## **ACKNOWLEDGEMENTS**

The author wishes to express his gratitude to Dr. Ion Stiharu for giving him the opportunity to work under his supervision. Dr. Stiharu's guidance, help, patience and kind nature combined with the exceptional atmosphere for doing research were essential in finishing this work.

The author wishes to thank his thesis co-supervisor, Dr. Muthukumaran Packirisamy, for encouraging him to develop independent thinking. The author also wishes to show his appreciation for Dr. Packirisamy's assistance in preparing this work.

The author wants to extend many thanks to Dan Juras, Technical Officer, for his help with the frame fabrication. Also, many thanks to Alex Macpherson, William Chicoine and Jose Esteves for their help with custom fabricated parts.

I owe a special note of appreciation to my colleagues Stefan, Dacian, Anas, Anand, Gino, and Arvind who supported me during my research.

Finally, I would like to thank my wife Cristina, my daughter Ana-Maria and my sister Ioana for all their support throughout this work. A very special thanks goes to my wife who has always been there for me; no one could ask for a better friend in life.

# TABLE OF CONTENTS

<b>LIST OF FIGURES .....</b>	<b>x</b>
<b>LIST OF TABLES .....</b>	<b>xv</b>
<b>NOMENCLATURE .....</b>	<b>xvi</b>
<b>Chapter 1 INTRODUCTION .....</b>	<b>1</b>
1.1 What are MEMS? .....	1
1.2 Mems fabrication.....	2
1.2.1 Deposition .....	2
1.2.2 Photolithography .....	3
1.2.3 Etching.....	6
1.2.3.1 Isotropic Etching .....	6
1.2.3.2 Anisotropic Etching.....	7
1.3 Bulk Micromachining.....	8
1.3.1 Surface Micromachining .....	10
1.3.2 Wafer Bonding .....	12
1.4 MEMS Applications.....	13
1.5 Plasma and Reactive Ion Etching.....	13
1.6 Xenon Difluoride.....	16
1.6.1 General considerations .....	16
1.6.2 Reaction mechanisms between $\text{XeF}_2$ and Si.....	18
1.6.3 Products from $\text{XeF}_2$ reaction with Si .....	21
1.6.4 Selectivity.....	21
1.6.5 $\text{XeF}_2$ etching equipment .....	22
1.7 Rationale of the Thesis .....	23
1.8 Objective of the Thesis.....	23
1.9 Thesis Overview.....	24
<b>Chapter 2 <math>\text{XeF}_2</math> ETCHING OF SILICON.....</b>	<b>26</b>
2.1 The influence of the process parameters .....	26

2.1.1 Influence of temperature.....	26
2.1.2 Pressure influence.....	31
2.1.3 Si doping level effects .....	33
2.2 Constant pressure etching versus pulse etching .....	35
<b>Chapter 3 EQUIPMENT DESIGN AND DEVELOPMENT .....</b>	<b>39</b>
3.1 Introduction .....	39
3.2 Design Constraints .....	40
3.2.1 Safety.....	41
3.2.2 Strategies to keep the design within the budget .....	41
3.2.3 Chambers volume and accessibility .....	41
3.2.4 Setup volume.....	42
3.2.5 Weight .....	42
3.3 Systems Components .....	44
3.3.1 Hardware Subsystem .....	44
3.3.2 Software subsystem .....	53
<b>Chapter 4 MODELING OF XENON DIFLUORIDE ETCHING OF SILICON.....</b>	<b>60</b>
4.1 Motivation .....	60
4.2 The etching model .....	61
4.2.1 Etching model for square opening mask .....	64
4.2.2 Circular opening mask model.....	67
<b>Chapter 5 VALIDATION OF THE PROPOSED ETCHING MODEL.....</b>	<b>69</b>
5.1 Experimental Procedure .....	69
5.1.1 Equipment Description.....	69
5.1.2 Sample Preparation.....	70
5.2 Validation for Square Opening.....	71
5.2.1 Experimental results .....	71
5.2.2 Theoretical results .....	76
5.2.3 Validation of theoretical results.....	77
5.2.4 Corner selectivity .....	81
5.2.5 Etched surface roughness .....	82
5.3 Validation for Circular Opening.....	84

5.3.1 Experimental results .....	84
5.3.2 Theoretical results .....	86
5.3.3 Validation of theoretical results.....	88
5.3.4 Surface roughness discussion .....	91
<b>Chapter 6 CONCLUSIONS AND FUTURE WORK.....</b>	<b>93</b>
6.1 Conclusions .....	93
6.2 Future Work .....	94
6.2.1 Design related future work .....	94
6.2.2 Model related future work.....	95
<b>REFERENCES.....</b>	<b>96</b>
<b>Appendix A DRAWINGS OF THE DEVELOPED EQUIPMENT .....</b>	<b>104</b>
<b>Appendix B MATLAB CODE FOR SQUARE OPENING .....</b>	<b>114</b>
<b>Appendix C MATLAB CODE FOR CIRCULAR OPENING .....</b>	<b>119</b>
<b>Appendix D PICTURES TAKEN DURING ASSEMBLING OF EQUIPMENT ..</b>	<b>124</b>

## LIST OF FIGURES

1-1	Isotropic wet etching : a) with agitation b) no agitation [8].	7
1-2	Anisotropic wet etching of silicon: a) (100) surface orientation; b) (110) surface orientation [8].	8
1-3	Bulk micromachined channel inlet [18].	10
1-4	Analog's Devices' ADXL50 accelerometer [19].	11
1-5	Fresnel lens [20].	11
1-6	Plasma etching setup	15
1-7	Reactive ion etching setup	16
1-8	Schematic diagram of the "tree" structure and the reaction processes for the etching products [42]	20
2-1	Temperature dependence of reaction coefficient $\epsilon$ [43].	28
2-2	Variation of the production coefficients $\delta_2$ and $\delta_4$ in the temperature range of 150 K to 900 K [43].	29
2-3	Etch rate dependence on substrate temperature [54]	30
2-4	The amount of silicon removed from a silicon film deposited on a quartz-crystal microbalance; silicon nitride ( $\text{Si}_3\text{N}_4$ ) and silicon oxide ( $\text{SiO}_2$ ) showed almost no etching [36].	31
2-5	Etch rate per 60 seconds pulse for a 175 $\mu\text{m}$ aperture width at different etching pressures [54]	32

2-6	Surface roughness evolution for samples etched at pressures between 65Pa and 390Pa [54].	33
2-7	Evolution of SiF <sub>4</sub> desorption in time [55].	34
2-8	Diagram of a XeF <sub>2</sub> etching setup without expansion chamber.	35
2-9	XeF <sub>2</sub> etching setup with expansion chamber.	36
3-1	Piping and instrumentation diagram of the designed XeF <sub>2</sub> etching system.	44
3-2	The XeF <sub>2</sub> supply chamber.	45
3-3	The complete etching system inside the fume hood.	45
3-4	Diagram of solenoid connection to the power supply.	46
3-5	CF type of flange and accessories.	48
3-6	KF type of flange, centering ring and clamp.	49
3-7	Plot of the system pressure during one hour of vacuum pumping.	51
3-8	Additional pressure regulator installed on the nitrogen line.	52
3-9	Flowchart of the LabView® code for an etching sequence where both etching and expansion chamber are purged with nitrogen.	55
3-10	Virtual Instrument's front panel.	56
3-11	Etching parameters front panel area.	57
3-12	System status area in auto mode.	59

3-13	System status area in manual mode; the valves icons act as on/off switches; when a valve icon is dark filled, the solenoid is not energized (valve is closed); when the valve is light filled the valve is open.	59
4-1	Variation of pressure in the etching chamber during one pulse.	61
4-2	Schematic of exposed silicon monolayers removal.	62
4-3	Schematics of the initial exposed area $A(0)$ and $A(1)$ - after one removed ML for a square opening.	66
4-4	Circular opening schematics of the initial exposed area $A(0)$ and $A(1)$ - after one removed ML.	68
5-1	Silicon sample with a 2.5mm X 2.5 mm square mask opening used to validate the theoretical model for square window openings.	72
5-2	Location of the lateral etch measurement points for the square opening. For each side of the square opening, measurements were taken at the maximum and minimum points.	73
5-3	Evolution of ED in microns during $\text{XeF}_2$ etching of a $2500\text{ }\mu\text{m}$ X $2500\text{ }\mu\text{m}$ for 25 pulses; the error bars represent $\pm 1$ standard deviation.	75
5-4	Measured lateral etch, of the etched square mask opening, using photos taken with a Nikon camera attached to the microscope ; the error bars represent $\pm 1$ standard deviation.	75
5-5	Matlab® contour plot representing the top view of a 2.5mm X 2.5 mm square opening; the blue contour lines represent the etched area after 5, 10, 15, 20 and 25 pulses.	76



5-6	Contour plot representing a cross-section through the middle of the square opening shown in previous figure.	77
5-7	Comparison between measured and theoretical obtained ED values; the error bars represent $\pm 1$ standard deviation.	80
5-8	Comparison between measured and theoretical lateral etch; the error bars represent $\pm 1$ standard deviation.	80
5-9	Comparison between measured and theoretical lateral etch. The picture in the background is a top view of the etched silicon chip after exposure to silicon for 25 pulses. The contour lines on top of the picture represent the plot generated by the theoretical model; a - concave etch fronts, b – convex etch fronts.	81
5-10	Evolution of the calculated standard deviation of etch depth measurement readings.	82
5-11	Pictures of etched surface (X500).	83
5-12	5000 $\mu\text{m}$ diameter circular mask opening sample used to validate the developed model.	84
5-13	Plot of etched depth measurements for circular opening; the error bars represent $\pm 1$ standard deviation.	85
5-14	Top view of theoretical contour plots generated by Matlab® for a 5000 $\mu\text{m}$ circular opening using the Delta P values saved when etched the 5 mm diameter circular mask opening.	87
5-15	Cross section view through the center of the top view; the figures have different scales.	87

5-16	Theoretical and experimental etch depth for a 5000 $\mu\text{m}$ diameter circular opening; the error bars represent $\pm 1$ standard deviation.	88
5-17	Plot of etch depth standard deviation values for the circular opening. Note that the values are very close except the 25th pulse one which is attributed to the onset of trenching.	91
5-18	Pictures of the circular mask opening etched surface (X500) after each set of five etching pulses.	92
D-1	Equipment parts in the FedEx shipping box.	124
D-2	Author while wiring the electromagnetic valves.	124
D-3	Author while wiring the electromagnetic valves.	125
D-4	The developed etching setup during pressure leak testing.	125

## **LIST OF TABLES**

1-1	Comparison of some bulk silicon etchants [8].	9
3-1	Design constraints.	40
3-2	Etching system subcomponents weight.	43
5-1	Etch depth measurements after five consecutive etch pulses for square mask opening sample.	73
5-2	Lateral etch measurements values for square mask opening experiment, approximated from photographs taken after sets of five consecutive pulses.	74
5-3	Experimental and theoretical results for a square opening etched for 25 pulses.	78
5-4	Experimental etch depth results obtained for a circular mask opening.	85
5-5	Experimental and theoretical etching results for the circular opening.	89

## NOMENCLATURE

<i>ED</i>	Etch Depth
AC	Alternating Current
BOE	Buffered Oxide Etch
BrF <sub>3</sub>	Bromine Trifluoride
CAIBE	Chemically Assisted Ion Beam Etching
CH <sub>3</sub> COOH	Acetic Acid
CMOS	Complementary Metal–Oxide–Semiconductor
DC	Direct Current
DRIE	Deep Reactive Ion Etch
EDP	Ethylene Diamine Pyrochat-Echol
HF	Hydrofluoric Acid
HNA	Hydrofluoric, Nitric, Acetic
HNO <sub>3</sub>	Nitric Acid
IBE	Ion Beam Etching
IC	Integrated-Circuits
KOH	Potassium Hydroxide
<i>L</i>	Lateral Etch

MEMS	Micro-Electro-Mechanical Systems
MERIE	Magnetically Enhanced Reactive Ion Etching
MIE	Magnetically Enhanced Ion Etching
ML	Monolayer
MST	Microsystems Technology
RF	Radio Frequency
RIE	Reactive Ion Etch
SD	Standard Deviation
SF <sub>6</sub>	Sulfur Hexafluoride
Si	Silicon
Si <sub>3</sub> N <sub>4</sub>	Silicon Nitride
SiC	Silicon Carbide
SiF <sub>3</sub>	Silicon Trifluoride
SiF <sub>4</sub>	Silicon Tetrafluoride
SiO	Silicon Oxide
SiO <sub>2</sub>	Silicon Dioxide
SOI	Silicon on Insulator
TMAH	Tetramethyl Ammonium Hydroxide

UHV	Ultra High Vacuum
$\text{XeF}_2$	Xenon Difluoride
$\Phi_s(\text{XeF}_2)$	$\text{XeF}_2$ flux arriving at the sample from the gas source
$\Phi(\text{XeF}_2)$	Nonused flux of $\text{XeF}_2$ leaving the sample
$\Phi(\text{SiF}_4)$	$\text{SiF}_4$ flux
$\Phi(\text{SiF}_2)$	$\text{SiF}_2$ flux
$\Delta P$	Difference between the pressure at the end of the etching cycle and the pressure at the beginning of the etching cycle
$n_{\text{SiF}_4}$	Number of $\text{SiF}_4$ moles
$P_{\text{SiF}_4}$	Partial pressure of $\text{SiF}_4$
$N_{\text{SiF}_4}$	Number of $\text{SiF}_4$ molecules desorbed during an etching pulse
$d_{(100)}$	Si interplanar spacing in (100) direction
$A_{(0)}$	Initial exposed silicon area
$A_{(1)}$	Silicon exposed area after one monolayer of silicon has been removed
$A_{(n)}$	Silicon exposed area after n monolayers of silicon have been removed
$t_{ML}$	Thickness of one monolayer

$ML(100)$	Silicon surface density for (100) surfaces
$N_{SiF_4}^r$	Number of remaining $SiF_4$ molecules in the etching chamber
CF	ConFlat
KF	Klein Flanche
LED	Light-emitting diode
$N_a$	Avogadro's number
$P_{final}$	Pressure in the etching chamber at the beginning and the end of the etching pulse
$P_{initial}$	Pressure in the etching chamber at the beginning of the etching pulse
$R$	Gas constant
$T$	Temperature inside the etching chamber
$V$	Volume of the etching chamber
VI	Virtual instrument
$\delta$	Production coefficient
$\varepsilon$	Reaction coefficient

# **CHAPTER 1**

## **INTRODUCTION**

### **1.1 WHAT ARE MEMS?**

MEMS, as they are known in North America is an acronym for Micro-Electro-Mechanical Systems. In Europe, this field is called MST, which stands for Microsystems Technology. MEMS are microfabricated structures comprised of a single or multiple mechanical, electrical or multi-physics miniature systems that perform a useful task.

It is generally accepted that the discovery of piezoresistive effect in germanium and silicon in 1954 [1] represents the birth of MEMS. However, the resonant gate transistor, considered by many the first MEMS device, was built more than ten years later by Nathanson et al. [2].

One of the most significant challenges in MEMS is the batch fabrication process to be used in accomplishing a specific device. In the last decade, the MEMS field has grown at a tremendous pace. According to a market research company, Business Communication of Norwalk, Connecticut, the global market for MEMS will reach \$12.5 billion US in 2010 while in 2005 it was about \$5 billion US [3].



## **1.2 MEMS FABRICATION**

The MEMS fabrication techniques evolved from Integrated-Circuits (IC). On the other hand, as the field expanded, new fabrication processes specifically developed for 3D MEMS such as, bulk micromachining, SU-8 molding using microstereolithography [4], directional controlled etching using deep reactive ion etching [5], electroplating [6] and conventional machining [7], have been developed.

Essentially there are two main streams in fabrication processes through which MEMS devices can be fabricated, namely, bulk micromachining [8] and surface micromachining [9]. Maluf and Williams [10] define micromachining as toolbox of MEMS, which comprises of design and fabrication tools, that can precisely machine structures and elements at microscale.

The general process flow in MEMS fabrication includes deposition, photolithography, patterning, etching which is done many times in a repetitive manner, and packaging.

### **1.2.1 Deposition**

Deposition is an additive process in which films of materials such as silicon dioxide, silicon nitride, metallic or other non-metallic films, are applied on the substrate to act as hard masks, sacrificial layers, conductors, insulators optical films or even organic layers.

Based on the reaction taking place at the substrate surface there are two categories of depositions: deposition due to a chemical reaction and deposition due to physical reaction.

In the deposition due to chemical reaction category the most used processes are: thermal oxidation, chemical vapor deposition, electrodeposition and epitaxial growth.

The most employed methods in the physical reaction deposition are electron beam deposition and sputtering.

Deposition processes are quite well established; research in this area is mostly directed in reactive depositions, controlled depositions and cost effective processes.

### **1.2.2 Photolithography**

Photolithography is a form of lithography using ultraviolet light used to fabricate MEMS structures. The photolithographic process consists of a multitude of steps.

After a thin layer of the material of choice has been deposited on the substrate surface, the wafer is placed in the resist spinner machine.

An abundant amount of photoresist is applied on the spinning silicon substrate, and depending on the spinning time, photoresist type and rotational speed, a thin layer of photoresist is formed on top of the wafer. Positive photoresist contains a sensitizer which

breaks down when exposed to light in the 200 – 450 nm range (ultraviolet to blue) and further dissolve in developer solution [10].

Subsequent to spin coating, the wafer is soft baked at 75 to 100°C to remove solvents and the potential interlaminar stress.

Using some type of optical marks, the mask layout is transferred to the photoresist layer after an alignment with previous patterns or the wafer flat is made.

Based on the position of the mask with respect to the silicon wafer there are 3 different methods for the layout transfer: contact, proximity and projection lithography.

In contact lithography, the mask touches the photoresist, whereas proximity lithography consists of a mask placed within 25 to 50  $\mu\text{m}$  above the photoresist layer. Projection lithography, also known as stepper lithography, is able to magnify or reduce the mask projection onto the photoresist layer using a complex optical system placed between mask and photoresist layers.

When using positive photoresist, the developer will dissolve the areas exposed to the light source, while the developer will dissolve the non-exposed areas when negative photoresist is used.

Last step of photolithography is post-baking which is performed after cleaning from developer is carried out, to improve the hardness of the photoresist mask before etching. The process described above represents the classic steps of the photolithographic process.

Although, as the demand for smaller MEMS devices has increased over the last years, there are some challenges that have to be solved. In terms of photolithography there are resist challenges and imaging challenges [11]. A good photoresist will coat the substrate uniformly. In addition, it will have a good adhesion to the substrate and will maintain integrity during etching. The biggest challenges in the imaging systems used for photolithography are the depth of focus and resolution, which are important in maintaining pattern accuracy across the substrate.

To overcome some of the challenges posed during photolithography many new lithographic processes have been proposed. Xia and Whitesides [12] presented a collection of non-photolithographic techniques called soft lithography. Cheng et al. [13] eliminated the use of a glass mask and experimented a dynamic photolithographic system using a Digital Micro-mirror Device, as a dynamic mask generator. A spray coating method replacing photoresist spinning, used in fabrication of high aspect ratio microstructures was presented by Singh and his colleagues [14]. However, it has to be noted that many of the new methods presented above are still in the experimental stage.

### 1.2.3 Etching

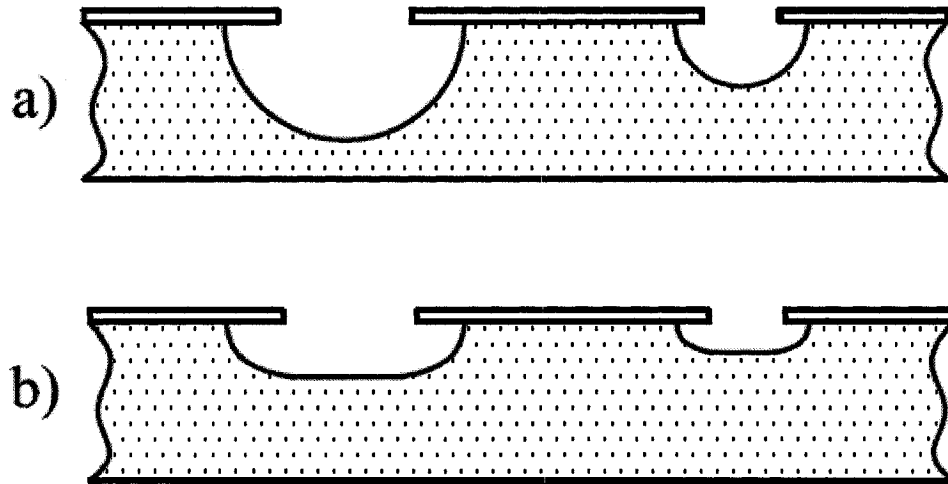
Etching is the process of selectively removing the material exposed through the patterned mask. The exposed material can be the silicon substrate or layers of deposited thin films, which can be subsequently used as masks for further etching.

There are a few etching methods based on isotropy, etch medium and selectivity [10]. The phase of the etchant, whether dry or wet, has a major influence on the etching steps and parameters. Wet etchants rely on aqueous chemistries while dry etching is based on vapor and plasma chemistry.

In general, the etching reactions take place as a result of the silicon reaction that forms compounds which can be removed from the substrate [8].

#### 1.2.3.1 Isotropic Etching

Isotropic etching is not influenced by the silicon crystallographic orientation; as a consequence of this property the resulting cross-sectional profile is round like shape as illustrated in Figure 1-1. One of the most used isotropic wet etchant is *HNA*, which is a mixture of hydrofluoric acid (HF), nitric acid (HNO<sub>3</sub>), and acetic acid (CH<sub>3</sub>COOH) [8]. As an isotropic dry etchant, XeF<sub>2</sub> gained much attention in the last few years. When using wet etchants, uniformity of the etched profile is difficult to control but stirring improves it a lot.

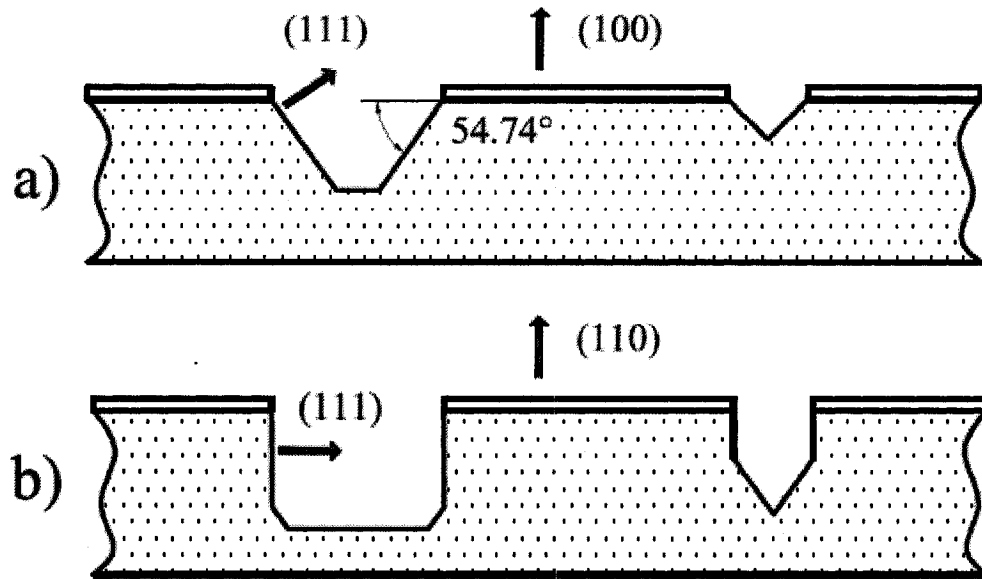


**Figure 1-1** Isotropic wet etching of silicon: a) with agitation b) no agitation [8].

#### 1.2.3.2 Anisotropic Etching

Anisotropic etching is orientation-dependant, in relation to Si crystallographic planes. The resulting etch profiles yield perfectly flat surfaces and well defined sharp angles [8]. In general, it is believed, that the orientation dependence in anisotropic etching comes from the dependence of etch chemistry with crystallographic planes. A possible factor influencing the anisotropy is the reaction mechanism of etchant with the silicon.

The mostly used anisotropic etchants are tetramethyl ammonium hydroxide (TMAH) and potassium hydroxide (KOH). For the TMAH the observed etch rate is  $\sim 1\mu\text{m}/\text{min}$  while for KOH the reported relative etch rates are 1 unit for (111) which was taken as reference, 400 units for (100) [15] and 600 units for (110) plane [16]. The etch reveal the crystallographic planes of slow etch as illustrated in Figure 1-2.



**Figure 1-2** Anisotropic wet etching: a) (100) surface orientation; b) (110) surface orientation [8].

### 1.3 BULK MICROMACHINING

Bulk micromachining consists of selectively removing the bulk of material from the substrate in order to release freestanding structures (membranes, beams, micro mirrors, etc) or three-dimensional features (holes, V grooves, micro-channels, as the one illustrated in Figure 1-3) [17]. Most of the bulk micromachining work employs single crystal silicon but there has been work involving glass, gallium arsenide and quartz. Etching of the silicon in bulk micromachining is done with all types of etchants, namely, wet, dry, isotropic and anisotropic (Table 1-1). In order to create suspended structures from the bulk of the silicon substrate the property of the etchants to etch under the oxide hard mask, called under etching, is used.

**Table 1-1** Comparison of some bulk silicon etchants [8].

<b>Comparison of Bulk Silicon Etchants</b>							
	<b>HNA</b> (HF+HNO <sub>3</sub> +Acetic Acid)	<b>Alkali- OH</b>	<b>EDP</b> (ethylene diamine pyrochat- echol)	<b>TMAH</b> (tetramethyl- ammonium hydroxide)	<b>XeF<sub>2</sub></b>	<b>SF<sub>6</sub> Plasma</b>	<b>DRIE</b> (Deep Reactive Ion Etch)
Etch Type	wet	wet	wet	wet	dry <sup>1</sup>	dry	dry
Anisotropic?	no	yes	yes	yes	no	varies	yes
Availability	common	common	moderte	moderate	limited	common	limited
Si Etch Rate μm/min	1 to 3	1 to 2	0.02 to 1	~1	1 to 3	~1	>1
Si Roughness	low	low	low	variable <sup>2</sup>	high <sup>3</sup>	variable	low
Nitride Etch	low	low	low	1 to 10 nm/min	?	low	low
Oxide Etch	10 to 30 nm/min	1 to 10 nm/min	1 to 80 nm/min	~1 nm/min	Low	low	low
Al Selective	no	no	no <sup>4</sup>	yes <sup>5</sup>	yes	yes	yes
Au Selective	likely	yes	yes	yes	yes	yes	yes
p++ Etch Stop?	no (n slows)	yes	yes	yes	no	no (some dopant effects)	no
Electrochemical Stop?	?	yes	yes	yes	no	no	no
CMOS Compatible? <sup>6</sup>	no	no	yes	yes	yes	yes	yes
Cost <sup>7</sup>	low	low	moderate	moderate	moderate	high	high
Disposal	low	easy	difficult	moderate	N/A	N/A	N/A
Safety	moderate	moderate	low	high	moderate?	high	high

1 Sublimation from solid source.

2 Varies with wt% TMAH, can be controlled to yield very low roughness.

3 Addition of Xe to vary stoichiometry in F or Br etch system can yield optically smooth surfaces.

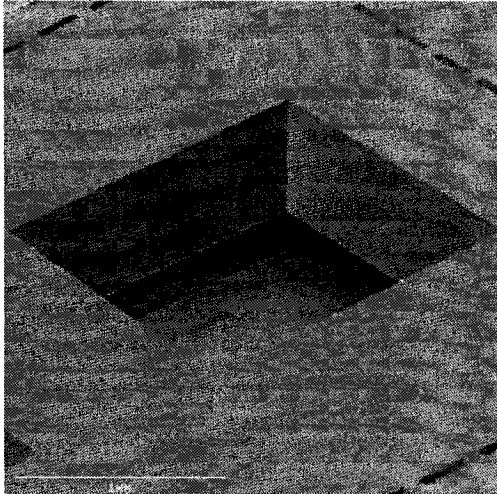
4 Some formulations do not attack Al, but are not common.

5 With added Si, polysilicic acid or pH control.

6 Defined as 1) allowing wafer to be immersed directly with no special measures and 2) no alkali ions.

7 Includes cost of equipment.



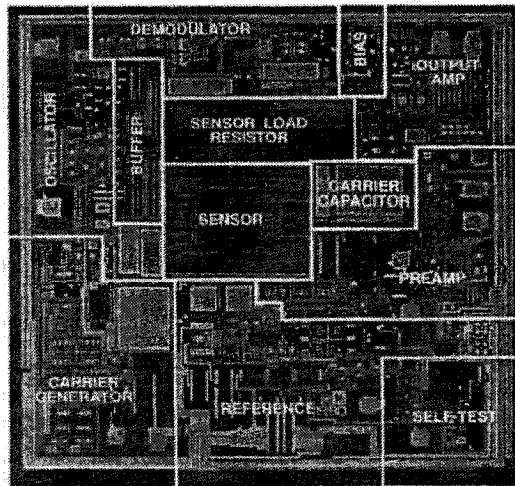


**Figure 1-3** Bulk micromachined channel inlet [18].

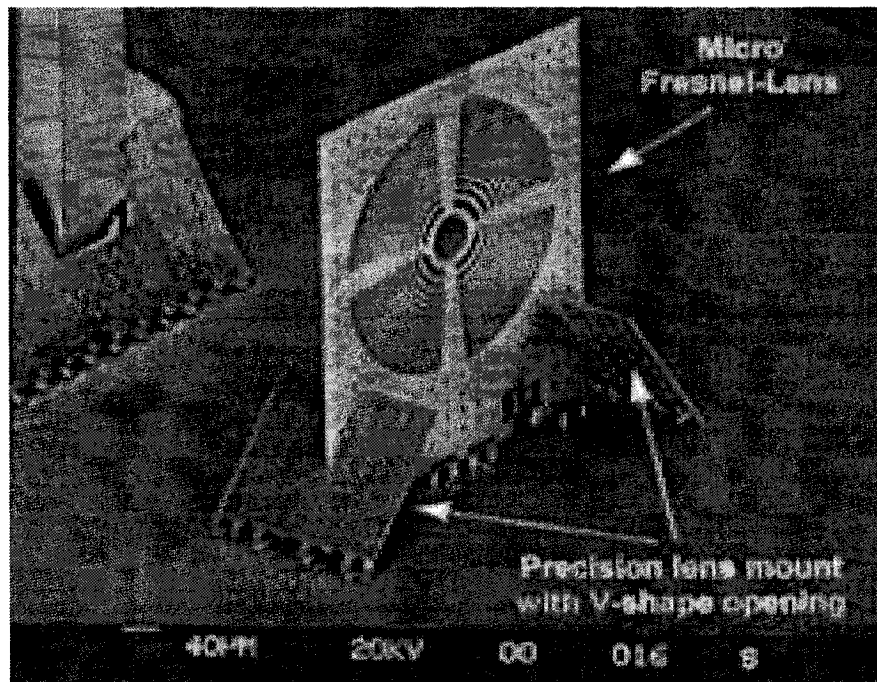
### **1.3.1 Surface Micromachining**

Surface micromachining has its roots in the integrated circuits fabrication and uses deposited thin films such as, silicon nitride and silicon oxides, to build three-dimensional structures, that are able to move and rotate freely from the substrate [9]. One of the key techniques in the surface micromachining process is the sacrificial etching through which suspended structures can be fabricated. In mid 1960's Nathanson et al.[2] used sacrificial etching to release one end of a cantilever fabricated from a deposited film, to build the field-effect transistor.

Today, the main application of surface micromachining is the accelerometer based on lateral resonators, developed by Analog Devices [19] and illustrated in Figure 1-4. Also, many optical micro-electro-mechanical systems devices are fabricated using surface micromachining, such as the self-assembled Fresnel lens [20], shown in Figure 1-5.



**Figure 1-4** Analog's Devices' ADXL50 accelerometer [19].



**Figure 1-5** Fresnel lens [20].

### 1.3.2 Wafer Bonding

Wafer bonding refers to mechanical fixation of two or more wafer to each other, and has been developed from the need to fabricate inexpensive and high quality SOI (silicon on insulator) films and assembling microstructures [21]. Lord Rayleigh [22] was the first one to investigate the adherence of pieces of silica at room temperature. Gosele and his colleagues [23] outlined the basic steps of the direct bonding (without involving an intermediate adhesive layer) process.

The first step is surface preparation of the wafers that will be bonded. One or two monolayers of water are applied to the wafers surface, which may or may not contain a native oxide or a thermally grown oxide layer.

In step two, the surfaces are brought into contact at room temperature in air or clean room conditions to avoid surface contamination with foreign particles, by pressing the wafers together. In a couple of seconds the bonded area spreads over the entire contact surface. The next step of the bonding process is the adhesion between the bonded surfaces, which takes place due to the van der Waals interactions. In applications where a higher bond energy is needed heating of the wafers takes place (for SOI applications the heating temperature is 1100°C).

There are also cases of bonding where an adhesive layer is used and the bonding process is called indirect bonding.

## **1.4 MEMS APPLICATIONS**

In his speech “There’s plenty of room at the bottom” [24] given to an audience at the annual meeting of the American Physical Society, on December 26<sup>th</sup>, 1959, Richard Feynman presents some interesting ideas about microfabrication. However, as he admits almost 25 years later, during another famous lecture “Infinitesimal Machinery” [25] held for the Jet Propulsion Laboratory scientists and engineers, he “was able to suggest no particular use for the small machines.”

Today, there are many commercially available sensors and actuators that incorporate MEMS devices ranging from pressure, temperature, gas, and motion sensors to accelerometers, micro pumps, and many optical applications.

## **1.5 PLASMA AND REACTIVE ION ETCHING**

Until late 1970s, the preferred etching method was wet etching because of low cost and high selectivity [26]. However, limitations in submicron feature sizes had forced researchers to look for an alternate etching method like gas-phase etching, also known as dry etching.

Based on the type of interaction between the etchant and the substrate there are several categories of dry etching [27]:

1. Dry etching without plasma ( $\text{XeF}_2$ ,  $\text{BrF}_3$ );

2. Physical dry etching employing ion bombardment (magnetically enhanced ion etching – MIE, ion beam etching – IBE);
3. Chemical dry etching through a chemical reaction with reactive species (plasma and barrel etching);
4. Combination of physical and chemical etching (reactive ion etching – RIE, chemically assisted ion beam etching – CAIBE, reactive ion beam etching – RIBE, magnetically enhanced ion etching – MERIE).

Out of all these dry etching processes the most widely used are plasma etching and RIE.

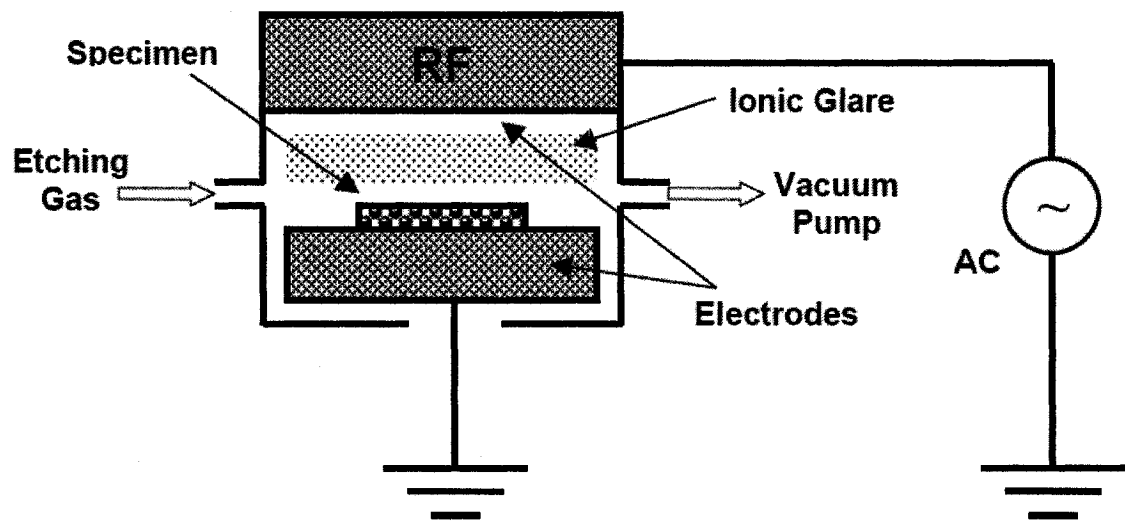
Plasma is obtained by applying a high voltage radio frequency AC signal (sometimes DC bias can be also employed) between two parallel electrodes, which produces active species from the ionization of the of the gas molecules in the electrical field [17].

In terms of equipment set up, the difference between plasma etching and RIE etching lies in the way the electrode holding the wafer is wired. If the electrode is grounded, a plasma etching is obtained, while when applying AC bias to the electrode, the RIE setup is achieved, as illustrated in Figure 1-7.

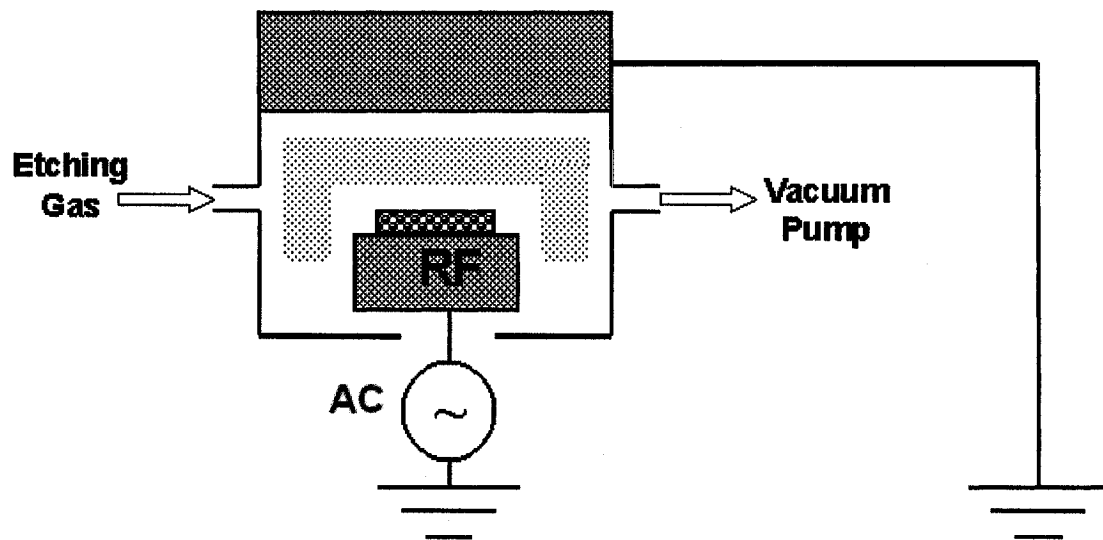
Plasma etching operates in the  $10^{-1}$  to 10 Torr while RIE operates in the  $10^{-3}$  to  $10^{-1}$  Torr pressure range. Both processes can generate isotropic or anisotropic etching profiles by

tuning the process parameters like gas composition, flow rate of the etching gas, power, pressure, temperature, etching time, RF excitation frequency and reactor geometry [28].

However, finding the best fit for all these parameters and achieving effective process control are very difficult tasks that researchers and designers have to accomplish. This makes dry etching using plasma and RIE expensive.



**Figure 1-6** Plasma etching setup



**Figure 1-7** Reactive ion etching setup

In addition, when RIE is used, there are other shortcomings, like surface damage to an extent that silicon can become polycrystalline or amorphous in the affected regions [29], and surface contamination [30, 31] . Therefore, non enhanced energetic etching methods would be preferred.

## **1.6 XENON DIFLUORIDE**

### **1.6.1 General considerations**

One of the major challenges in IC and MEMS fabrication is finding an etchant with high selectivity and etch rate, which requires a simple and inexpensively setup that will work at room temperature.

During 1980's a few research groups in North America focused on the reaction of  $\text{XeF}_2$  with silicon and studied the similarities between the  $\text{XeF}_2$  and F-atom reactions with Si and  $\text{SiO}_2$  [32], gaseous products from the reaction of  $\text{XeF}_2$  with silicon [33] and reaction probability [34], just to name a few.

Xenon Difluoride is a solid white crystalline with a sublimation pressure of about 4 Torr at room temperature [35].

In 1979, Winters and Coburn [36] proved that Xenon Difluoride ( $\text{XeF}_2$ ) [37] can etch silicon at room temperature without plasma enhancement, with etch rates in the range of 120 to 7000 Å/min at different conditions.

Etching of solid materials exposed to gas-phase etchants follows a sequence of steps [36] :

1. Nondissociative adsorption of gas species at the surface of solid etched;
2. Dissociation of the adsorbed gas;
3. Reaction between solid and adsorbed atoms which forms an adsorbed product molecule ( $\text{SiF}_4$  in the case of  $\text{XeF}_2$  – Si reaction);
4. Desorption of the product molecule;



## 5. Non-reactive product removal.

For Si/XeF<sub>2</sub> reaction, out of many other possibilities, Chuang [38] mentioned the following reaction steps as important ones:

1.  $\text{Si(s)} + \text{XeF}_2(\text{g}) \rightarrow \text{SiF}_2(\text{ads}) + \text{Xe(g)}\uparrow,$
2.  $\text{SiF}_2(\text{ads}) + \text{XeF}_2(\text{g}) \rightarrow \text{SiF}_4(\text{ads}) + \text{Xe(g)}\uparrow,$
3.  $\text{SiF}_4(\text{ads}) + \text{Si(s)} \rightarrow 2\text{SiF}_2(\text{ads}),$
4.  $\text{SiF}_4(\text{ads}) \rightarrow \text{SiF}_4(\text{g}) \uparrow.$

### 1.6.2 Reaction mechanisms between XeF<sub>2</sub> and Si

For many years it was believed that the reaction of XeF<sub>2</sub> with silicon was similar to the reaction between F atoms with silicon [36, 39]. However, the experimental results of Ibbotson [32] and his colleagues showed that etch rate and temperature dependence of XeF<sub>2</sub>/Si and F-atoms/Si reactions are different.

The reaction of XeF<sub>2</sub> with Si is a sequential chemical reaction [40] which requires development of a thick fluorosilyl layer SiF<sub>x</sub> (x = 1, 2, 3) at the exposed surface before etching begins [41].

There is a debate about the thickness of the  $\text{SiF}_x$  layer. Lo et al.[42] reported a thickness of 4 ML ( monolayer - atoms surface density ; for (111) surfaces -  $7 \times 10^{14}$  atoms/cm<sup>2</sup>, while for Si(100) the surface density is  $6.86 \times 10^{14}$  atoms/cm<sup>2</sup> [41]), Vugts et al. [43] estimated a thickness of 5.5 ML, McFeely et al. [44] are confident that the thickness is about 7 ML, Winters and Coburn [41] suggested 13 ML , and even a thickness of 38 ML was reported by Vugts and his colleagues [45]. However, the large values (13 ML and 38 ML) might be the result of surface roughening as suggested by Vugts' group [43].

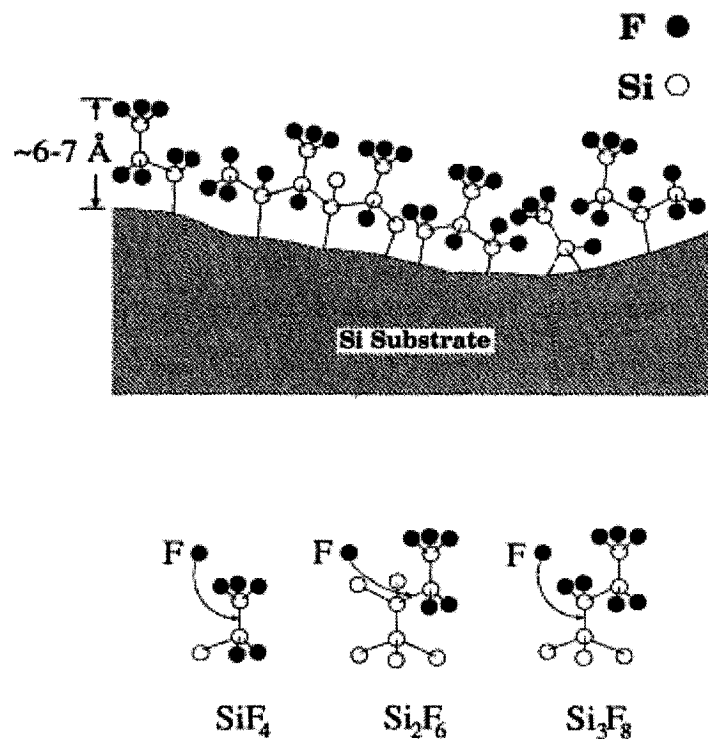
$\text{SiF}_x$  layer growth is controlled by two or more reaction paths that include the reaction between fluorine with silicon dangling bonds on the surface and insertion into the Si-Si bonds in the bulk of the silicon [41]. The initial growth caused by the attachment of fluorine atoms to the silicon dangling bonds is very rapid and concerns the formation of the first 1.5 ML [46]. After 1.5 ML the  $\text{SiF}_x$  layer continues to grow at a slower rate until “saturation” is reached [47] and etching begins.

Lo et al [42] studied the evolution of the  $\text{SiF}_x$  reaction layer as a function of  $\text{XeF}_2$  exposure (amount of  $\text{XeF}_2$  that silicon had been exposed to – in Langmuirs; 1L =  $1 \times 10^{-6}$  Torr·s) and divided their results into four regimes.

In the initial exposure ( $\text{XeF}_2$  exposure < 200L), the reaction involves mainly fluorination of the exposed surface, while in the second regime ( $\text{XeF}_2$  exposure between 200L and 2000L), a quasiequilibrium regime between  $\text{SiF}_x$  growth and etching is reached. In this regime the reaction layer is mainly composed of about 1 ML of SiF. As etching carries on

the defects appear on the surface because of the heat generated during formation of the Si-F bonds. Between 2000 and 30000 L transition to steady-state etching occurs because of sufficient substrate disorder, which modify the reaction layer composition into “tree structures of fluosilyl chains terminated by  $\text{SiF}_3$  groups” (Figure 1-8). When the tree structures are completely developed, etching reaches a steady state.

Studies showed that fluorine concentration in the surface layer did not change after the  $\text{XeF}_2$  flux was terminated. However, when the samples were exposed to temperatures above  $100^\circ\text{C}$ , the  $\text{SiF}_x$  layer begun to decompose [41].



**Figure 1-8** Schematic diagram of the “tree” structure and the reaction processes for the etching products [42]

### 1.6.3 Products from XeF<sub>2</sub> reaction with Si

Etching of silicon with XeF<sub>2</sub> proceeds through unselectively fluorination of silicon atoms, to form a sole stable product at room temperature (SiF<sub>4</sub>), and small quantities of radicals which evaporate from the substrate [48]. Winters and Houle [33] studied the products of the XeF<sub>2</sub>/Si reaction and concluded that, at room temperature, SiF<sub>4</sub> is the primary etch product (>84%); the rest is SiF, SiF<sub>2</sub> and SiF<sub>3</sub>.

### 1.6.4 Selectivity

In MEMS and IC fabrication, the knowledge about etch rates of all materials involved in the process is essential because it helps the user design, choose and tune up the appropriate fabrication process. Etch selectivity, defined as the ratio between the etch rate of the target material and the etch rate of other materials involved in the fabrication, plays an important role in MEMS fabrication, because of desirable high etch rates and high aspect ratio structures.

Winters and Coburn [36] reported that, at room temperature and without external radiation, XeF<sub>2</sub> does not etch SiO, SiO<sub>2</sub>, Si<sub>3</sub>N<sub>4</sub> and SiC. However, they observed etching of SiO, Si<sub>3</sub>N<sub>4</sub> and SiC when XeF<sub>2</sub> was combined with electron or ion bombardment.

Joyce et al. [49] confirmed Winters and Coburn's conclusions by studying the reaction between XeF<sub>2</sub> and thermally grown SiO<sub>2</sub>.

Ibbotson and his colleagues [32] studied the reaction of  $\text{XeF}_2$  with Si and  $\text{SiO}_2$  in the temperature range  $-17$  to  $360^\circ\text{C}$  and pressures between 0.05 and 2 Torr. They concluded that  $\text{SiO}_2$  was not etched under any condition while Si was etched quickly under all conditions.

A  $\text{XeF}_2$  selectivity of about 1000:1 to  $\text{SiO}_2$ , OCG 825 and AZ 5214 photoresist, aluminum, copper, acrylic, titanium-nickel alloy, gold and several polyamides was experienced by Chang et al. [50].

### **1.6.5 $\text{XeF}_2$ etching equipment**

The first group that used  $\text{XeF}_2$  as a silicon etchant to release MEMS structures was the one at University of California at Berkeley [50]. In 1994 they presented a conference paper in which they described a simple  $\text{XeF}_2$  etching system and two different etching methods they employed during the experiments.

Their setup comprised of an etching chamber that was pumped down by a vacuum pump, a pressure meter, electrical feedthroughs, nitrogen inlet and a stainless steel  $\text{XeF}_2$  source chamber.

Few years later, the same group, inspired by a paper published in the 1980's [51], added an expansion chamber to the system, and changed the manual with pneumatic valves.

## 1.7 RATIONALE OF THE THESIS

Xenon Difluoride is a very dangerous chemical product. It is corrosive to the exposed tissues, and vapor inhalation may cause chemical pneumonitis [52].

One of the challenges encountered in designing and building a safe  $\text{XeF}_2$  etching setup is due to the dangers involved in handling and storage of the  $\text{XeF}_2$ , as well as purging and releasing the reaction products.  $\text{SiF}_4$  which is the main reaction product, is a poisoning and corrosive gas [53].

Until the year 2000, when Xactix started to offer their Xetch<sup>™</sup> etching systems, there was no commercial  $\text{XeF}_2$  equipment available for silicon etching. However, at a base price of over \$100,000 US, the Xetch<sup>™</sup> system is prohibitive to many universities, including Concordia.

Also, since the announcement of the first  $\text{XeF}_2/\text{Si}$  etching lab setup for MEMS [50], there was a low interest in assessing the equipment performance versus the process parameters.

## 1.8 OBJECTIVE OF THE THESIS

A Xenon Difluoride silicon etching system, controlled by a Windows PC running LabView<sup>®</sup>, was fully designed and fabricated. Also, a Matlab<sup>®</sup> code, able to calculate the etch depth based on the pressure increase in the chamber during etching, was written and validated by the experimental results.

The main objective of this work is to advance the knowledge of micromachining through experimental investigation of the Si isotropic etch with  $\text{XeF}_2$ .

The specific objectives of the research are:

- i. to develop an etching model that is based on an atomic model of etching;
- ii. to design and install a fully automatic, second generation,  $\text{XeF}_2$  equipment that enables an optimal etching process of Si;
- iii. to validate the etching model through experimental work.

## **1.9 THESIS OVERVIEW**

In Chapter 1 of the thesis, the reader is introduced to MEMS field and xenon difluoride. Fabrication methods, applications and etching equipment for MEMS are described, while reactions mechanisms, reaction products and etching equipment layout for the  $\text{XeF}_2/\text{Si}$  reaction are presented.

The influence of process parameters and etching methods for etching of silicon with xenon difluoride are discussed in Chapter 2.

Chapter 3 presents the design constraints and systems components of the designed etching equipment.

The motivation for developing an etching model for xenon difluoride etching of silicon is discussed in the 4<sup>th</sup> Chapter. Also, the model is presented in detail for square and circular mask openings.

In Chapter 5 the etching model is validated against experimental results for both square and circular openings.

Conclusions and suggestions for future work are discussed in Chapter 6.



## CHAPTER 2

### **XeF<sub>2</sub> ETCHING OF SILICON**

#### **2.1 THE INFLUENCE OF THE PROCESS PARAMETERS**

It has been found that reaction between xenon difluoride and silicon is very sensitive to the process parameters such as temperature, etching pressure, doping level of Si, aperture width, aperture inclination and external excitation.

##### **2.1.1 Influence of temperature**

Vugts et al. [43] studied temperature dependence of Si/XeF<sub>2</sub> etching in a molecular beam setup. The UHV chamber had a background pressure of 10<sup>-8</sup> Torr and was temperature controlled, in the range of 100 K to 1000 K. The XeF<sub>2</sub> flux, which was supplied at an angle of 52° with the surface normal, could be varied from 0.06 ML s<sup>-1</sup> to 3.6 ML s<sup>-1</sup> on a 3 mm diameter sample detection area. A mass spectrometer positioned in a separate UHV was used to monitor the species desorbing from the detection area.

Before each experiment they heated the sample to a temperature of 900 K to clean it, then they cool it to the desired temperature in the range of 150 K to 900 K. After cleaning, the sample was exposed for 2400s to a XeF<sub>2</sub> flux of 1 ML s<sup>-1</sup> to reach steady state, and the reaction products were monitored using a mass spectrometer. They defined two

coefficients, namely, reaction coefficient  $\varepsilon$  and production coefficient  $\delta$  in order to determine the temperature dependence of the Si/XeF<sub>2</sub> reaction.

The reaction coefficient  $\varepsilon$  is the flux of fluorine used at the sample, normalized to the total flux arriving at the sample:

$$\varepsilon = \frac{\Phi_s(XeF_2) - \Phi(XeF_2)}{\Phi_s(XeF_2)} \quad (2-1)$$

where  $\Phi_s(XeF_2)$  is the XeF<sub>2</sub> flux arriving at the sample from the gas source and,  $\Phi(XeF_2)$  is the nonused flux of XeF<sub>2</sub> leaving the sample.

The production coefficient  $\delta$  was defined as the flux of fluorine atoms produced, bound to desorbing products, normalized to the total flux of fluorine atoms arriving at the sample. The expression is composed of two terms corresponding to the two major etching products, SiF<sub>4</sub> and SiF<sub>2</sub> etching products.

$$\delta = \delta_4 + \delta_2 \quad (2-2)$$

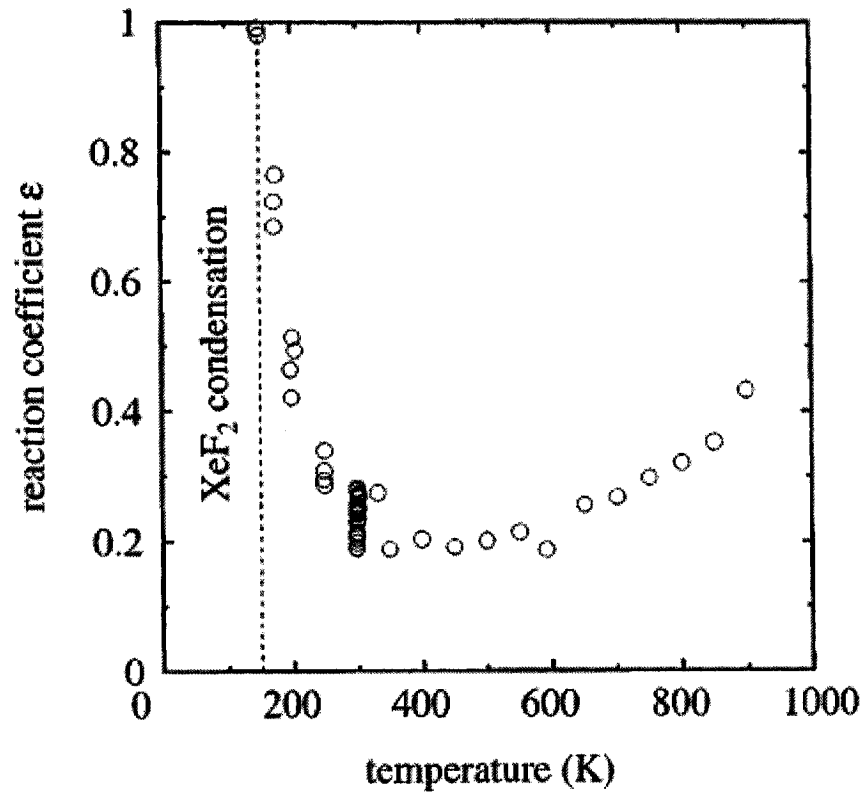
$$\delta_4 = \frac{2\Phi(SiF_4)}{\Phi_s(XeF_2)} \quad (2-3)$$

$$\delta_2 = \frac{\Phi(SiF_2)}{\Phi_s(XeF_2)} \quad (2-4)$$

in which,  $\Phi(\text{SiF}_4)$  is the  $\text{SiF}_4$  flux and  $\Phi(\text{SiF}_2)$  is the  $\text{SiF}_2$  flux.

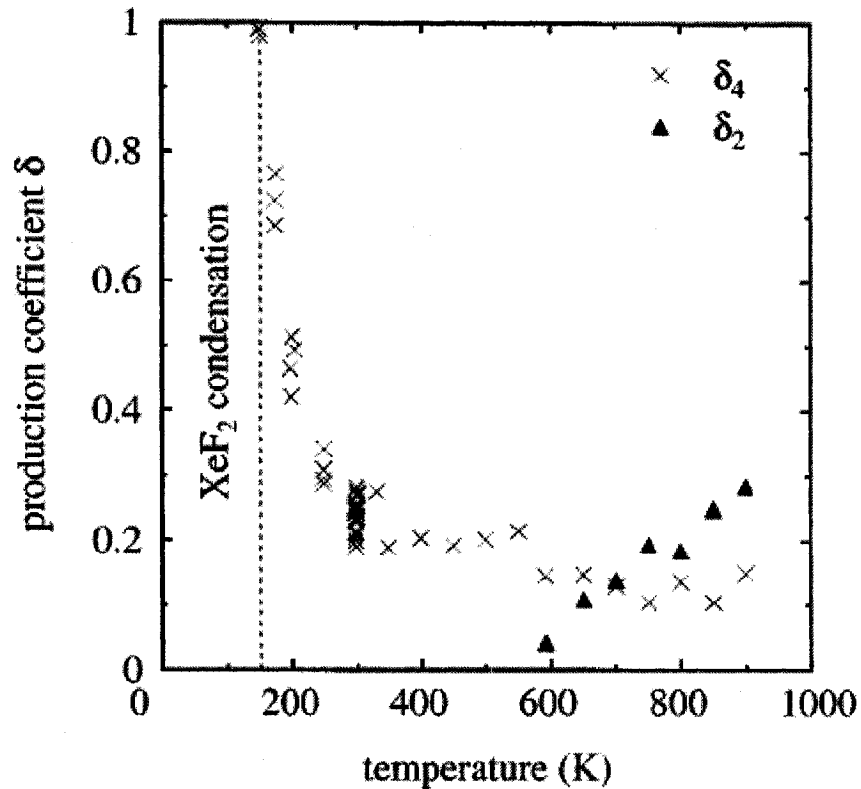
As the authors were interested in steady state regime of  $\varepsilon = \delta$ , or the flux of the incoming fluorine as  $\text{XeF}_2$  is equal with desorbing fluorine as etch products.

For the reaction coefficient, maximum value  $\varepsilon = 1$  was around 150 K while the minimum  $\varepsilon = 0.2$  was reached around 400 K. After 600 K there is an increasing trend reaching a value of  $\varepsilon = 0.45$  at 900 K (Figure 2-1).



**Figure 2-1** Temperature dependence of reaction coefficient,  $\varepsilon$  [43].

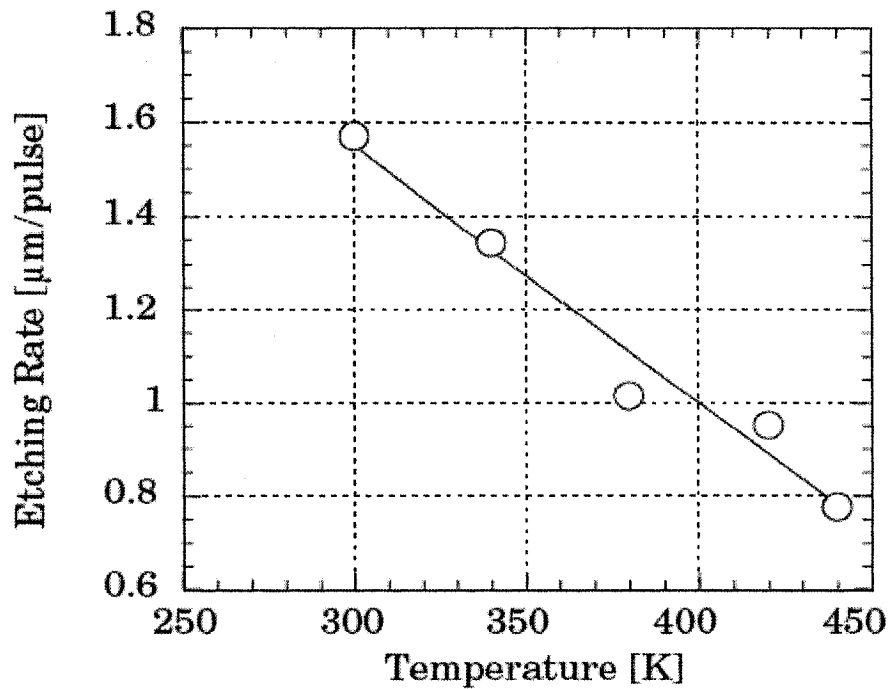
The variation of production coefficient as a function of temperature is shown in Figure 2-2. Below 600 K, the  $\text{SiF}_2$  production is insignificant or none, but starts to increase above this temperature reaching a value of  $\delta_2 = 0.12$  at around 700 K where  $\delta_2 = \delta_4$  and reaches a maximum of about  $\delta_2 = 0.24$  at 900 K. The  $\text{SiF}_4$  production is maximum in the lower range of temperatures with  $\delta_4 = 1$  at  $T = 175$  K, then it decreases in the range of  $\delta_4 = 0.2 - 0.3$  at room temperature. Between 300 K and 575 K there is a floor in the production of  $\text{SiF}_4$  with a value of  $\delta_4 = 0.2$ . Above 600 K  $\delta_4$  had random values between 0.5 and 0.7. Also we have to note that above 700 K,  $\delta_2 > \delta_4$ .



**Figure 2-2** Variation of the production coefficients  $\delta_2$  and  $\delta_4$  in the temperature range of 150 K to 900 K [43].

It has to be mentioned that no experiments were performed below 150 K due to  $\text{XeF}_2$  condensation, which blocks the reaction.

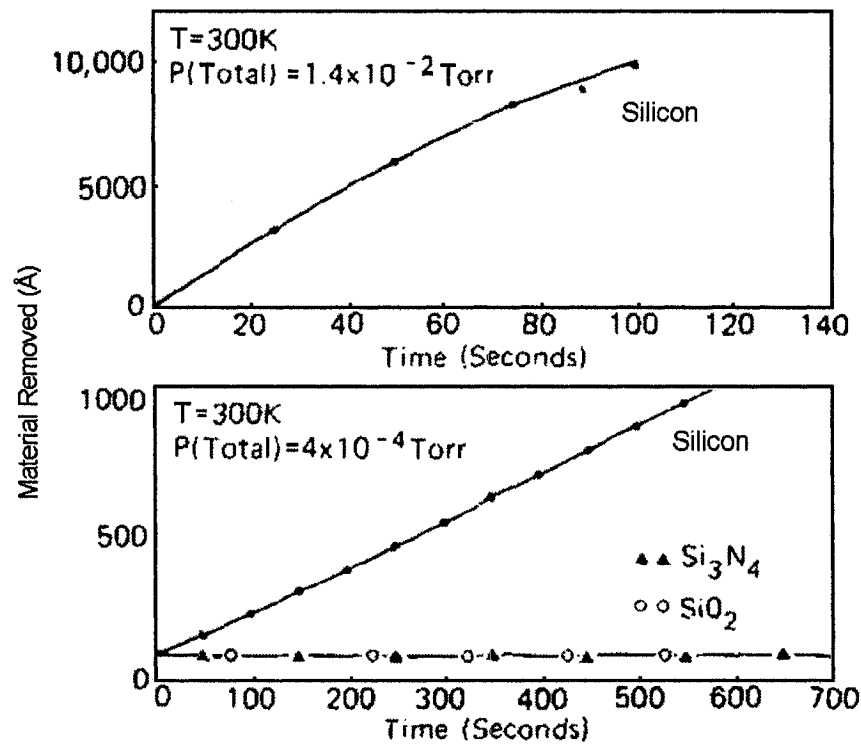
The same trend was found by Sugano and Tabata [54] when they compared the etch rate for different sample temperatures in the range of 300 K to 440 K. They used wagon wheel patterned silicon samples exposed to  $\text{XeF}_2$  for five pulses of 60 seconds in the temperature range stated above. The measurements were taken at an aperture width of 175  $\mu\text{m}$ . At 300 K the etch rate per pulse was about 1.5  $\mu\text{m}$  and it decreased linearly to approximately 0.7  $\mu\text{m}$  at 440 K (Figure 2-3).



**Figure 2-3** Etch rate dependence on substrate temperature [54]

### 2.1.2 Pressure influence

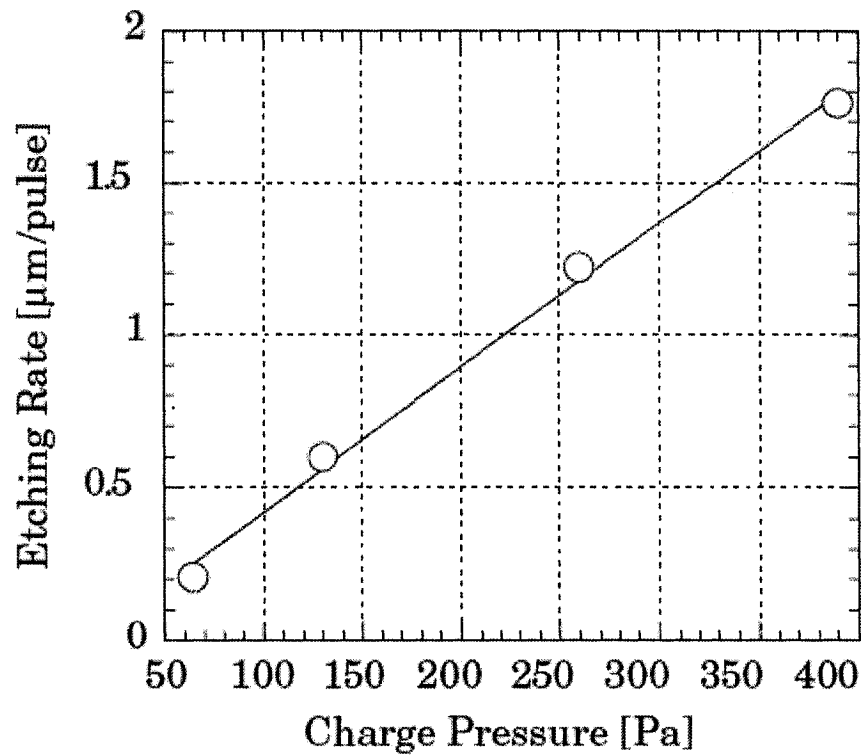
Winters and Coburn [36] monitored the removal rate of silicon when exposed to  $\text{XeF}_2$  at 300 K. The exposed silicon was a  $2\mu\text{m}$  thick film deposited by e-beam evaporation, and the change in mass was monitored using a quartz crystal microbalance. After a minute of exposure they found an approximate etch rate of  $7000 \text{ \AA}/\text{min}$  at  $1.4 \times 10^{-2} \text{ Torr}$ , while for a pressure of  $4 \times 10^{-4} \text{ Torr}$  the etch rate decreased to  $120 \text{ \AA}/\text{min}$  (Fig. 2-4).



**Figure 2-4** The amount of silicon removed from a silicon film deposited on a quartz-crystal microbalance; silicon nitride ( $\text{Si}_3\text{N}_4$ ) and silicon oxide ( $\text{SiO}_2$ ) showed almost no etching [36].

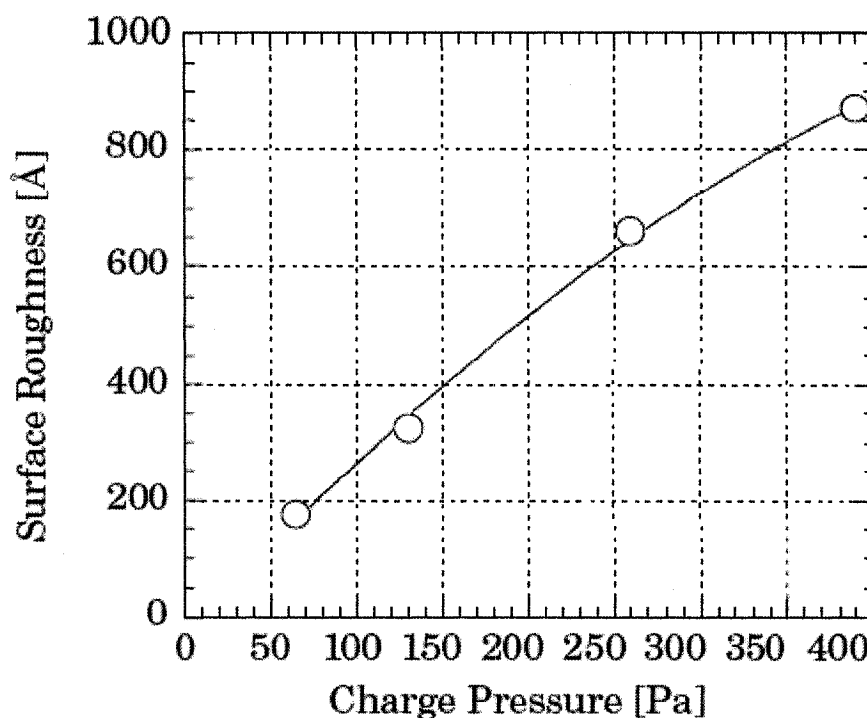
Sugano and Tabata [54] did some experiments trying to find the influence of etching pressure on etching rate and surface roughness.

They found that the etching rate is linearly increasing in the range of 65Pa and 390Pa for a pulse of 60 seconds. For a pressure of 65Pa the etch rate found was 0.21  $\mu\text{m}$  while for a starting etching pressure of 390 Pa the etch rate was 1.76  $\mu\text{m}$ ; the sample aperture width was 175  $\mu\text{m}$  (Figure 2-5).



**Figure 2-5** Etch rate per 60 seconds pulse for a 175  $\mu\text{m}$  aperture width at different etching pressures [54]

Another experiment done by the authors was to compare the surface roughness at the same etch depth, for samples etched at different etching pressure. As in the case of the etch rate, the surface roughness presented almost a linear increase with pressure in the 65Pa to 390Pa range, as it can be seen in Figure 2-6.



**Figure 2-6** Surface roughness evolution for samples etched at pressures between 65Pa and 390Pa [54].

### 2.1.3 Si doping level effects

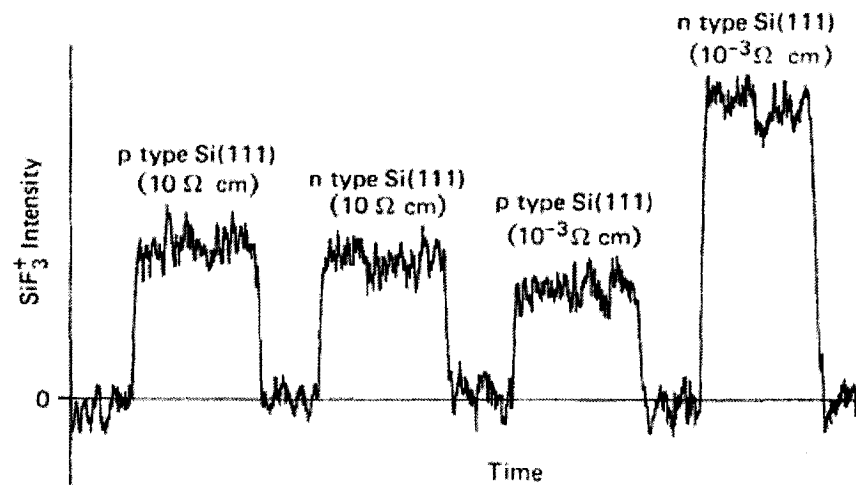
For many years it was believed that the trends observed in plasma-assisted etching regarding effects of doping would also occur in the  $\text{XeF}_2/\text{Si}$  etching reaction. Winters and Haarer [55] revealed that etch rate depends upon the concentration and type of dopant and, also upon the thickness of the fluorosilyl layer.

They used a bakeable ultrahigh-vacuum system in which atomically clean silicon samples were exposed to  $\text{XeF}_2$  and a small sample of the etch product was detected using a mass spectrometer. Up to eight Si(111) samples were mounted on a manipulator for



comparison, accomplished by rotating them such as a different sample was placed in front of the detector's aperture.

All the samples were exposed to a flux of  $1 \times 10^{19}$  XeF<sub>2</sub> molecules/cm<sup>2</sup> and the etch rate was monitored through SiF<sub>4</sub> evolution, which is the intensity of the SiF<sub>3</sub><sup>+</sup> signal detected by the spectrometer. They found that lightly doped *p*- and *n*-type silicon have about the same etch rate while heavily doped *n*<sup>+</sup>-type has a much larger etch rate than *p*<sup>+</sup>-type (Figure 2-7).



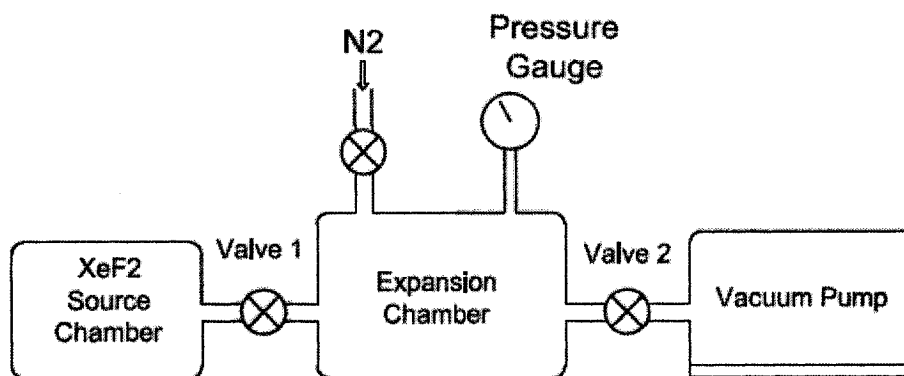
**Figure 2-7** Evolution of SiF<sub>4</sub> desorption in time [55].

## 2.2 CONSTANT PRESSURE ETCHING VERSUS PULSE ETCHING

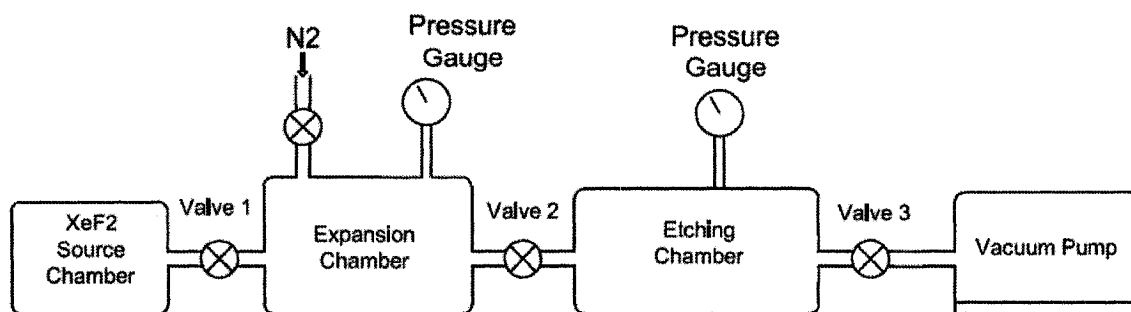
There are two types of etching setups that are currently being used.

The first type comprises of a  $\text{XeF}_2$  source chamber, an etching chamber, a vacuum pump, a pressure measurement device to monitor the pressure in the etching chamber and valves which connect the source chamber, vacuum pump and liquid nitrogen tank (Figure 2-8).

Second type of etching system has an additional chamber between the source and the etching chambers, which permit a known volume of  $\text{XeF}_2$  to be injected in the etching chamber (Figure 2-9).



**Figure 2-8** Diagram of a  $\text{XeF}_2$  etching setup without expansion chamber.



**Figure 2-9** XeF<sub>2</sub> etching setup with expansion chamber.

Chang et al. [50] reported two methods for XeF<sub>2</sub>/Si etching, namely constant pressure etching and pulse etching outlined below.

Constant pressure etching is used in general with etching systems that do not have an expansion chamber. This etching method proceeds as it follows:

1. The etching chamber is pumped down until a pressure of ~20 mTorr is reached;
2. Valve 1 is opened and the XeF<sub>2</sub> crystals sublime into the etching chamber and the etching commences;
3. Using valve 2 the pressure is fine tuned around 1.8 to 2 Torr;
4. When the desired etch time is reached valve 1 is closed.

A pulse etching done in a  $\text{XeF}_2$  setup with expansion chamber will have the following sequence:

1. Valves 2 and 3 are open, valve 1 is closed;
2. Expansion chamber and etching chamber are pumped down to approximately 20 mTorr;
3. When this pressure is reached, valves 2 and 3 will close and valve 1 will open letting the  $\text{XeF}_2$  sublimate in the expansion chamber;
4. Valve 1 will close when  $\text{XeF}_2$  pressure in the expansion chamber will reach 3 Torr moment in which valve 2 will open letting the  $\text{XeF}_2$  vapors in the etching chamber and the etching pulse count begins;
5. When the pressure in the etching chamber reaches 1.8 Torr, valve 2 will be closed;
6. The expansion and etching chamber are purged with nitrogen when the pulse counter reaches 60 seconds by opening nitrogen valve and valves 2 and 3.

The same sequence is repeated for the number of desired pulses.

Chang et al. [50] employed both methods using an etching system without expansion chamber. They found that the pulse method averaged between 5 and 10  $\mu\text{m}$  per pulse while using constant pressure etching at 2.5 Torr the etch rates were 3 to 5  $\mu\text{m}$  per minute. When compared the etch uniformity across the wafer, they found similarities between the methods with highest etch rates near the  $\text{XeF}_2$  inlet and the slowest at the center of the wafer.

## **CHAPTER 3**

### **EQUIPMENT DESIGN AND DEVELOPMENT**

#### **3.1 INTRODUCTION**

Using the experience acquired from operating our previous Xenon Difluoride etching system [56], a completely new and improved Xenon Difluoride etching system for silicon, has been designed and built.

The new design focuses mainly on eliminating custom fabrication in order to keep the price down, increasing the process repeatability through minimizing the human intervention in the process, and improving the system ergonomics by using human factors engineering design principles.

Another improvement of the new system over previous setup is the addition of an expansion chamber which allows a known quantity of  $\text{XeF}_2$  to be injected in the main chamber. Also, by designing an expansion chamber with a volume more than twice of the volume of etching chamber, the duration of the etching process is minimized by eliminating the need to purge and vacuum the expansion chamber every pulse. Instead, the  $\text{XeF}_2$  gas that is in the expansion chamber is used to fill the etching chamber twice.

### 3.2 DESIGN CONSTRAINTS

The main constraints of the design process (explained in Table 3-1), could be classified in the following groups: safety, price, process, chambers volume, setup volume, and weight constraints.

**Table 3-1** Design constraints.

Design Constraint	Reason	Design Solution
Safety	<ul style="list-style-type: none"><li>• XeF<sub>2</sub> is a very dangerous substance; in contact with moisture forms HF.</li></ul>	<ul style="list-style-type: none"><li>• Placed the setup in a fume hood.</li><li>• Operator has to wear safety equipment.</li></ul>
Budget	<ul style="list-style-type: none"><li>• Limited budget.</li></ul>	<ul style="list-style-type: none"><li>• Avoid custom fabrication;</li><li>• Work with only a few suppliers in order to be able to negotiate a volume discount and save on shipping cost.</li></ul>
Chambers volume and accessibility	<ul style="list-style-type: none"><li>• Ability to fill up the etching chamber with XeF<sub>2</sub> twice from the expansion chamber.</li><li>• Possibility of etching wafers up to 4 inches in diameter.</li><li>• Visual access to the etching process.</li></ul>	<ul style="list-style-type: none"><li>• The chambers volume ratio was designed as 2 to 1.</li><li>• The etching chamber is fitted with a 4 inch diameter access door and a top glass viewport.</li></ul>
Setup volume	<ul style="list-style-type: none"><li>• Due to safety reasons, the setup has to operate inside a standard fume hood.</li></ul>	<ul style="list-style-type: none"><li>• The designed setup is very compact; the components are connected with very short tubes.</li></ul>
Weight	<ul style="list-style-type: none"><li>• Increase systems portability and easy maintenance.</li></ul>	<ul style="list-style-type: none"><li>• Adopted a modular design; the system is formed from many smaller modules that attach to another using quick connect flanges.</li></ul>

### **3.2.1 Safety**

Due to the dangerous nature of  $\text{XeF}_2$ , safety of operation is the most important factor one has to take into account when designing a setup; safety is the reason why the system is placed inside a fume hood. Furthermore, the system was leak-tested for two weeks, and an emergency stop button was integrated in the software interface. Aside from a safety oriented design there is also standard safety equipment that the operator is required to wear when the samples are prepared and the system is running.

### **3.2.2 Strategies to keep the design within the budget**

The price constraint is the one that imposed a design based on standard parts rather than custom fabricated parts. The objective was to stay within an assigned budget, and for that matter a time consuming supplier search, which could provide all or at least 90% of the parts, at an negotiated discounted price and in one shipment, was done.

### **3.2.3 Chambers volume and accessibility**

Chambers volume ratio, which had to be at least 2 to 1 in favor of the expansion chamber, was one of the main process constraints. An expansion chamber with a bigger volume would be preferred, but the advantages of using such a chamber versus the increase in system's weight and the quantity of xenon difluoride that is wasted in the purging cycle do not make economic sense. An access door of at least four inches



diameter to accommodate medium sized wafers, a viewport mounted on top of the chamber which would allow for future film recording of the etching process, a larger flange on one of the chamber sides to allow future devices attachment through a multiport flange, a bottom flange where we could attach a rotating mechanism for the silicon chips, were all very important design constraints for the etching chamber that imposed us a six-way cross design for the etching chamber.

#### **3.2.4 Setup volume**

The volume constraints were related to the volume of the fume hood. One of the main objectives of the design was to accommodate all the components, including the vacuum pump, inside a fume hood. By doing this, a compact installation was designed, with low noise pollution and minimum length connection tubes. However, staying within the volume constraints resulted in other ergonomic challenges that had to be taken into account. The etching setup was designed to accommodate 95% percentile of men. The dial pressure gauges had to be elevated at the eye level, which is about 1.65 meters, the door knob had also to be within easy reach while the top of the liquid nitrogen trap was placed at about 1.2 meters from the floor to be at the elbow height.

#### **3.2.5 Weight**

The whole etching system is formed of several smaller modules which are connected together using quick connect flanges. This modular type of design assures systems

portability, when service or maintenance operations are performed, by enabling quick disassembling into smaller subassemblies, which can be moved around by a single person. The main subcomponents of the system are: etching chamber, expansion chamber, vacuum pump, liquid nitrogen trap, vacuum valves, capacitance manometers, dial manometers and XeF<sub>2</sub> supply bottle; their weight is listed in Table 3-2.

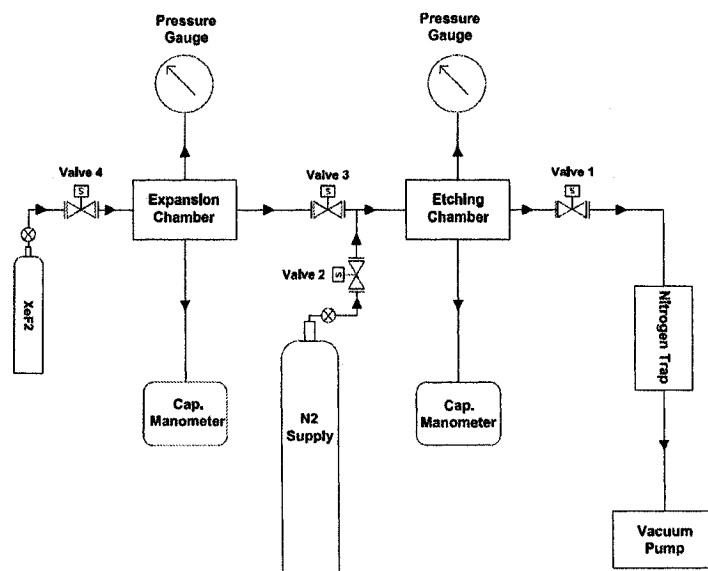
**Table 3-2 Etching system subcomponents weight.**

<b>Subcomponent</b>	<b>Number of Parts</b>	<b>Unit Weight [lb]</b>	<b>TOTAL Weight [lb]</b>
Expansion Chamber	1	42	42
Etching Chamber	1	45	45
Vacuum Pump	1	59.5	59.5
Liquid Nitrogen Trap	1	6	6
Vacuum Valves	4	2.2	8.8
Capacitance Manometers	2	1.5	3.0
Dial Manometers	2	0.5	1.0
Tubes	3	0.5	1.5
Connectors	5	0.5	2.5
Clamps	17	0.25	4.25
Frames	1	25	25
XeF <sub>2</sub> Supply Chamber	1	2.2	2.2
Bolts, nuts and gaskets			30
<b>TOTAL</b>			<b>230.75</b>

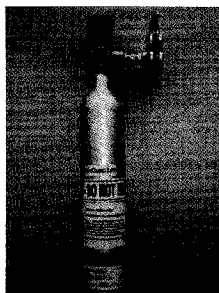
### 3.3 SYSTEMS COMPONENTS

#### 3.3.1 Hardware Subsystem

The hardware subsystem consists of the following components: vacuum pump, liquid nitrogen trap, electromagnetic valves, etching chamber, expansion chamber, XeF<sub>2</sub> supply chamber, dial manometers and pressure transducers for the expansion and etching chamber, connecting tubes, flanges and flanges accessories, and the supporting frame. The hardware parts are interconnected as shown in the piping and instrumentation diagram, shown in Figure 3-1. Systems components are all made of stainless steel, except for the XeF<sub>2</sub> supply chamber, which is made of aluminum as provided by the supplier, and is connected to the system through a manual stainless steel safety valve. The XeF<sub>2</sub> supply chamber is shown in Fig. 3-2.

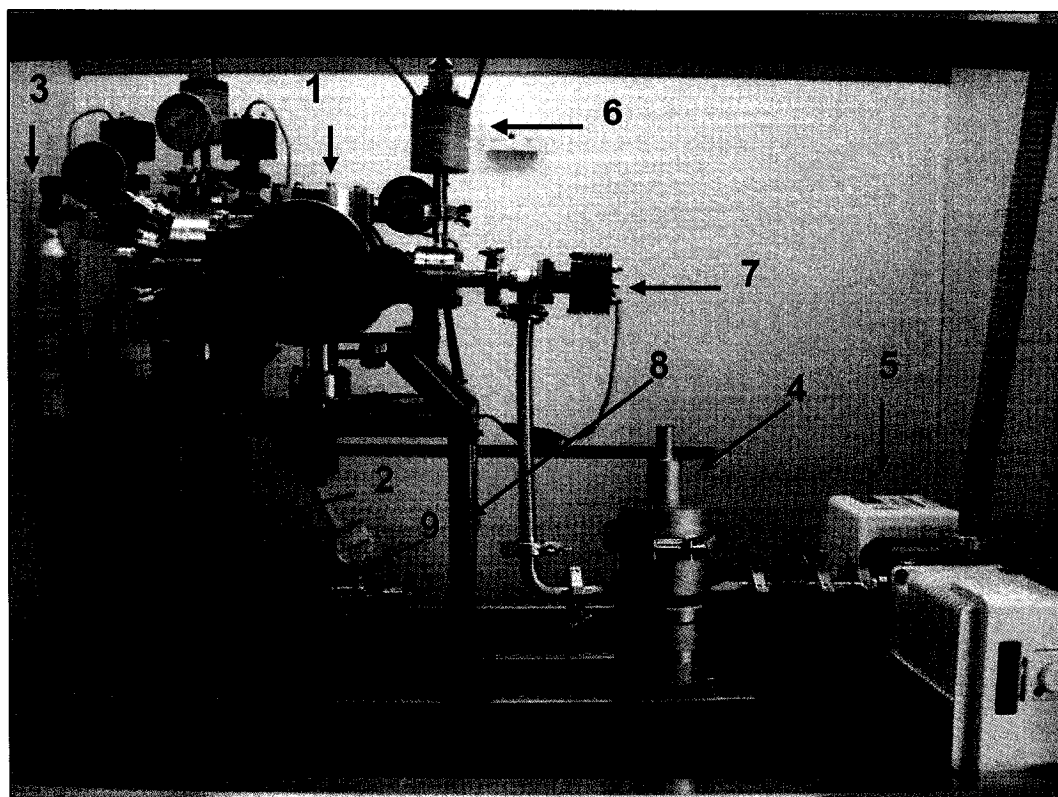


**Figure 3-1** Piping and instrumentation diagram of the designed XeF<sub>2</sub> etching system.



**Figure 3-2** The  $\text{XeF}_2$  supply chamber, supplied by SynQuest Labs, Inc.

A picture of the etching system placed inside the fume hood is shown in Figure 3-3.

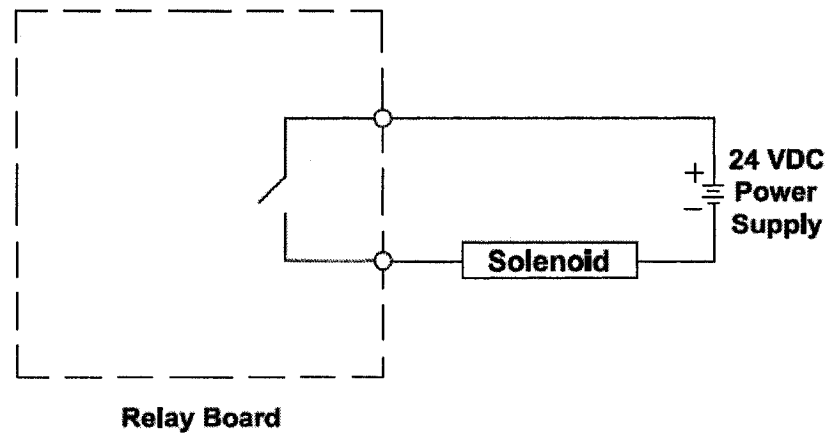


- 1 – Etching Chamber; 2 – Expansion Chamber; 3 –  $\text{XeF}_2$  Supply Chamber;
- 4 – Liquid Nitrogen Trap; 5 – Vacuum Pump; 6 – Pressure Transducer;
- 7 – Electromagnetic Valve; 8 – Supporting Frame;
- 9 – Nitrogen Pressure Regulator;

**Figure 3-3** The complete etching system inside the fume hood.

The etching chamber has a volume of about 2.7 liters and is of spherical shape with a front-loading door, a top viewport, and on one of the sides it has a multiport that can be used to attach other instruments in the future. A simple nipple blanked at one end connected to the system through a flexible tube and with a volume of about 5.6 liters acts as expansion chamber.

To keep the system as simple as possible, to eliminate the need for a supplementary air supply, and because of the excellent response time they are providing, electromagnetic solenoids are used for valves' actuation. The solenoids require 24 VDC at 1.4A at the initial actuation but the power consumption goes down to 0.28A after startup. The electromagnetic vacuum valves are connected to the PC through a four channel relay device because of the high initial power consumption. The connection diagram between the power supply and the solenoids is shown in Figure 3-4.

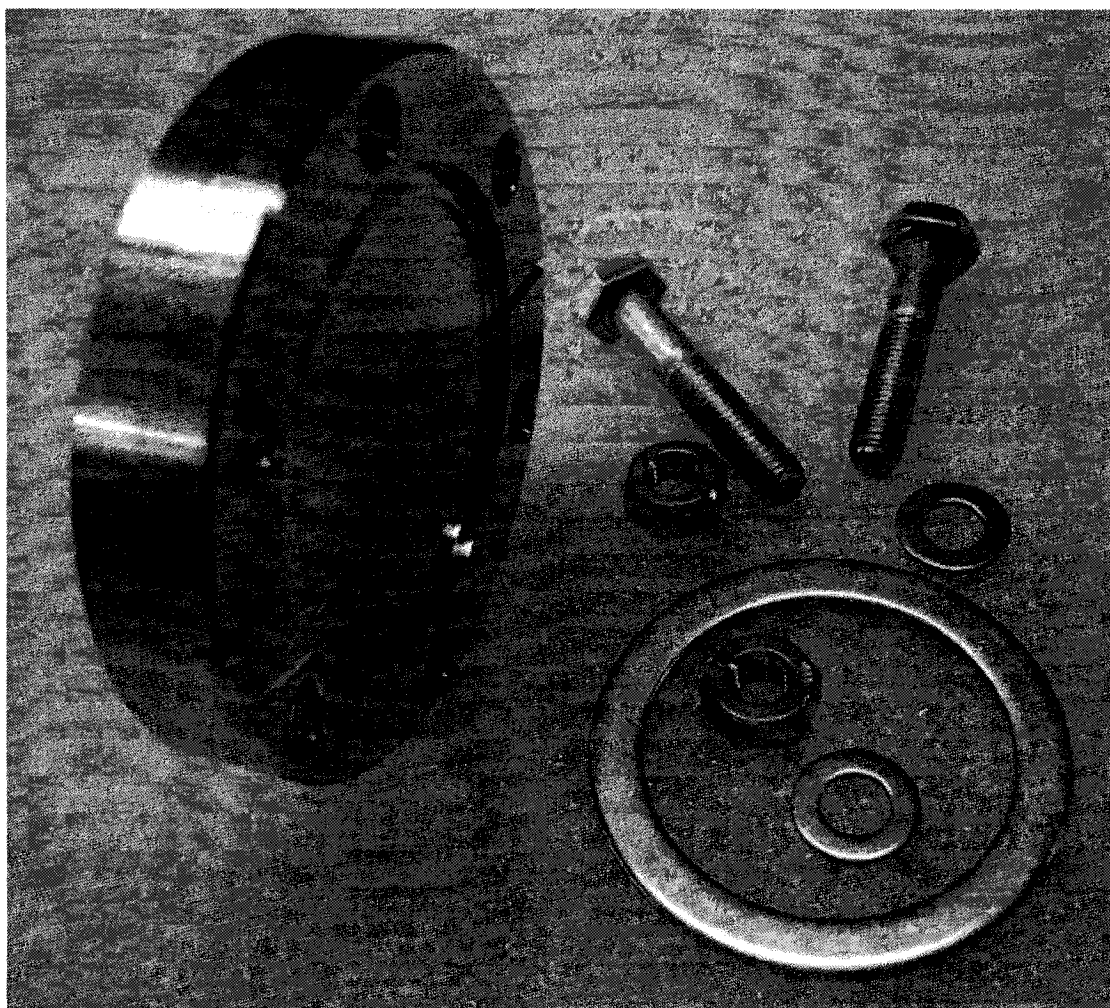


**Figure 3-4** Diagram of solenoid connection to the power supply.

The connections between systems components are made with ConFlat flanges and KF (Klein Flanche) also known as quick release flanges.

CF are sexless flanges, designed to work between 760 Torr to  $1 \times 10^{-13}$  Torr, and they attach to each other using stainless steel bolts lubricated with an anti-seize compound or stainless steel bolts coated with silver. The sealing is realized by two knife edges, one on each flange, which are machined below flange faces. When the bolts are tightened a softer metal gasket, usually copper, is pressed between the knife edges and a leak-tight seal results. When tightening the bolts of CF assemblies, a crisscross star pattern was used. The bolts were first hand tightened and afterwards a torque wrench was used to gradually tighten in a quarter or half turn increments, until the desired torque was reached. Following of this procedure for each CF flange ensured an even compressed gasket.

The KF flanges are also sexless and attach to each other using a clamp tightened by a butterfly nut. An o-ring mounted on a centering ring aligns the flanges and seals the assembly in a pressure range from atmospheric to  $1 \times 10^{-8}$  Torr. In Figure 3-5 a 2.75 CF blank, a copper gaskets and stainless steel bolts, nuts and washers are shown. Figure 3-6 shows a KF16 clamp, a 90 degrees elbow, and a centering ring.



**Figure 3-5** CF type of flange and accessories.



**Figure 3-6** KF type of flange, centering ring and clamp.

To prevent condensed vapors entering the oil-sealed vacuum pump and reduce the oil lubrication properties, and also to prevent oil from backstreaming into the etching chamber, a liquid nitrogen cooled trap was placed in between the etching chamber and the pump.

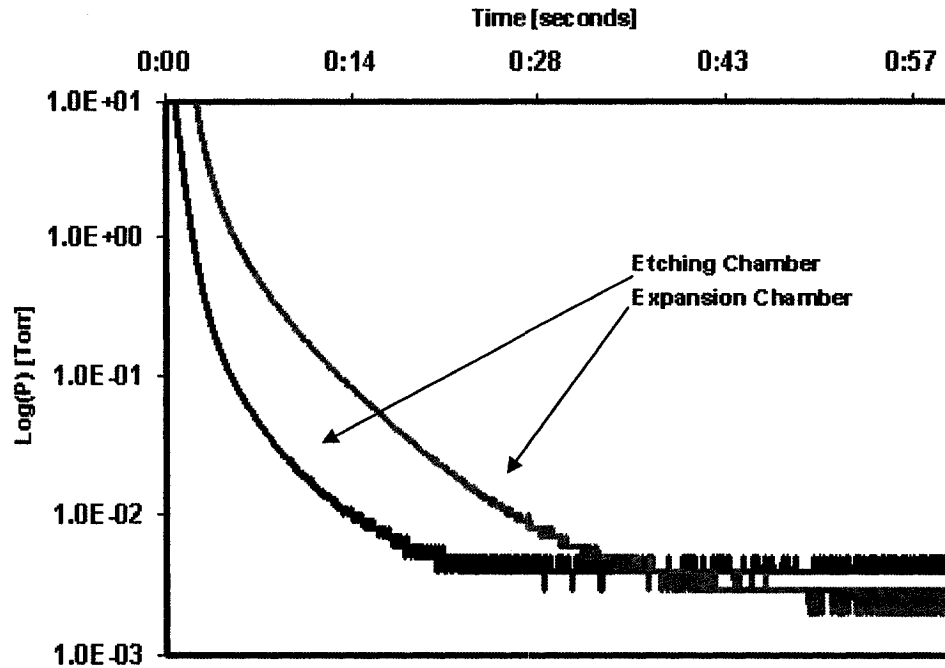
The pressure in both chambers is measured using two capacitance manometers, which can measure in the range 0 to 10 Torr. To power up the manometers and transform the voltage readings, a controller was used for both gauges. Also, the controller communicates with the PC through a serial interface. Prior to experiments, to eliminate a



possible zero offset, the pressure transducers had the zero adjusted in a vacuum system at a pressure below  $5 \times 10^{-4}$  Torr.

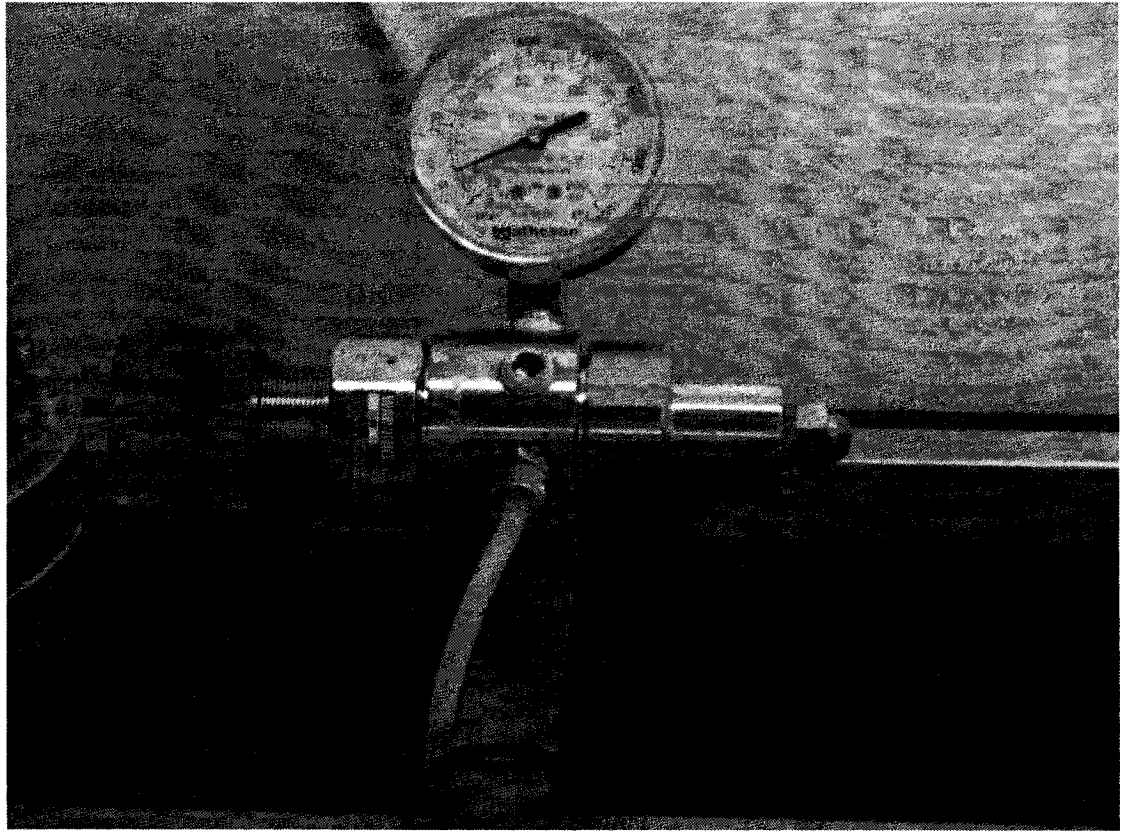
To decrease the duration of an etching pulse a two stage rotary vane pump, with a flow rate of  $18 \text{ m}^3/\text{h}$ , is used. The vacuum system was pumped down in order to find what is the vacuum speed of the pump. The results are plotted in Figure 3-7. It can be seen that the lowest attainable vacuum pressure for the designed system is 2 mTorr. The 1 mTorr pressure variation that can be observed in on the graph is due to the rounding of capacitance manometers voltage readings.

The lowest pressure was 3 mTorr in the expansion chamber and 4 mTorr in the etching chambers. However, these are approximate values, as the transducers were not zeroed before the test was done, and for a transducer with 10 Torr full scale reading, the manufacturer suggests accurate readings in the 10 Torr to 5 mTorr vacuum ranges; for the same reasons the pressure readings oscillate in the 5 mTorr zone. The plot shows that the etching chamber reaches 4 mTorr after approximate 30 minutes of pumping down from atmospheric pressure, while the expansion chamber reaches the same pressure 5 minutes later. A vacuum pressure delay is observed in the plot, for the expansion chamber, and this is due to the higher volume of the expansion chamber and because it is further away from the vacuum pump.



**Figure 3-7** Plot of the system pressure during one hour of vacuum pumping.

The impossibility of the pressure transducers to measure above 10 Torr had created a few design challenges, all related to the nitrogen purge of the system in between etching cycles when the pressure inside the chambers goes well above the transducers measurement range and there is no feedback pressure. To eliminate the risks of over-pressurizing the etching system we had designed a few backup systems. One is the fact that we added an extra pressure regulator on the nitrogen purge line. In case of a failure of the first pressure regulator, the second one will reduce the nitrogen pressure to a maximum of 30 psi, which will not allow a pressure increase in the system of higher than 100 Torr when the vacuum pump is running. The additional pressure regulator is represented in Figure 3-8.



**Figure 3-8** Additional pressure regulator installed on the nitrogen line.

A second backup safety feature to eliminate overpressure in the chambers was added by positioning the electromagnetic valve which isolates the etching chamber from the vacuum pump such way that the valve will open if the pressure is above 35 psi.

The last over-pressure safety feature is realized by the way the chamber door was designed. The chamber door is sealed with an o-ring; when the pressure inside the chamber is below atmospheric pressure, the door is pressed on the o-ring and a perfect sealing is done. However, when the chamber pressure reaches 15 psi, the door surface moves away from the o-ring acting as a relief valve.

All the hardware parts are supported by a custom made frame. The frame was designed by the author and fabricated by an external machine shop from 304 stainless steel rectangular tubes with a thickness of 0.065 inch.

### **3.3.2 Software subsystem**

To control the hardware subsystem, a control program was created using LabView®. Contrary to the usual programming languages, which use text based instructions, in LabView® the programmer uses icons arranged in a flowchart like manner. A LabView® program is called virtual instrument (VI) because of the resemblance of physical instruments such as oscilloscopes and gauges.

To ease the troubleshooting of the LabView® programs, when creating complex VIs, it is a good practice to group related controls and indicators into smaller VIs and place them in the desired VI as subVI.

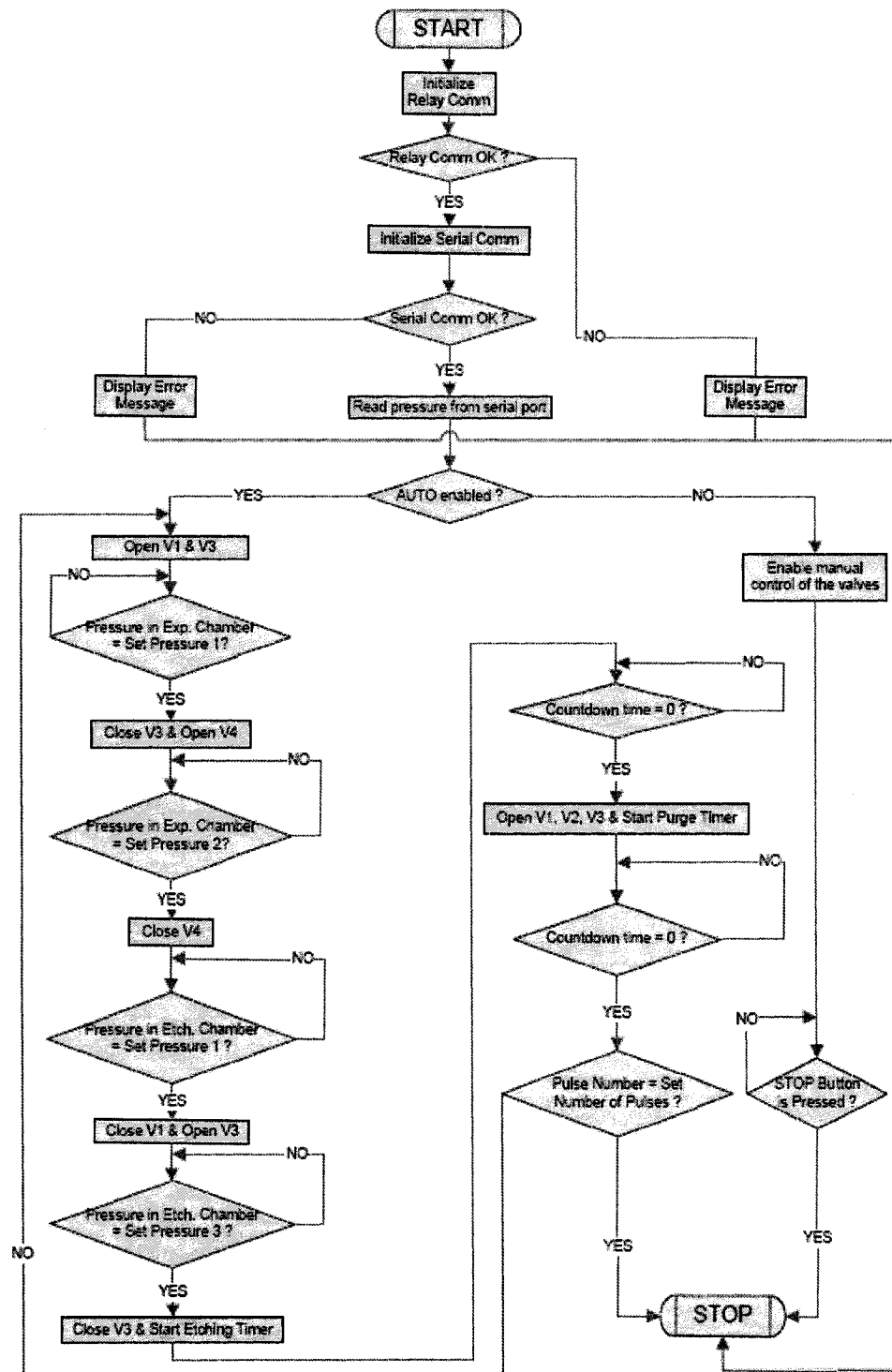
The LabView® VI has a user interface also referred to as front panel, where all the controls and indicators are placed, but the connection between them is done in another interface known as block diagram.

A complete library of controls and indicators is available for the programmer. LabView® controls are push buttons, dials and knobs; they simulate input devices and supply data to

the block diagram. The indicators, which simulate instrument output devices, are graphs, LEDs, and other displays [57].

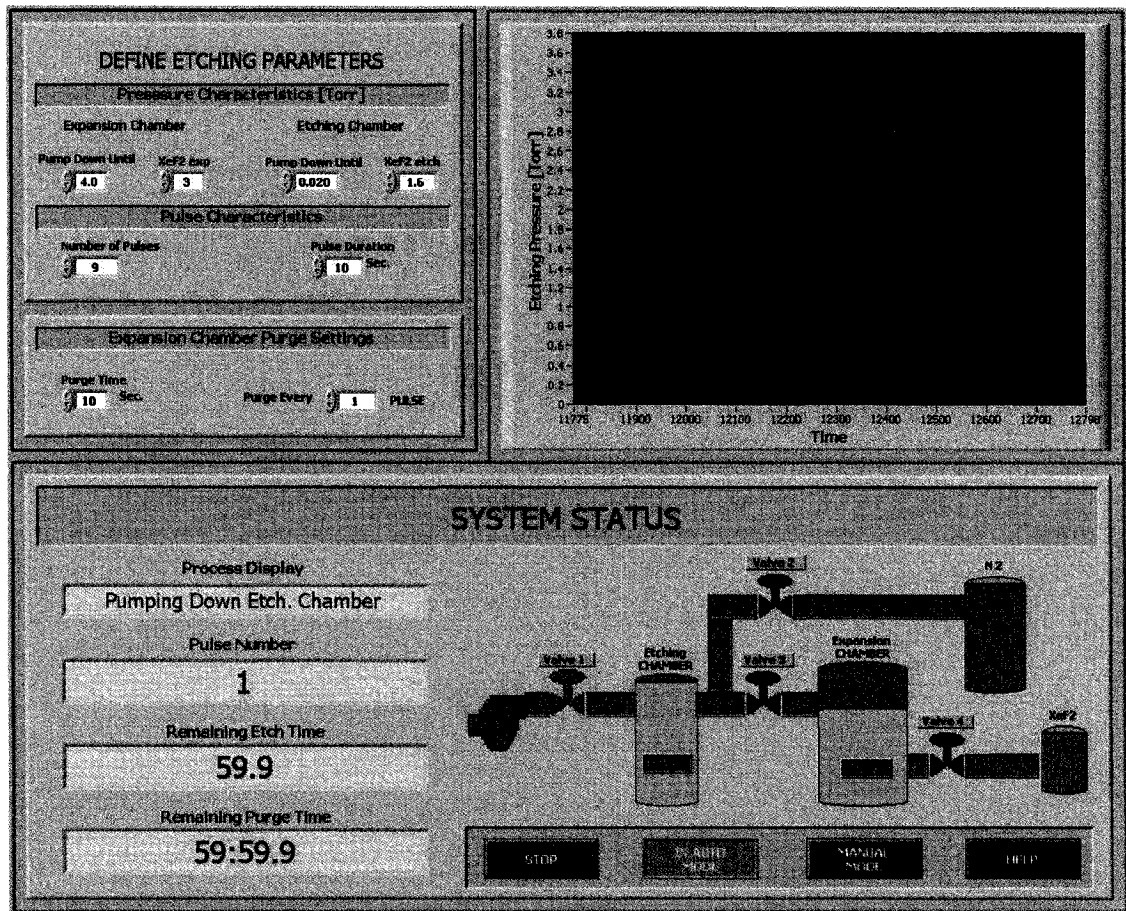
Feedback from the pressure sensing devices is used by LabView® to open and close the electromagnetic valves and to control the process flow. The pressure values are read from the serial port by a loop and passed out using local variables.

The LabView® energizes the valve solenoids by sending binary commands to the relay control board which connects or disconnects the power to the solenoids. A simplified flowchart diagram of the program that controls the etching process is pictured in Figure 3- 9.



**Figure 3-9** Flowchart of the LabView® code for an etching sequence where both etching and expansion chamber are purged with nitrogen.

The designed code has a very intuitive user interface from where the operator controls and fine-tunes the whole etching process. The front panel of the LabView<sup>®</sup> code is shown in Figure 3-10.



**Figure 3-10** Virtual Instrument's front panel.

The user interface is divided in three areas. The upper left side is the area where the user defines the etching parameters, as shown in Figure 3-11. There are three categories of parameters that can be adjusted: the pressure characteristics, the pulse characteristics, and purge characteristics.

## DEFINE ETCHING PARAMETERS

---

### Presssure Characteristics [Torr]

Expansion Chamber		Etching Chamber	
Pump Down Until	XeF <sub>2</sub> exp	Pump Down Until	XeF <sub>2</sub> etch
1.0	3	0.020	1.8

---

### Pulse Characteristics

Number of Pulses	Pulse Duration
25	60 Sec.

---

### Purge Settings

Purge Time	Purge Expansion Chamber Every
10 Sec.	1 PULSE

**Figure 3-11** Etching parameters front panel area.

The pressures at which both chambers are pumped down before and after filling with XeF<sub>2</sub> can be adjusted in the pressure characteristics area.

Number of pulses and pulse duration are adjusted in pulse characteristics zone while purge time and the purging frequency of the expansion chamber are set in the purge settings.

In the upper right area a graph displays in real time the pressure in the etching chamber.



The bottom half of the front panel shows system status. System status area of the front panel has three distinct zones. There is the process information area, which is functional only in the auto mode. In this area the process sequence, the pulse number, and time counters for etching pulse and purge sequence are displayed. It has to be noted that the nitrogen purge sequence is time based and not pressure based because of the impossibility of the pressure transducers to measure above 10 Torr.

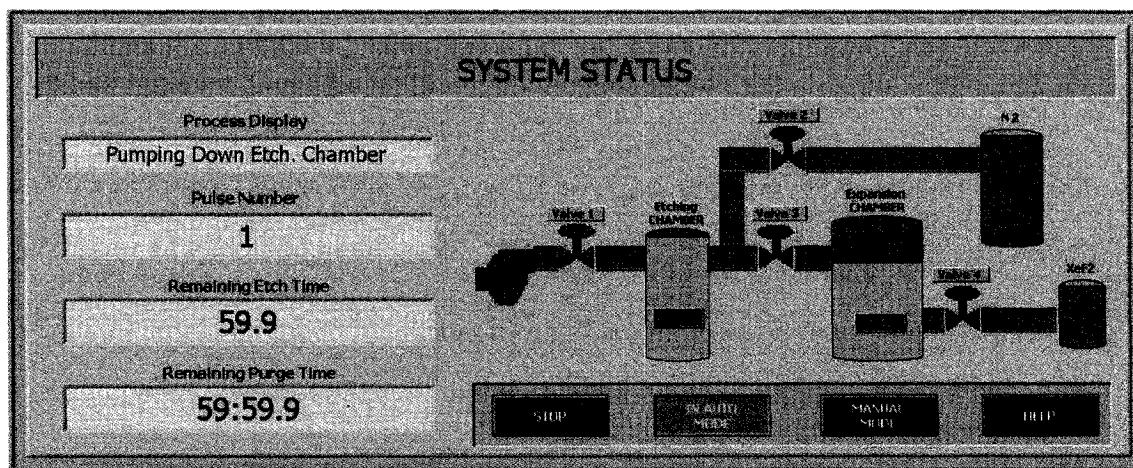
Another area is the process diagram that shows the state of the valves and indicates the pressure in both chambers.

In the bottom right are located the emergency stop, the auto and manual mode and the help buttons.

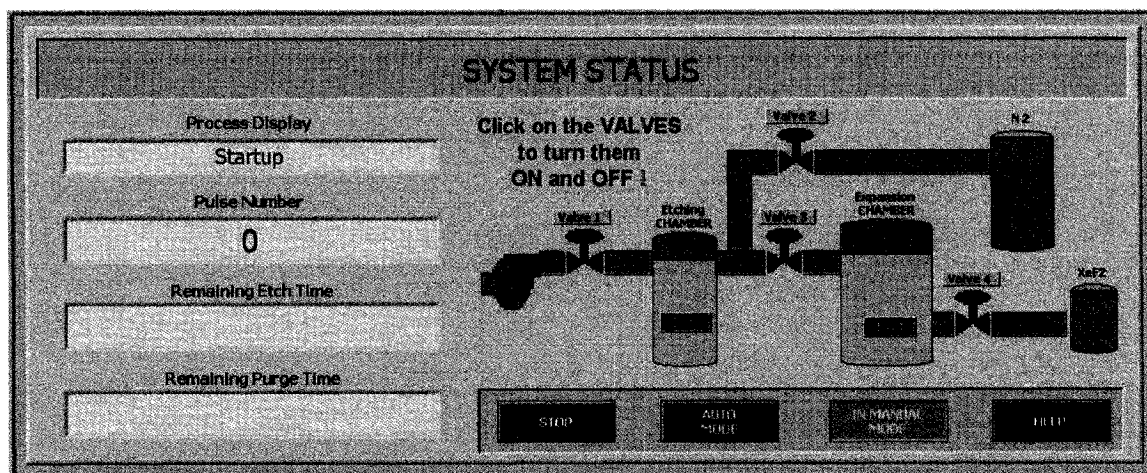
When first started, the VI runs in automatic mode in which it follows the process sequence based on the pressure variation inside chambers, the number and duration of etching pulses and the nitrogen purge settings.

In manual mode the valves icons from the process diagram function as on/off buttons, which open and close the valves. The only feedback that user gets in the manual mode is the pressure measurement inside chambers, the process sequence is established by the user and, in fact, the manual mode is used to charge the chambers with nitrogen after the etching is finished or if for some reasons the user wants to override the programmed sequence.

Figures 3-12 and 3-13 show for comparison the system status area of the front panel in both auto and manual mode. It can be seen that in the manual mode the user is alerted of the fact that the valves icons can be clicked on to open and close the valves.



**Figure 3-12** System status area in auto mode.



**Figure 3-13** System status area in manual mode; the valves icons act as on/off switches; when a valve icon is red filled, the solenoid is not energized (valve is closed); when the valve is green filled the valve is open.

## **CHAPTER 4**

# **MODELING OF XENON DIFLUORIDE ETCHING OF SILICON**

### **4.1 MOTIVATION**

The main issue associated with dry isotropic etching of silicon is related to the lack of predictive etching models, which under certain circumstances may be of fundamental importance to provide information about the etched and under-etched structures. For example, resonant structures built in microsystems technologies, may dramatically change their resonant frequency due to change in the boundary conditioning, which is likely to occur when under or over-etching conditions are attained.

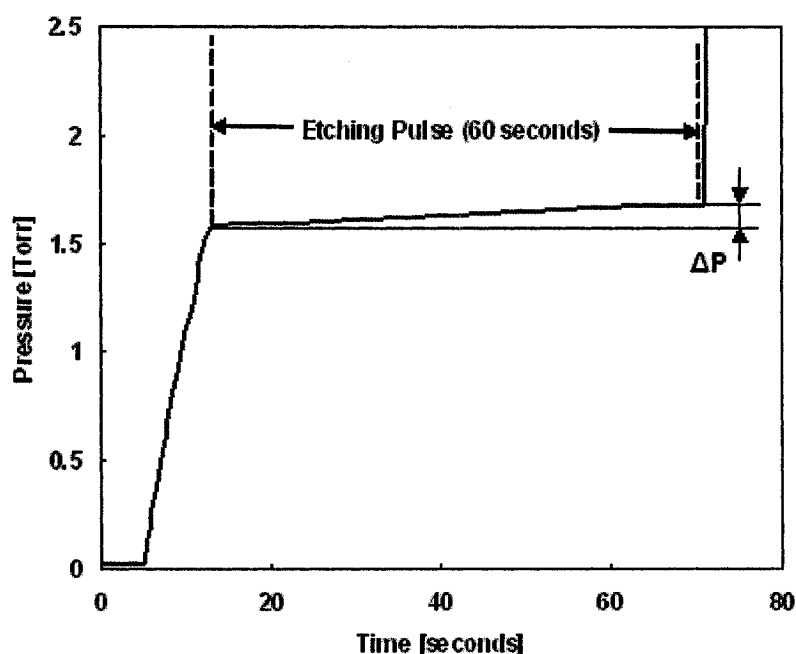
Chemical milling or etching is sensitive to process parameters, and they are very difficult to be included in an etching model. Reasonable isotropic etching models of the reaction process are used instead of robust models, because the robust models would impose strict process requirements to manufacturers.

While etching silicon with  $\text{XeF}_2$  using the first generation equipment [56], many situation had been encountered in which, because of the wide range of attainable etch rates, the silicon samples were over etched. To overcome this problem and help inexperienced users, an etching model capable of calculating the etch rate per pulse has been developed.

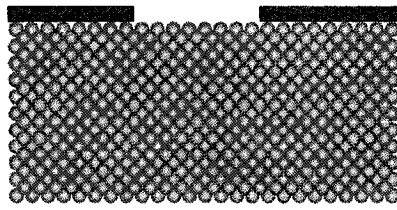
## 4.2 THE ETCHING MODEL

During the etching of silicon, there is a pressure increase in the etching chamber due to the formation of volatile products, as shown in Figure 4-1. Delta P, the difference between the pressure at the end of the etching cycle and the pressure at the beginning of the etching cycle, is the partial pressure of  $\text{SiF}_4$ ; (ie)  $\Delta P = P_{\text{SiF}_4}$  as shown in Figure 4-1.

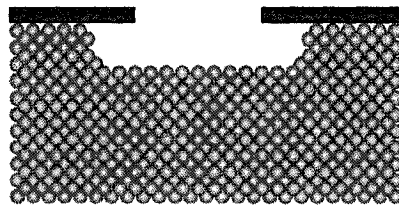
The developed etching model, based on the assumption that the etching proceeds through a sequential removal of the exposed silicon monolayers (Figure 4-2), calculates the etch depth, lateral etch, and generates a plot of the etch profile after each pulse, as a function of the pressure increase in the etching chamber and the exposed surface area of silicon.



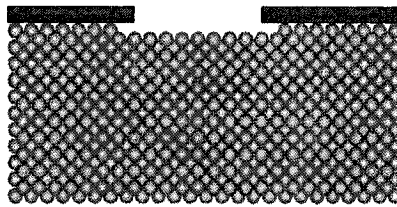
**Figure 4-1** Typical variation of pressure in the etching chamber during one pulse [60].



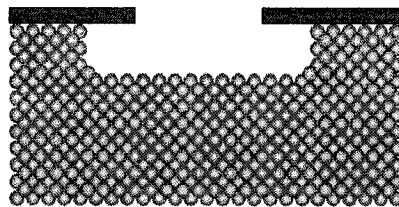
a) Initial substrate



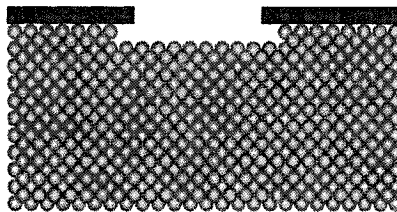
e) 4 ML removed



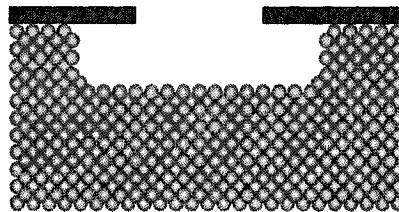
b) 1 ML removed



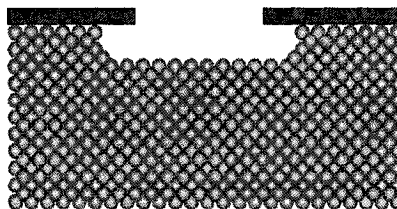
f) 5 ML removed



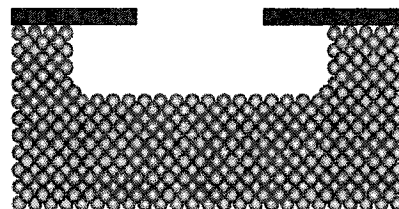
c) 2 ML removed



g) 6 ML removed



d) 3 ML removed



h) 7 ML removed

**Figure 4-2** Schematic of exposed silicon monolayers removal.

It is assumed that  $\text{XeF}_2$  etches silicon isotropically and the assumed chemical reaction at room temperature is the following:



Using the measured  $\text{SiF}_4$  partial pressure  $P_{\text{SiF}_4}$ , the number of  $\text{SiF}_4$  moles in the reaction chamber at the end of the pulse can be easily found as,

$$n_{\text{SiF}_4} = \frac{P_{\text{SiF}_4} \times V}{R \times T} \quad (4-2)$$

where  $P_{\text{SiF}_4}$  is expressed in atmospheres,  $V$  is the volume of the etching chamber in liters,  $R$  is the gas constant, and  $T$  is the temperature inside the etching chamber in K.

Multiplying the number of moles,  $n_{\text{SiF}_4}$ , with Avogadro's number  $N_a = 6.02205 \times 10^{23} \text{ atoms/mole}$ , one learns how many  $\text{SiF}_4$  molecules have desorbed during an etching pulse.

$$N_{\text{SiF}_4} = n_{\text{SiF}_4} \times N_a \quad (4-3)$$

Knowing the atoms surface density for Si(100) surfaces ( $6.86 \times 10^{14} \text{ atoms/cm}^2$ ), the number of Si atoms removed, and area of the exposed silicon surface, the etch rate per

pulse can be calculated. The diamond-like lattice of Si has the interplanar spacing in (100) direction:

$$d_{(100)} = \frac{a}{4} = \frac{5.43}{4} = 1.35 \text{ \AA} \quad (4-4)$$

#### 4.2.1 Etching model for square opening mask

For a square opening (Figure 4-3), the exposed silicon area in  $\mu\text{m}^2$  can be expressed in the following form, after one monolayer of silicon has been removed:

$$A_{(1)} = A_{(0)} + 4 \times \sqrt{A_{(0)}} \times (1.35 \times 10^{-4}) + \pi \times (1.35 \times 10^{-4})^2 \quad (4-5)$$

where,  $A_{(0)}$  is the initial exposed area in  $\mu\text{m}^2$ .

After 2 monolayers have been removed, the exposed silicon area has the following form:

$$A_{(2)} = A_{(1)} + 4 \times \sqrt{A_{(0)}} \times (1.35 \times 10^{-4}) + \pi \times [(2 \times 1.35 \times 10^{-4})^2 - (1.35 \times 10^{-4})^2] \quad (4-6)$$

If the thickness of one monolayer and the silicon surface density for (100) surfaces  $ML(100)$  are defined as in the equations (4-7) and (4-8) respectively:

$$t_{ML} = 1.35 \times 10^{-4} [\mu m] \quad (4-7)$$

$$ML(100) = 6.86 \times 10^6 \text{ atoms} / \mu m^2 \quad (4-8)$$

Then, if  $N_{SiF_4}^r \geq A_{(n-1)} \times ML(100)$ , the area after  $n$  monolayers have been removed is:

$$A_{(n)} = A_{(n-1)} + S + \pi \times [t_{ML}^2 \times (2n-1)] \quad (4-9)$$

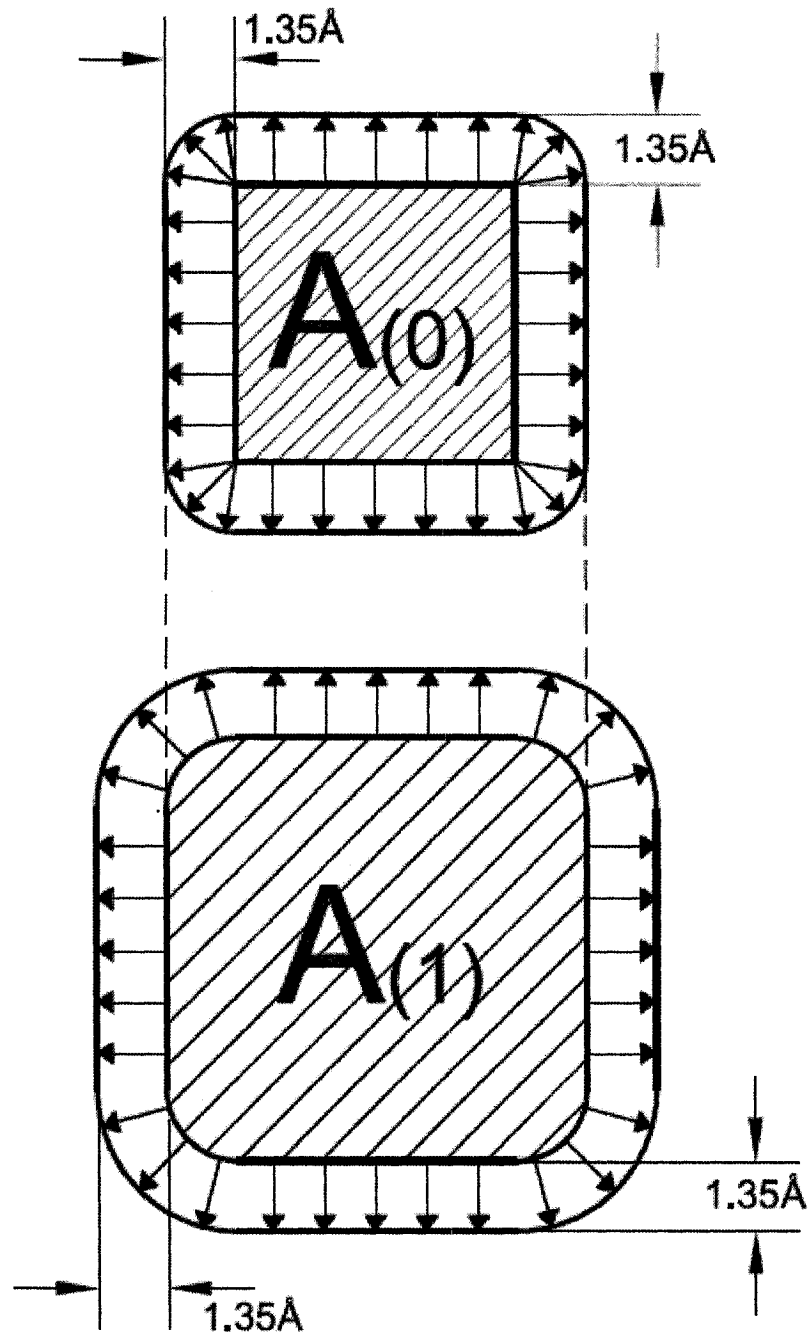
Where, the number of remaining  $SiF_4$  molecules in the etching chamber is:

$$N_{SiF_4}^r = N_{SiF_4} - \sum_{n=1} [A_{(n)} \times ML(100)] \quad (4-10)$$

and,

$$S = 4 \times \sqrt{A_{(0)}} \times t_{ML} \quad (4-11)$$





**Figure 4-3** Schematic of the initial exposed area  $A_{(0)}$  and  $A_{(1)}$  - after one removed ML for a square opening.

Etch depth ( $\mu\text{m}$ ) is given by the following equation:

$$ED = n \times t_{ML} \quad (4-12)$$

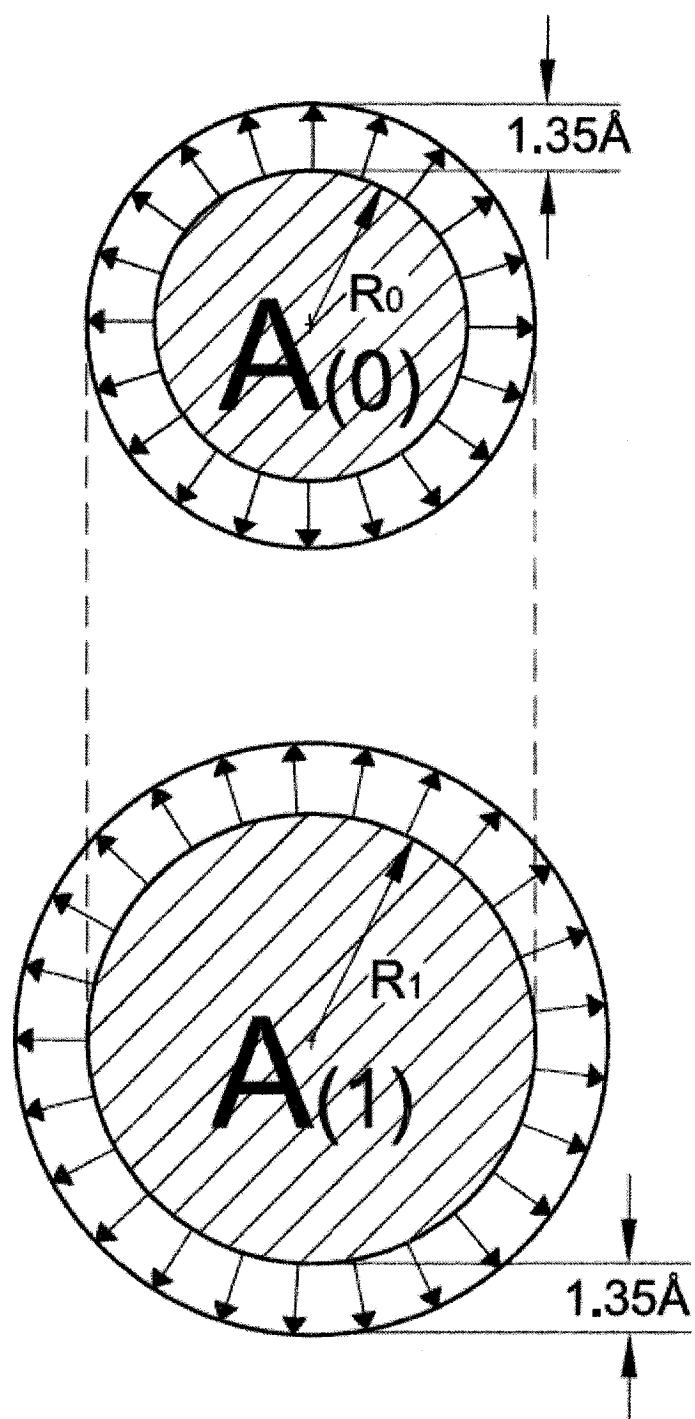
Some of the available F atoms do not have the chance to react with Si and will be released with the  $\text{N}_2$  flush from the chamber.

#### 4.2.2 Circular opening mask model

For a circular opening mask, shown in Figure 4-4, the area after n monolayers removed is:

$$A_{(n)} = \pi \times [R_0 + n \times t_{ML}]^2 \quad (4-13)$$

Where,  $R_0$  is the radius of the patterned circular opening. Etch depth (ED) is calculated with the same equation (4-12) as for the square opening mask.



**Figure 4-4** Circular opening schematic of the initial exposed area  $A_{(0)}$  and  $A_{(1)}$  - after one removed ML.

## **CHAPTER 5**

### **VALIDATION OF THE PROPOSED ETCHING MODEL**

#### **5.1 EXPERIMENTAL PROCEDURE**

##### **5.1.1 Equipment Description**

Piping and instrumentation diagrams of the  $\text{XeF}_2$  setup used in the experiments are shown in Figure 3-1. The etching apparatus is comprised of a vacuum pump, an etching chamber, an expansion chamber, a  $\text{XeF}_2$  source chamber, pressure measurement devices and a nitrogen purging system.

The etching is done in 60 second pulses. A typical etching pulse has the following sequence: (1) valves 2 and 4 are closed, valves 1 and 3 are opened; (2) etching and expansion chambers are pumped down until the pressure in the expansion chamber reaches 1 Torr and valve 3 is closed; (3) etching chamber is pumped down until it reaches 20 mTorr and valve 1 is closed; (4) valve 4 opens and  $\text{XeF}_2$  sublimate in the expansion chamber until pressure reaches 3 Torr and valve 3 opens and 4 closes; (5) the  $\text{XeF}_2$  flows into etching chamber until pressure reaches 1.5 Torr, moment in which valve 3 closes and the etching pulse begins; at the end of the 60 seconds, valve 2 opens and the etching chamber is filled with nitrogen until it reaches about 5 psi when valve 1 opens and the etching chamber is pumped down until it reaches 20 mTorr and valve 1 is closed; (6) the

expansion chamber is filled with xenon difluoride by opening valve 4 until it reaches 3 Torr, valve 4 is closed and valve 3 is opened. Steps (5) and (6) are repeated for as many pulses as the operator desires. It has to be noted that the expansion chamber is only pumped down once during an experiment and, because of the volume ratio of the two chambers, step (6) can be done only once for two etching pulses. When the total number of pulses has been reached, both chambers are purged with nitrogen before the silicon chips are removed. Also, when not in use, the system is pressurized with nitrogen at 5 psi for safety reasons and to avoid humidity in the chamber.

### **5.1.2 Sample Preparation**

All the samples were *p*-type (100) silicon wafers. The edges and the back of the specimens were covered with photoresist and baked for 15 minutes at 120°C to prevent etching. To remove the native oxide from the exposed areas, the samples were dipped into BOE (Buffered Oxide Etch) solution containing HF and ammonium fluoride in a 1:4 ratio for 10 seconds. Also, to prevent formation of a silicon polymer layer on top of the substrate surface which can slow the etching [58], the samples were dehydrated at 120°C for 5 minutes.

To validate the etching model proposed in previous chapter, samples with square and circular opening were etched in the designed apparatus.

## **5.2 VALIDATION FOR SQUARE OPENING**

### **5.2.1 Experimental results**

The first experiment was carried on the sample shown in Figure 5-1, which had a 2500  $\mu\text{m}$  X 2500  $\mu\text{m}$  square opening patterned on top of the silicon and was etched for 25 pulses of 60 seconds each.

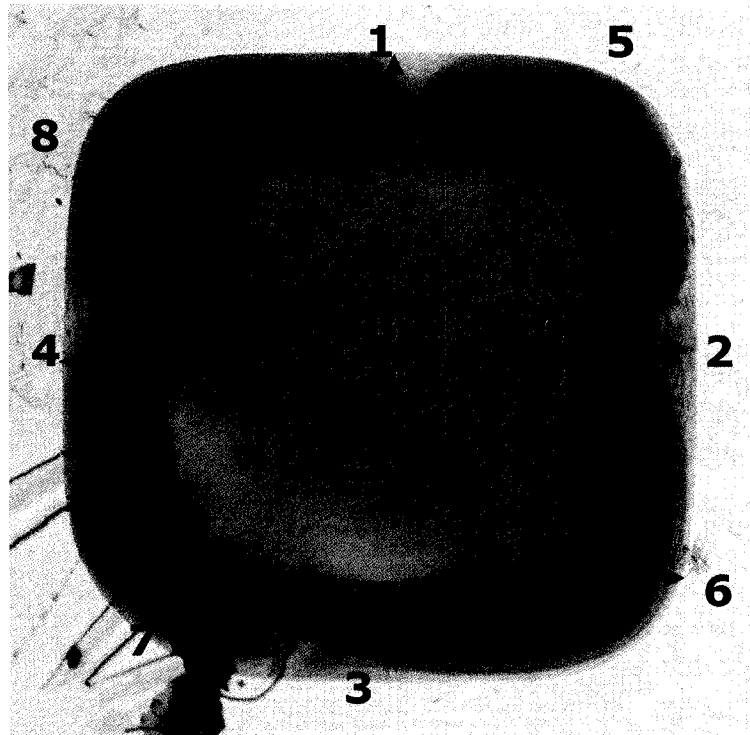
The back and edges of the sample were covered in photoresist to prevent etching. The sample was etched continuously for 5 pulses and then the etch depth was measured using an Olympus BX60M microscope, focusing first on the mask and then on the bottom. After the etch depth was measured, in at least 3 different places, the sample was again placed in the reactor for another set of 5 pulses and then the etch depth was measured.

The lateral etch was measured in eight points from the pictures taken with a Nikon camera attached to the microscope. In Figure 5-2 the location of the lateral etch measurement points is shown. The dark shaded area represents the lateral etch area and the orange colored area from the center of the picture is the photoresist (which can be seen after a through hole was etched in the chip) applied to protect the backside of the silicon from contact with xenon difluoride.



**Figure 5-1** Silicon sample with a 2.5mm X 2.5 mm square mask opening used to validate the theoretical model for square window openings.

The etch depth and lateral etch depth measurements values are tabulated in Table 5-1 and Table 5-2 respectively.



**Figure 5-2** Location of the etch measurement points for the square opening. For each side of the square opening, measurements were taken at the maximum and minimum points. (1-8 refer to lateral etch; A-C refer to etch depth)

**Table 5-1** Etch depth measurements after five consecutive etch pulses for square mask opening sample.

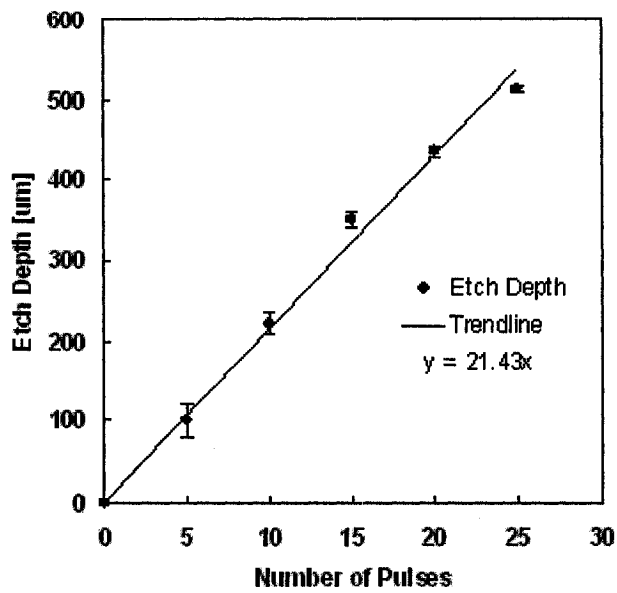
Pulse Number	Etch Depth [ $\mu\text{m}$ ] measured at point			Average Etch Depth [ $\mu\text{m}$ ]	Standard Deviation [ $\mu\text{m}$ ]
	A	B	C		
5	80	100	120	100	20
10	225	205	235	222	15
15	350	340	360	350	10
20	435	440	430	435	5
25	510	510	515	512	3



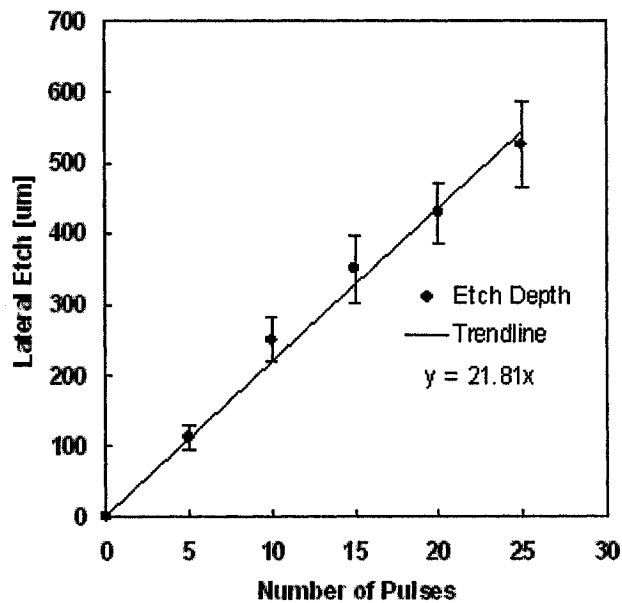
**Table 5-2** Lateral etch measurements values for square mask opening experiment, approximated from photographs taken after sets of five consecutive pulses.

Pulse Number	Lateral Etch [ $\mu\text{m}$ ] measured at point								Average Lateral Etch [ $\mu\text{m}$ ]	Standard Deviation [ $\mu\text{m}$ ]
	1	2	3	4	5	6	7	8		
5	111	83	125	139	111	97	111	111	111	17
10	277	277	263	277	222	194	222	249	248	32
15	402	402	374	402	305	305	305	305	350	49
20	471	471	457	471	388	388	388	388	428	43
25	582	582	554	609	471	471	471	471	526	61

Figures 5-3 and 5-4 represent plots of the etch depth (ED) and lateral etch (L) for the square opening. On the ED versus number of pulses graph (Figure 5-3), the value of the last measurement is not plotted, as the abscissa is not exactly known. It is believed that the silicon sample was completely etched through around pulse 23 because the thickness of the silicon sample was about 500  $\mu\text{m}$ . Both graphs have a linear increase characteristic which was previously reported [59]. As it can be seen from comparing the ED and L values, during the first ten pulses the lateral etch shows higher etch rate than the etch depth and this could be explained by very high surface roughness and limited number of etch depth measurements. Another factor that could explain the increased lateral etch over the etch depth could be the fact that around the edges of the mask opening there is a zone of increased reaction probability due to xenon difluoride molecules that might be trapped under the overhanging hard mask.



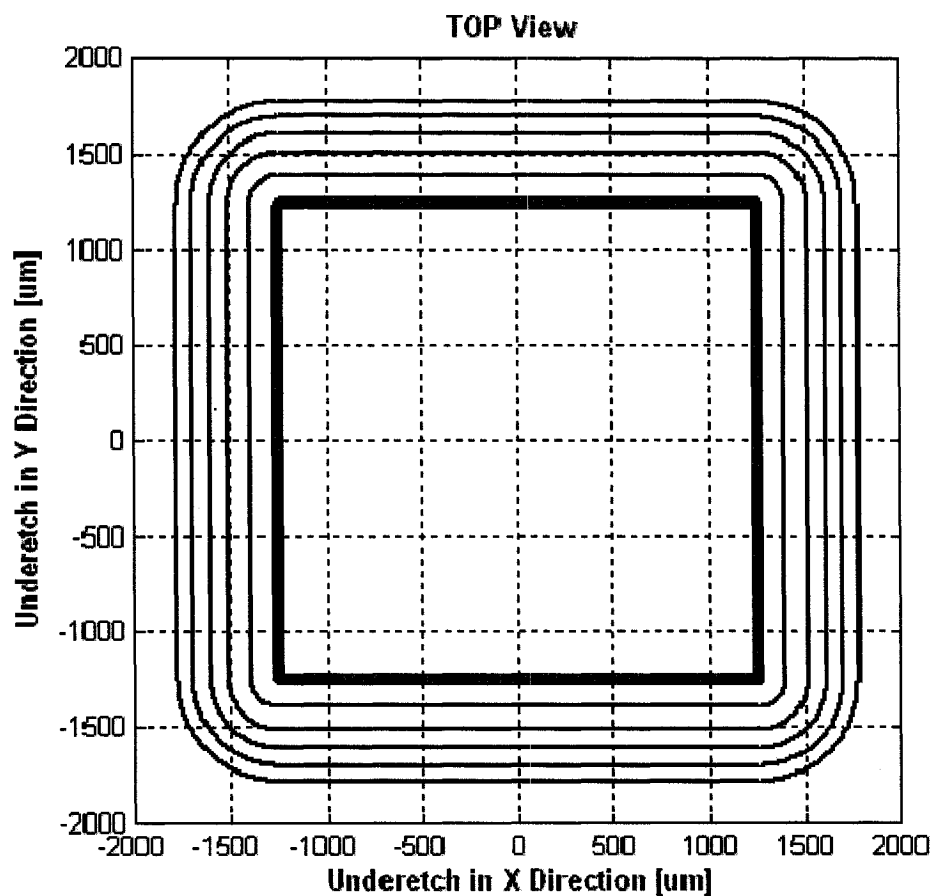
**Figure 5-3** Evolution of ED in microns during  $\text{XeF}_2$  etching of a  $2500\ \mu\text{m} \times 2500\ \mu\text{m}$  for 25 pulses; the error bars represent  $\pm 1$  standard deviation.



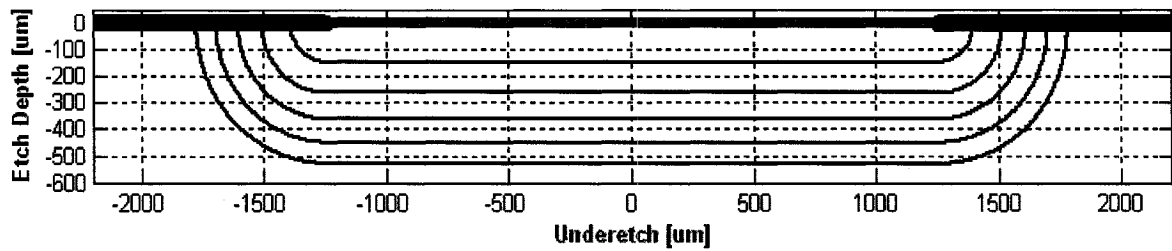
**Figure 5-4** Measured lateral etch, of the etched square mask opening, using photos taken with a Nikon camera attached to the microscope ; the error bars represent  $\pm 1$  standard deviation.

### 5.2.2 Theoretical results

The etching chamber pressure readings, during experiments, were saved to a text file, and then “plugged” into a Matlab<sup>®</sup> script developed based on the proposed etching model. The script calculates the etch depth, lateral etch and it is also capable of generating contour plots, shown in Figures 5-5 and 5-6, of the etched sample based on the pressure increase during etching pulse, size and shape of the exposed silicon area.



**Figure 5-5** Matlab<sup>®</sup> contour plot representing the top view of a 2.5mm X 2.5 mm square opening; the blue contour lines represent the etched area after 5, 10, 15, 20 and 25 pulses.



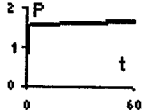
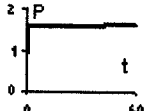
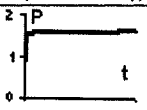
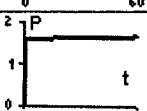
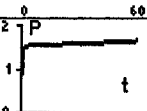
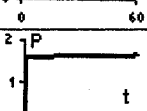
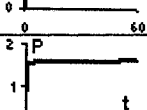
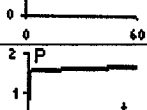
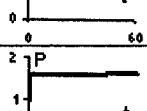
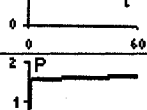
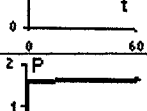
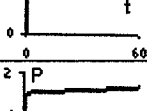
**Figure 5-6** Contour plot representing a cross-section through the middle of the square opening shown in previous figure.

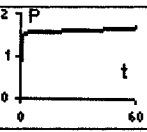
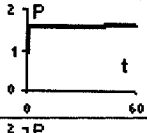
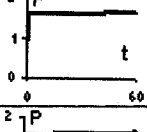
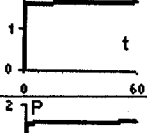
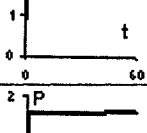
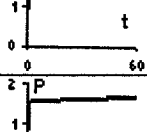
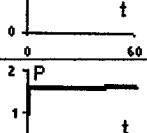
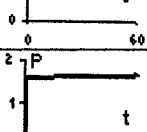
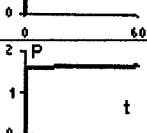
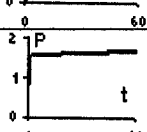
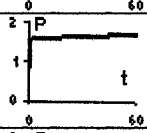
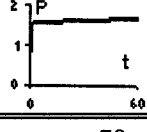
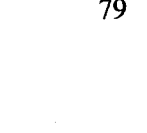
### 5.2.3 Validation of theoretical results

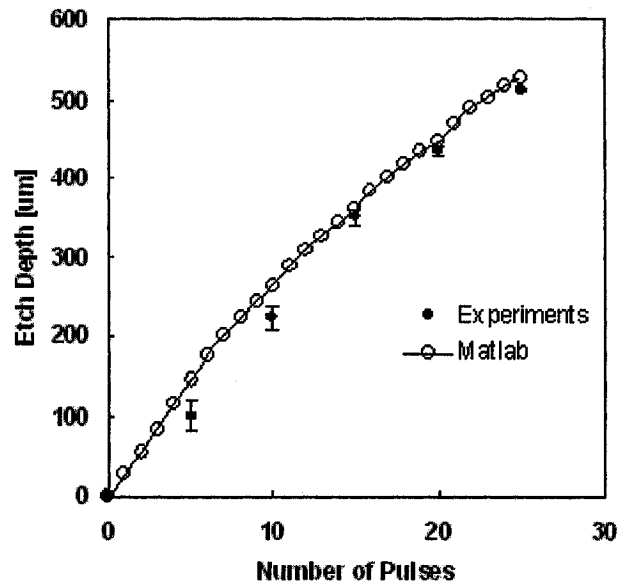
The experimental results are compared with the Matlab<sup>®</sup> results in Figures 5-7 and 5-8 for both ED and L. The slight differences for etch depth between the proposed model and experimental results are due to the high variation of etched surface roughness, relatively large exposed silicon area and, significant changes of experimental etching conditions such as humidity, temperature gradients or onset growth of an oxide layer when the sample was removed from the etching chamber for measurements. In Figure 5-8 it can be seen that for lateral etch the model predicts almost perfectly the experimental results.

In Table 5-3 both the experimental results are shown for the square opening sample. Pressure data columns contain the values of the pressure in the etching chamber.  $P_{\text{initial}}$  and  $P_{\text{final}}$  are the pressure at the beginning and at the end of the etching pulse, and the  $\Delta P = P_{\text{initial}} - P_{\text{final}}$  are the pressure values used to calculate the theoretical etch depth and lateral etch.

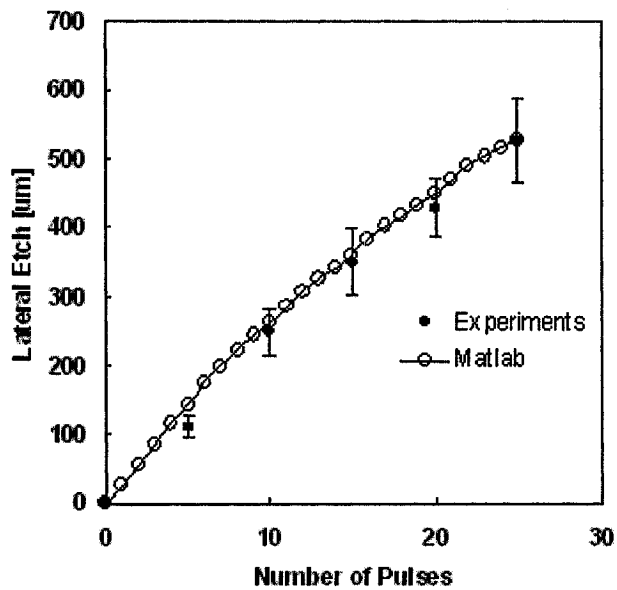
**Table 5-3** Experimental and theoretical results for a square opening etched for 25 pulses.

Pulse #	Pressure Data [Torr]			Etch Pressure Graph	Average Etch Depth [ $\mu\text{m}$ ]	Matlab Etch Depth [ $\mu\text{m}$ ]	Average Lateral Etch [ $\mu\text{m}$ ]	Matlab Lateral Etch [ $\mu\text{m}$ ]
	P <sub>initial</sub>	P <sub>final</sub>	$\Delta P$					
1	1.516	1.685	0.169			27		27
2	1.553	1.651	0.098			54		54
3	1.534	1.650	0.116			84		84
4	1.518	1.643	0.125			115		115
5	1.514	1.703	0.189		100	144	111	144
6	1.561	1.697	0.136			175		175
7	1.641	1.755	0.114			200		200
8	1.592	1.755	0.163			223		223
9	1.554	1.651	0.097			243		243
10	1.500	1.655	0.155		222	262	248	262
11	1.571	1.698	0.127			287		287
12	1.517	1.699	0.182			307		307

Pulse #	Pressure Data [Torr]			Etch Pressure Graph	Average ED [ $\mu\text{m}$ ]	Matlab ED [ $\mu\text{m}$ ]	Average L [ $\mu\text{m}$ ]	Matlab L [ $\mu\text{m}$ ]
	P <sub>initial</sub>	P <sub>final</sub>	$\Delta P$					
13	1.528	1.707	0.179			325		325
14	1.559	1.653	0.094			342		342
15	1.522	1.612	0.090		350	359	350	359
16	1.563	1.696	0.133			382		382
17	1.583	1.686	0.103			400		400
18	1.506	1.603	0.097			417		417
19	1.589	1.745	0.156			433		433
20	1.592	1.682	0.090		435	448	428	448
21	1.558	1.688	0.130			469		469
22	1.557	1.678	0.121			489		489
23	1.519	1.673	0.154			503		503
24	1.501	1.658	0.157			516		516
25	1.536	1.682	0.146		512	528	526	528



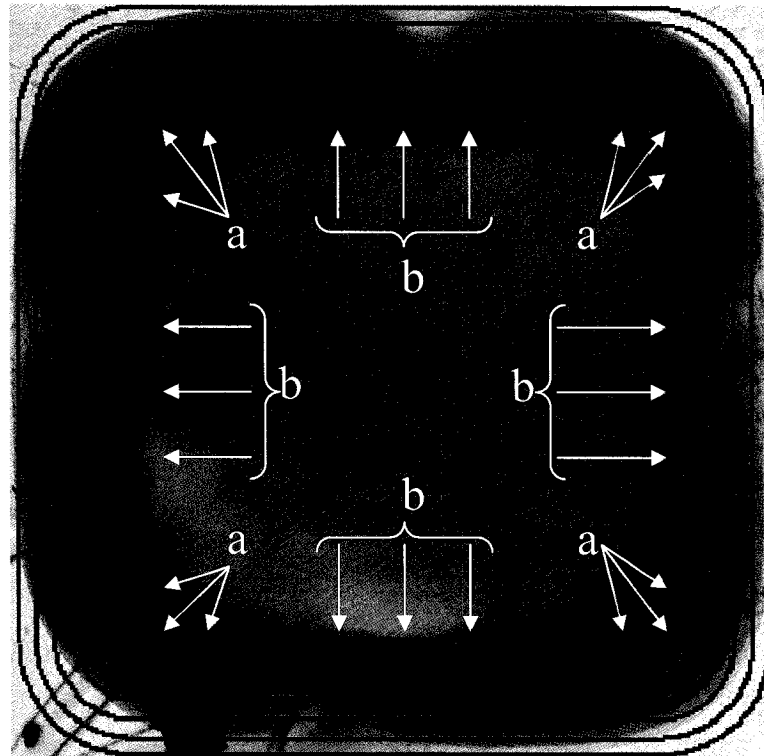
**Figure 5-7** Comparison between measured and theoretical ED values for square opening; the error bars represent  $\pm 1$  standard deviation.



**Figure 5-8** Comparison between measured and theoretical lateral etch for square opening; the error bars represent  $\pm 1$  standard deviation.

#### 5.2.4 Corner selectivity

In Figure 5-9 the theoretical top contour plot is compared with a top picture of the etched silicon chip. Areas of convex etch rate (b) are very well predicted by the model but there is a difference between the model and the experimental results for the concave etch rate areas (a). The experiments show that the convex zones have a higher average etch rate than the concave ones, a phenomenon previously reported for isotropic etching of silicon with XeF<sub>2</sub> [56].



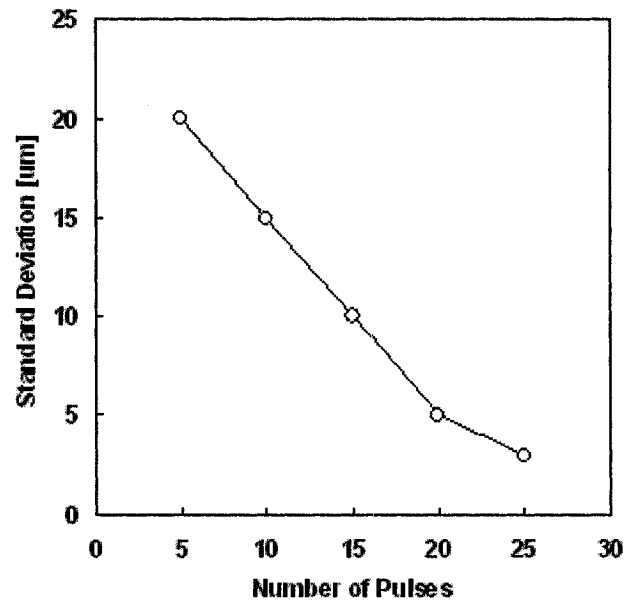
**Figure 5-9** Comparison between measured and theoretical lateral etch. The picture in the background is a top view of the etched silicon chip after exposure to silicon for 25 pulses.

The contour lines on top of the picture represent the plot generated by the theoretical model; **a** - concave etch fronts, **b** – convex etch fronts.

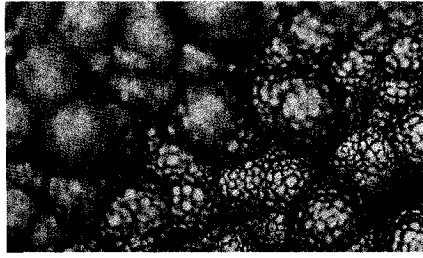


### 5.2.5 Etched surface roughness

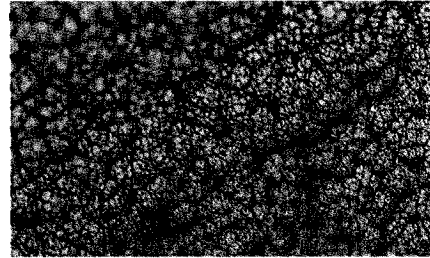
As it can be seen in Figure 5-10, the standard deviation values of the etch depth measurement decreases as the xenon difluoride etches deeper into the silicon. One conclusion that can be drawn from these observations is that the surface roughness actually improves with the increase in the number of pulses. In Figure 5-11, pictures of the etched surface, taken after each set of 5 etching and magnified 500 times, are shown and they support the previous conclusion.



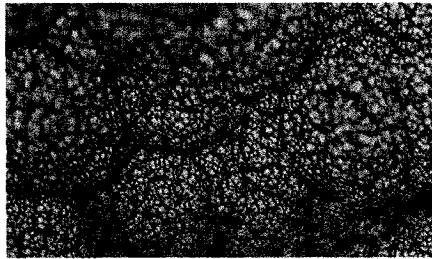
**Figure 5-10** Evolution of the calculated standard deviation of etch depth measurement readings.



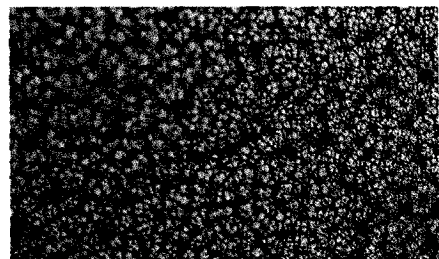
*a) Etched surface after 5 pulses*



*c) Etched surface after 15 pulses*



*b) Etched surface after 10 pulses*



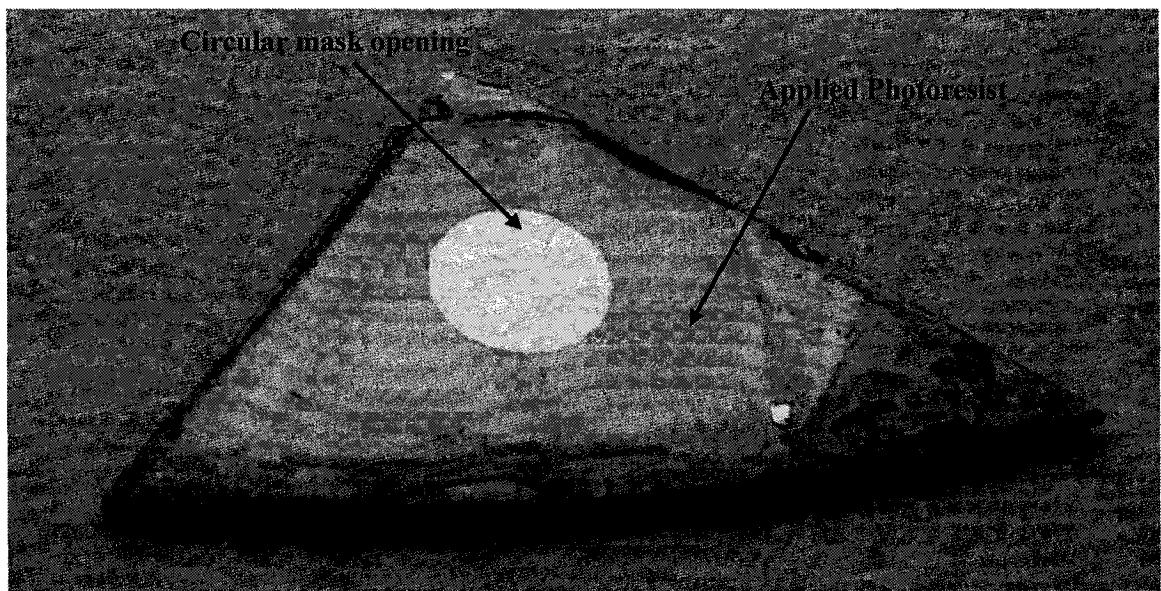
*d) Etched surface after 20 pulses*

**Figure 5-11** Pictures of etched surface (X500).

## 5.3 VALIDATION FOR CIRCULAR OPENING

### 5.3.1 Experimental results

The second set of experiments, similar with the previous ones, were carried on a silicon chip, with a 5000  $\mu\text{m}$  diameter circular opening on the photoresist mask , as shown in Figure 5-12. The sample was etched for a total of 25 pulses of 60 seconds each and the etch depth was measured at three points after each set of 5 pulses.



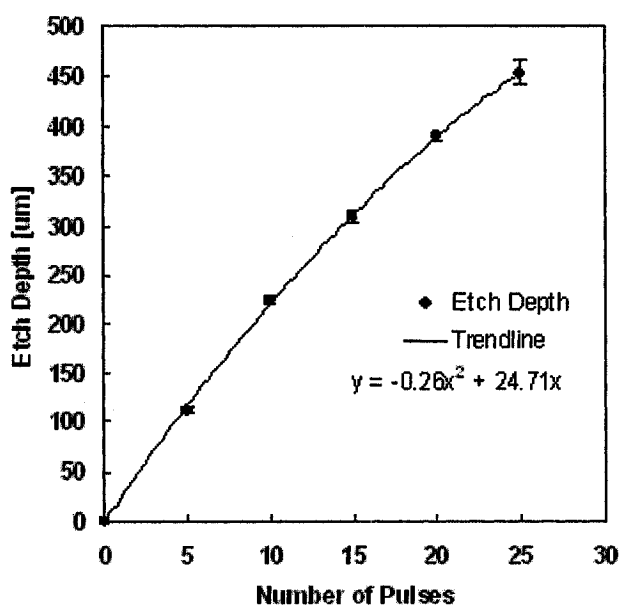
**Figure 5-12** 5000  $\mu\text{m}$  diameter circular mask opening sample used to validate the developed model.

The etch depth results, tabulated in Table 5-4, were measured at three points across the bottom of the etched surface. Because of very high etch area, it was impossible to focus

the whole opening under the microscope and thus lateral etch measurements were not taken.

**Table 5-4** Experimental etch depth results obtained for a circular mask opening.

Pulse Number	Etch Depth [ $\mu\text{m}$ ] measured at point			Average Depth [ $\mu\text{m}$ ]	Standard Deviation [ $\mu\text{m}$ ]
	A	B	C		
5	115	110	110	112	3
10	225	220	230	225	5
15	310	315	305	310	5
20	385	390	394	390	5
25	440	460	460	453	12



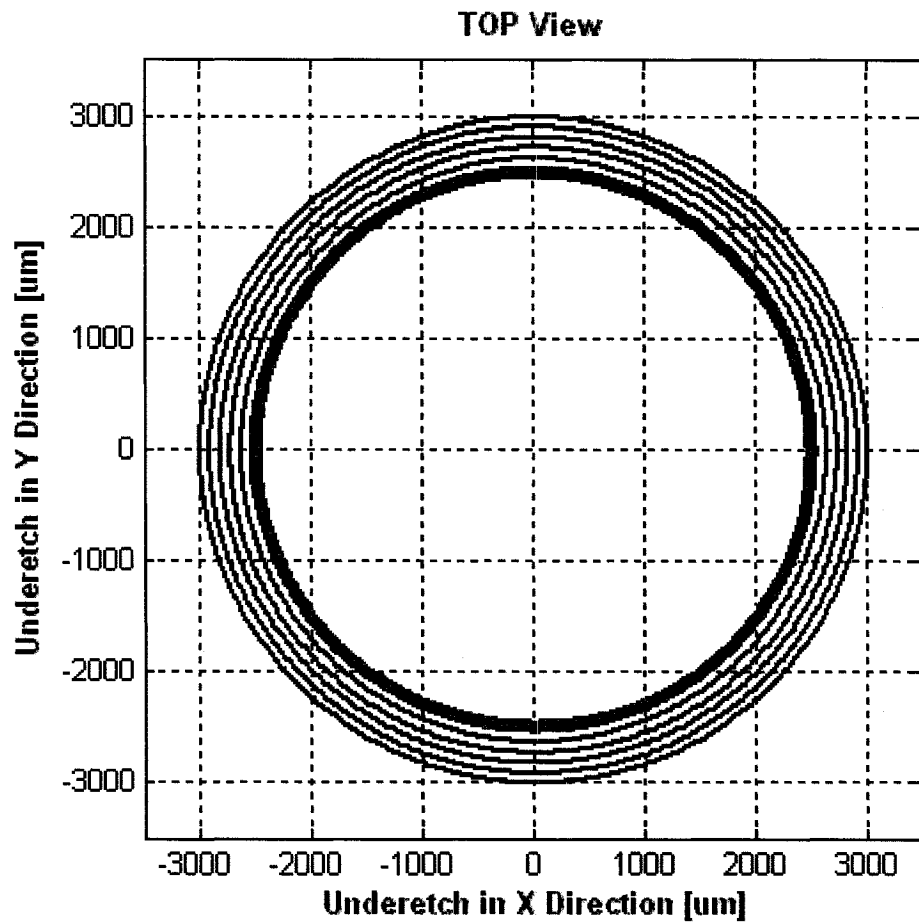
**Figure 5-13** Plot of etched depth measurements for circular opening; the error bars represent  $\pm 1$  standard deviation.

The progress of etch depth is plotted in Figure 5-13 and is very well approximated by a quadratic equation. The decrease in the silicon etch rate with the increase in the number of pulses is probably because of the increase in the exposed silicon area while the available xenon difluoride remains practically the same for each etch pulse. However, this etch rate trend is also closely correlated with the volume of the etching chamber and  $\text{XeF}_2$  partial pressure at the beginning of the etch pulse.

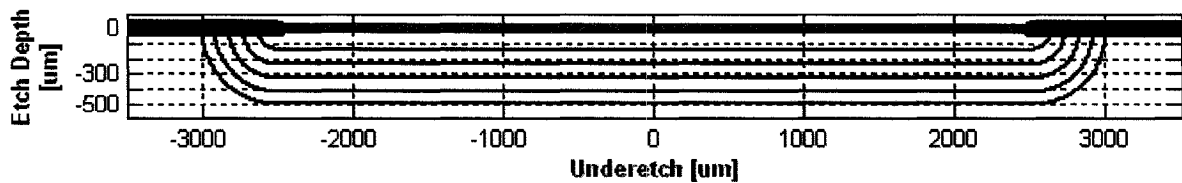
### 5.3.2 Theoretical results

The experimental etch parameters, such as, the pressure difference between the starting etch pressure and final etch pressure for each pulse, etch temperature, initial mask opening shape and area, were used in the Matlab<sup>®</sup> code to predict the etch depth, lateral etch and generate the contour plots of the etched sample.

The contour plots showing the etched area evolution with the etched time are shown in the next two figures. Figure 5-14 represents the top view of the circular etched area. The red colored circle and the blue circles represent the lateral etch after 5, 10, 15, 20, and 25 pulses represent the initial exposed silicon. In Figure 5-15 which is a center cross section, the thick blue lines represents the photoresist mask, the redline is the initial size of the developed pattern, and the thin blue lines represent the etch fronts corresponding to the blue lines shown in the top view.



**Figure 5-14** Top view of theoretical contour plots generated by Matlab® for a 5000  $\mu\text{m}$  circular opening using the Delta P values saved when etched the 5 mm diameter circular mask opening.

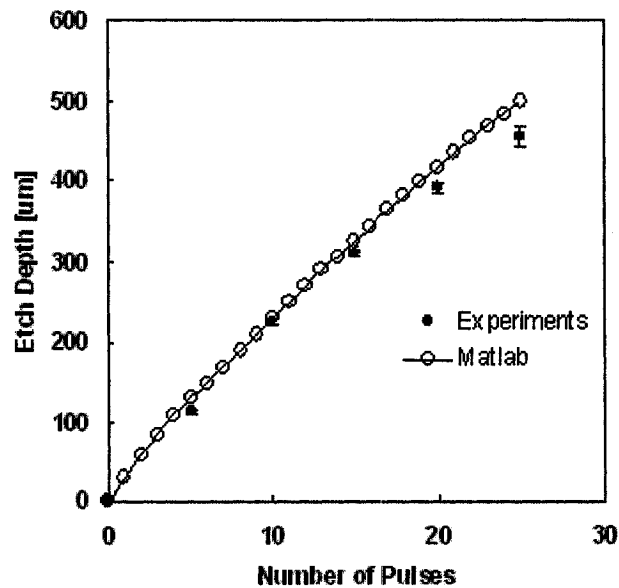


**Figure 5-15** Cross section view through the center of the top view; the figures have different scales.

### 5.3.3 Validation of theoretical results


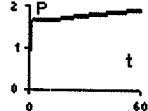
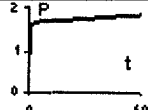
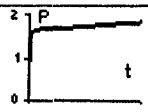
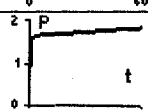
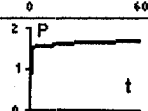
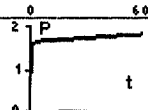
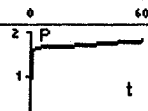
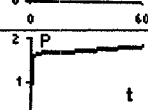
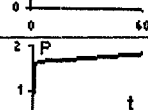
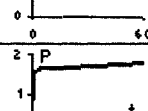
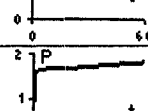
For the first 20 pulses there is a good agreement between the proposed etch model and the experimental results, however after pulse 20 there is a decrease in the slope of the measured etch depth. The difference could be due to a trenching phenomenon, where the etch depth at the center of the opening is slightly lower than the etch depth at the sides, observed after the 25<sup>th</sup> etch pulse. Trenching happens for large apertures, when there is sufficient lateral etch which subsequently trap the xenon difluoride molecules under the overhanging hard mask.

Experimental and Matlab<sup>®</sup> results are tabulated in Table 5-5, whereas the etch depths are compared in the graph pictured in Figure 5-16.

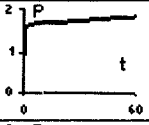
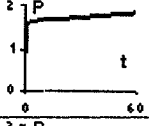
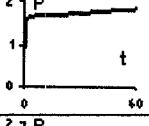
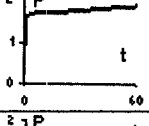
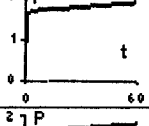
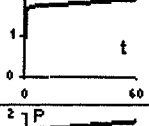
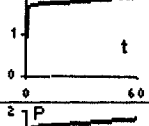
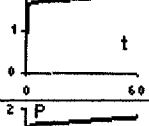
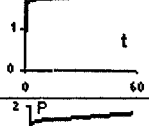
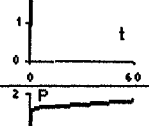
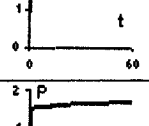
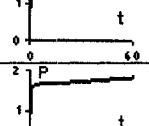
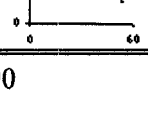


**Figure 5-16** Theoretical and experimental etch depth for a 5000  $\mu\text{m}$  diameter circular opening; the error bars represent  $\pm 1$  standard deviation.

**Table 5-5** Experimental and theoretical etching results for the circular opening.

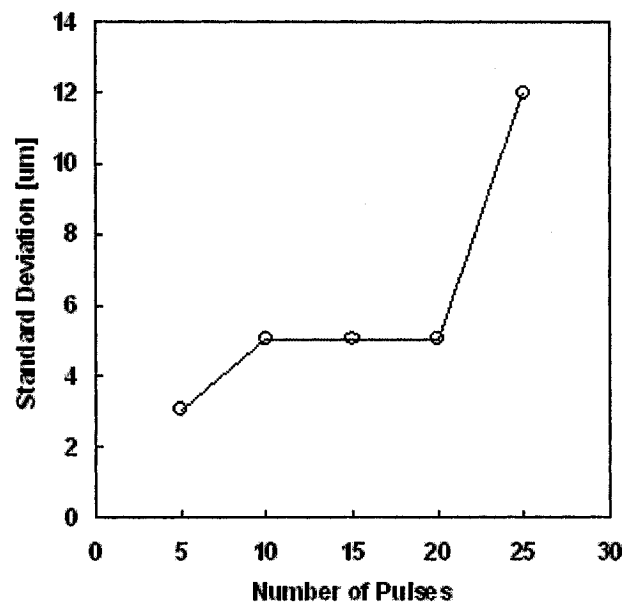
Pulse #	Pressure Data [Torr]			Etch Pressure Graph	Average Etch Depth [ $\mu\text{m}$ ]	Matlab Etch Depth [ $\mu\text{m}$ ]
	P <sub>initial</sub>	P <sub>final</sub>	$\Delta P$			
1	1.576	1.897	0.321			29
2	1.545	1.892	0.347			59
3	1.541	1.825	0.284			84
4	1.513	1.783	0.270			108
5	1.503	1.772	0.269		112	130
6	1.509	1.725	0.216			148
7	1.553	1.819	0.266			169
8	1.519	1.768	0.249			189
9	1.546	1.808	0.262			210
10	1.525	1.776	0.251		225	229
11	1.519	1.789	0.270			250
12	1.553	1.805	0.252			269



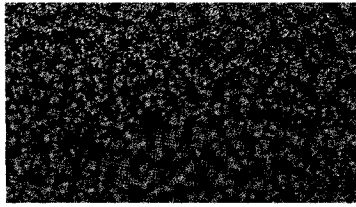
Pulse #	Pressure Data [Torr]			Etch Pressure Graph	Average ED [ $\mu\text{m}$ ]	Matlab ED [ $\mu\text{m}$ ]
	P <sub>initial</sub>	P <sub>final</sub>	$\Delta P$			
13	1.519	1.753	0.234			286
14	1.545	1.797	0.252			305
15	1.507	1.752	0.245		310	323
16	1.51	1.775	0.265			342
17	1.538	1.788	0.250			361
18	1.533	1.794	0.261			379
19	1.57	1.819	0.249			397
20	1.514	1.773	0.259		390	415
21	1.511	1.786	0.275			434
22	1.54	1.793	0.253			451
23	1.511	1.745	0.234			467
24	1.537	1.793	0.256			484
25	1.524	1.766	0.242		453	499

### 5.3.4 Surface roughness discussion

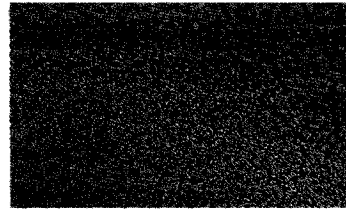
In contrast with the previous experiments carried on the square opening, the surface roughness tends to stay within the same range when the circular opening silicon chip was etched. This is also confirmed by the standard deviation values of etch depth measurements shown in Table 5-4, which are almost constant, and pictures of the etched surface taken through a microscope objective, shown in Figure 5-18. The high rise in the standard deviation for the last set of etch pulses is due to trenching phenomenon; the etch depth measured in the center of the surface is  $440\text{ }\mu\text{m}$  while on each sides of the center the etch depth values are  $460\text{ }\mu\text{m}$ .



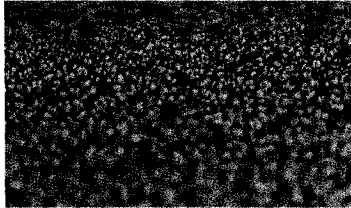
**Figure 5-17** Plot of etch depth standard deviation values for the circular opening. Note that the values are very close except the 25<sup>th</sup> pulse one which is attributed to the onset of trenching.



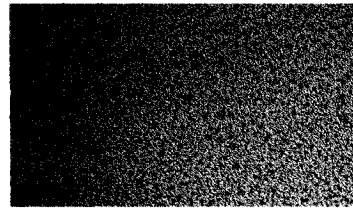
*a) Etched surface after 5 pulses*



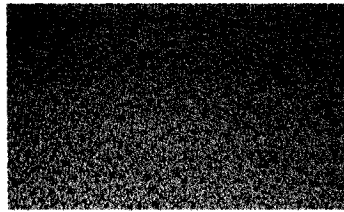
*c) Etched surface after 15 pulses*



*b) Etched surface after 10 pulses*



*d) Etched surface after 20 pulses*



*e) Etched surface after 25 pulses*

**Figure 5-18** Pictures of the circular mask opening etched surface (X500) after each set of five etching pulses.

## **CHAPTER 6**

### **CONCLUSIONS AND FUTURE WORK**

#### **6.1 CONCLUSIONS**

In the present work, reaction between  $\text{XeF}_2$  and silicon was investigated. Based on the theoretical and experimental knowledge acquired, a model for the reaction was developed and a Matlab<sup>®</sup> script to predict the etch depth, lateral etch and contour plots of the etched area was developed.

To verify the model a new experimental setup was designed and installed. To ease the etching process and eliminate the human error, a Labview<sup>®</sup> program, which controls the whole etching process, was created. The control program is very versatile; all the etching parameters can be changed and, it can be run in automatic as well as in manual mode.

The proposed model is simple and robust and it is capable of predicting the etch rate, etch depth and material removal rate with reasonable accuracy. More experimental investigations and optimization are required to fully characterize the influences of the geometry of the hard mask, the influence of the impurities in the Si substrate, temperature and humidity.

## **6.2 FUTURE WORK**

Future work recommendations can be divided in two categories: design related and model related.

### **6.2.1 Design related future work**

The design related type of recommendations refers to fitting new devices in the existing setup to allow further investigation of the reaction between xenon difluoride and silicon, such as:

1. Heating and cooling the sample;
2. Rotating and tilting the sample;
3. Bending the silicon sample;

Also, replacing the capacitance manometers with new ones that would be able to measure over a wider pressure range, for example 0 to 1000 Torr will allow for more flexibility in the setup's purge sequence.

Another suggestion could be the use of a more powerful computer to integrate both Labview<sup>®</sup> and Matlab<sup>®</sup> in an attempt to get real time etch depth and lateral etch predictions.

### **6.2.2 Model related future work**

The proposed etching model could be more developed to account for surface roughness, to compensate for the trenching phenomenon and to compensate for the etch difference between the convex and concave etch fronts.

## REFERENCES

- [1] Smith, C.S., "Piezoresistance effect in germanium and silicon", Physical Review, 1954. 94(1), p. 42-49.
- [2] Nathanson, H. C., Newell, W. E., Wickstrom, R. A., and Davis, J. R., Jr., "The resonant gate transistor", IEEE Transactions on Electron Devices, 14(3), 1967, p. 117-133.
- [3] Military and Aerospace Electronics, "MEMS market to reach \$12.5 billion by 2010", ([http://mae.pennnet.com/Articles/Article\\_Display.cfm?Section=ARTCL&ARTICLE\\_ID=259780&VERSION\\_NUM=2&p=32](http://mae.pennnet.com/Articles/Article_Display.cfm?Section=ARTCL&ARTICLE_ID=259780&VERSION_NUM=2&p=32) ).July 1st, 2006
- [4] Bertsch, A., Lorenz, H., and Renaud, P.. "Combining microstereolithography and thick resist UV lithography for 3D microfabrication". Sensors and Actuators A-Physical, vol. 73, (1-2) (1999), p. 14-23.
- [5] Ayon A. A., Nagle S., Frechette L., Epstein A., and Schmidt M. A., "Tailoring etch directionality in a deep reactive ion etching tool", Journal of Vacuum Science & Technology B: Microelectronics and Nanometer Structures, 2000. 18(3): p. 1412-1416.
- [6] Beuret, C., Racine, G. A., Gobet, J., Luthier, R., and de Rooij, N. F., "Microfabrication of 3D multidirectional inclined structures by UV lithography and electroplating", IEEE Workshop on Micro Electro Mechanical Systems, 1994, MEMS '94, p. 81-85.

- [7] Jin, W. L. and Mote C. D., Jr., "Development of a six-component miniature force sensor using silicon micromachining and conventional machining technologies [for microrobotics application]", IEEE Transactions on Instrumentation and Measurement,, 1998. 47(3): p. 715-719.
- [8] Kovacs, G.T.A., Maluf N. I., and Petersen K. E., "Bulk micromachining of silicon", Proceedings of the IEEE, 1998. 86(8): p. 1536-1551.
- [9] Bustillo, J.M., Howe R. T., and R.S. Muller, "Surface micromachining for microelectromechanical systems", Proceedings of the IEEE, 1998. 86(8): p. 1552-1574.
- [10] Maluf, N. and Williams K., "An introduction to microelectromechanical systems engineering". 2nd ed. 2004, Boston: Artech House. xx, 283 p.
- [11] Craven, D., "Photolithography challenges for the micromachining industry", 16th Annual BACUS Symposium on Photomask Technology and Management, 1996 Proc. SPIE Vol. 2884, p. 498-507.
- [12] Xia, Y.N. and Whitesides G. M., "Soft lithography", Annual Review of Materials Science, 1998. 28, p. 153-184.
- [13] Yih-Lin C., Meng-Long L., Jiang-Hong L., Jia-Hung L., Chang-Tai K., and Yu-Chia H., "Development of dynamic mask photolithography system", IEEE International Conference on Mechatronics, 2005. ICM '05. , 10-12 July 2005, p. 467- 471.



- [14] Singh, V. K., Sasaki, M., Hane, K., Watanabe, Y., Kawakita, M., and Hayashi, H., "Photolithography on three-dimensional structures using spray coated negative and positive photoresists", The 13th International Conference on Solid-State Sensors, Actuators and Microsystems. Digest of Technical Papers. TRANSDUCERS '05, Vol. 2, p. 1445-1448.
- [15] Petersen, K.E., "Silicon as a mechanical material", Proceedings of the IEEE, 1982. 70(5): p. 420-457.
- [16] Bean, K.E., "Anisotropic etching of silicon", IEEE Transaction on Electron Devices, 1978. 25(10): p. 1185-1193.
- [17] Liu, C., "Foundations of MEMS", 2006, Upper Saddle River, NJ: Pearson Prentice Hall. xxii, 530 p.
- [18] kanal.jpg, microFAB Bremen GmbH.  
<http://www.microfab.de/technologies/bulkmm.htm> [June,2006].
- [19] Patel, H., "Silicon that moves-towards the smart sensor". IEEE Review, 1992. 38(7): p. 268-269.
- [20] Lin, L. Y., Lee, S. S., Pister, K. S. J., and Wu, M. C., "Micro-machined three-dimensional micro-optics for integrated free-space optical system", Photonics Technology Letters, IEEE, 1994. 6(12): p. 1445-1447.
- [21] Gosele, U.M., M. Reiche, and Q.Y. Tong, "Wafer bonding: an overview", 4th International Conference on Solid-State and Integrated Circuit Technology, 24-28 Oct 1995, p. 243-247.

- [22] Lord Rayleigh, "A Study of Glass Surfaces in Optical Contact", Proceedings of the Royal Society of London. Series A, Mathematical and Physical Sciences, Vol. 156, No. 888 (Aug. 17, 1936), pp. 326-349.
- [23] Gosele, U., Alexe, M., Kopperschmidt, P., and Tong, Q. Y., "Semiconductor wafer bonding. A flexible approach to materials combinations in microelectronics; micromechanics and optoelectronics", International Semiconductor Conference. 1997, Vol. 1, p. 23-32.
- [24] Feynman, R.P., There's plenty of room at the bottom [data storage]. Journal of Microelectromechanical Systems, 1992. 1(1): p. 60-66.
- [25] Feynman, R., "Infinitesimal machinery", Journal of Microelectromechanical Systems 1993. 2(1): p. 4-14.
- [26] Dry etching for microelectronics edited by R. A. Powell. Journal of Applied Crystallography, 1985. 18(1): p. 54.
- [27] Madou, M.J., "Fundamentals of microfabrication : the science of miniaturization". 2nd ed. 2002, Boca Raton, Fla.: CRC Press. 723 p.
- [28] Sugano, T., "Applications of plasma processes to VLSI technology", 1985, New York: Wiley. xiv, 394 p.
- [29] Tieer G., Ditizio R. A., Fonash S. J., Awadelkarim O. O., Ruzylo J., Collins R. W., and Leary H. J., "Damage to Si substrates during SiO<sub>2</sub> etching: A comparison of reactive ion etching and magnetron-enhanced reactive ion etching", Journal of Vacuum Science & Technology B: Microelectronics and Nanometer Structures, 1994. 12(2): p. 567-573.

- [30] Oehrlein G. S., Tromp R. M., Tsang J. C., Lee Y. H., and Petrillo E. J., "Near-Surface Damage and Contamination after CF<sub>4</sub>/H<sub>2</sub> Reactive Ion Etching of Si", *Journal of The Electrochemical Society*, 1985. 132(6): p. 1441-1447.
- [31] Stephen, J.F., "An overview of dry etching damage and contamination effects", *Journal of The Electrochemical Society*, 1990. 137(12): p. 3885-3892.
- [32] Ibbotson D. E., Flamm D. L., Mucha A. J., and Donnelly V. M., "Comparison of XeF<sub>2</sub> and F-atom reactions with Si and SiO<sub>2</sub>", *Applied Physics Letters*, 1984. 44(12): p. 1129-1131.
- [33] Winters, H.F. and Houle F. A., "Gaseous products from the reaction of XeF<sub>2</sub> with silicon", *Journal of Applied Physics*, 1983. 54(3): p. 1218-1223.
- [34] Vasile, M.J., "The reaction probability of XeF<sub>2</sub> with silicon", *Journal of Applied Physics*, 1983. 54(11): p. 6697-6704.
- [35] Holloway, J.H., "Noble-gas chemistry", 1968, London,: Methuen. viii, 213 p.
- [36] Winters, H.F. and Coburn J. W., "The etching of silicon with XeF<sub>2</sub> vapor", *Applied Physics Letters*, 1979. 34(1): p. 70-73.
- [37] Smith, D.F., "Xenon Difluoride", *The Journal of Chemical Physics*, 1963. 38(1): p. 270-271.
- [38] Chuang, T.J., "Electron spectroscopy study of silicon surfaces exposed to XeF<sub>2</sub> and the chemisorption of SiF<sub>4</sub> on silicon", *Journal of Applied Physics*, 1980. 51(5): p. 2614-2619.

- [39] Gerlach-Meyer, U., Coburn J. W., and Kay E., "Ion-enhanced gas-surface chemistry: The influence of the mass of the incident ion", *Surface Science*, 1981. 103(1): p. 177-188.
- [40] Aliev, V.S. and Kruchinin V. N., "Development of Si(100) surface roughness at the initial stage of etching in F<sub>2</sub> and XeF<sub>2</sub> gases: ellipsometric study", *Surface Science*, 1999. 442(2): p. 206-214.
- [41] Winters, H.F. and Coburn J. W., "Surface science aspects of etching reactions. *Surface Science Reports*", 1992. 14(4-6): p. 162-269.
- [42] Lo, C. W., Shuh, D. K., Chakarian, V., Durbin, T. D., Varekamp, P. R., and Yarmoff, J. A., "XeF<sub>2</sub> etching of Si(111): The geometric structure of the reaction layer", *Physical Review B*, 1993. 47(23): p. 15648-15659.
- [43] Vugts M. J. M., Verschueren G. L. J., Eurlings M. F. A., Hermans L. J. F., and Beijerinck H. C. W., "Si/XeF<sub>2</sub> etching: Temperature dependence", *Journal of Vacuum Science & Technology A: Vacuum, Surfaces, and Films*, 1996. 14(5): p. 2766-2774.
- [44] McFeely, F.R., Morar J. F., and Himpsel F. J., "Soft X-ray photoemission study of the silicon-fluorine etching reaction", *Surface Science*, 1986. 165(1): p. 277-287.
- [45] Vugts M. J. M., Joosten G. J. P., van Oosterum A., Senhorst H. A. J., and Beijerinck H. C. W., "Spontaneous etching of Si(100) by XeF<sub>2</sub>: Test case for a new beam surface experiment", *Journal of Vacuum Science & Technology A: Vacuum, Surfaces, and Films*, 1994. 12(6): p. 2999-3011.

- [46] Engstrom J.R., Nelson M. M., and Engel T., "The adsorption and reaction of fluorine on the Si(100) surface", *Surface Science*, 1989. 215(3): p. 437-500.
- [47] Yarmoff J.A., Joyce S.A., Lo C. W., and Song J., "Desorption Induced by Electronic transition - DIET IV". Eds. G. Betz and P. Varga (Springer, Berlin, 1990): p. 65.
- [48] Houle, F.A., "A reinvestigation of the etch products of silicon and XeF<sub>2</sub>: Doping and pressure effects", *Journal of Applied Physics*, 1986. 60(9): p. 3018-3027.
- [49] Joyce, S., Langan J. G., and Steinfeld J. I., "Reactions of XeF<sub>2</sub> with thermally grown SiO<sub>2</sub>", *Surface Science*, 1988. 195(1-2): p. 270-282.
- [50] Floy I. C., Yeh R., Lin G., B. Chu P. B., Hoffman E. G., Kruglick E. J., Pister K. S. J., and Hecht M. H., "Gas-phase silicon micromachining with Xenon Difluoride", *Microelectronic Structures and Microelectromechanical Devices for Optical Processing and Multimedia Applications*, SPIE, 1995, Vol. 2641, p. 117-128.
- [51] Hecht H. H., Vasquez R. P., Grunthaner F. J., Zamani N., and Maserjian J., "A novel x-ray photoelectron spectroscopy study of the Al/SiO<sub>2</sub> interface", *Journal of Applied Physics*, 1985. 57(12): p. 5256-5261.
- [52] MSDS-XeF<sub>2</sub>, <http://eweb.processplants.boc.com/msds/gases/na/english/g86.pdf>, June, 2006.
- [53] MSDS-SiF<sub>4</sub>, <http://eweb.processplants.boc.com/msds/gases/na/english/g77.pdf>, June, 2006.

- [54] Sugano, K. and Tabata O., "Reduction of surface roughness and aperture size effect for etching of Si with XeF<sub>2</sub>", Journal of Micromechanics and Microengineering, 2002. 12(6): p. 911-916.
- [55] Winters, H.F. and Haarer D., "Influence of doping on the etching of Si(111)", Physical Review B, 1987. 36(12): p. 6613.
- [56] Muthukumaran P., "Boundary conditioning concept applied to the synthesis of microsystems using fuzzy logic approach", PhD Thesis, 2000, Concordia University, Montreal, Canada.
- [57] User Manual, National Instruments, LabView® 2007.
- [58] Chu P. B., Chen J. T., Yeh R., Lin G., Huang J. C.P., Warneke B. A., and Pister K. S. J., "Controlled Pulse-Etching with Xenon Difluoride", International Conference on Solid State Sensors and Actuators, 1997, Vol. 1, Issue , 16-19 Jun 1997, p. 665 – 668.
- [59] Sugano, K. and Tabata O., "Study on XeF<sub>2</sub> pulse etching using wagon wheel pattern", Proceedings of 1999 International Symposium on Micromechatronics and Human Science, 1999, p. 163 - 167.
- [60] Bhaskar, A. K., "Synthesis of electrostatically actuated optical micromirrors", MAsC Thesis, 2004, Concordia University, Montreal, Canada.

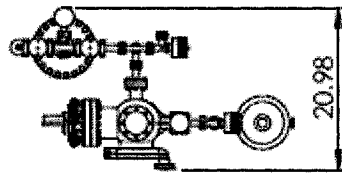
## **APPENDIX A**

### **DRAWINGS OF THE DEVELOPED EQUIPMENT**

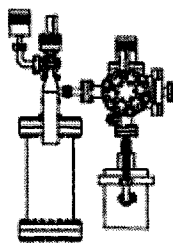
This appendix shows the last SolidWorks® drawings done during equipment design stage.

In order to choose the optimum solution that complies with the design constraints, standard parts chosen from manufacturers catalog and different designs were done in order to choose the optimum solution.

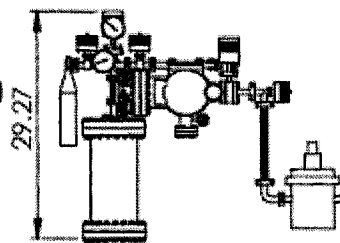
All drawings are shown using third angle projection technique, and for visual clarity, the supporting frame and the pump are not shown.



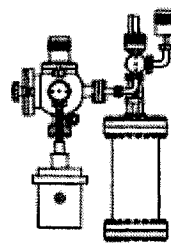
TOP VIEW



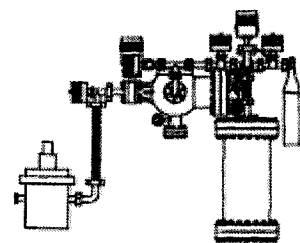
LEFT SIDE VIEW



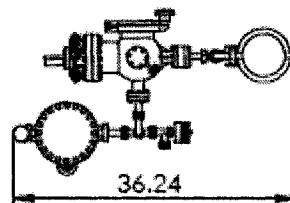
FRONT VIEW



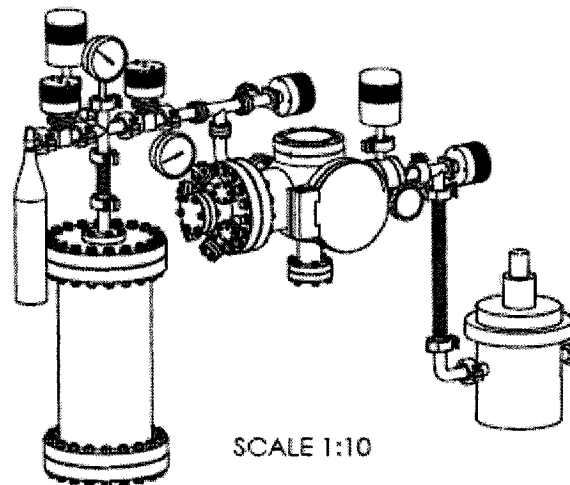
RIGHT SIDE VIEW




REAR VIEW



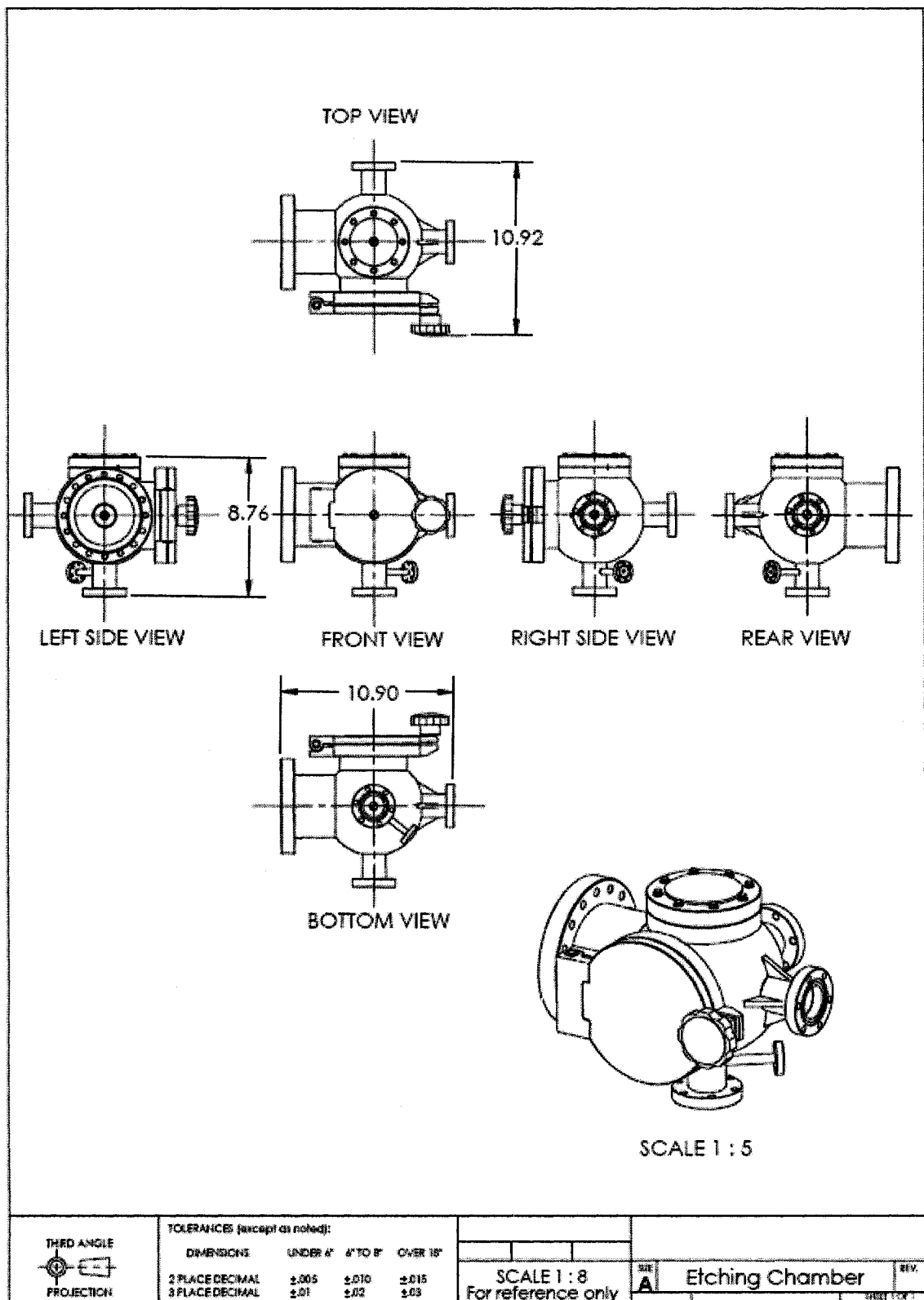
BOTTOM VIEW

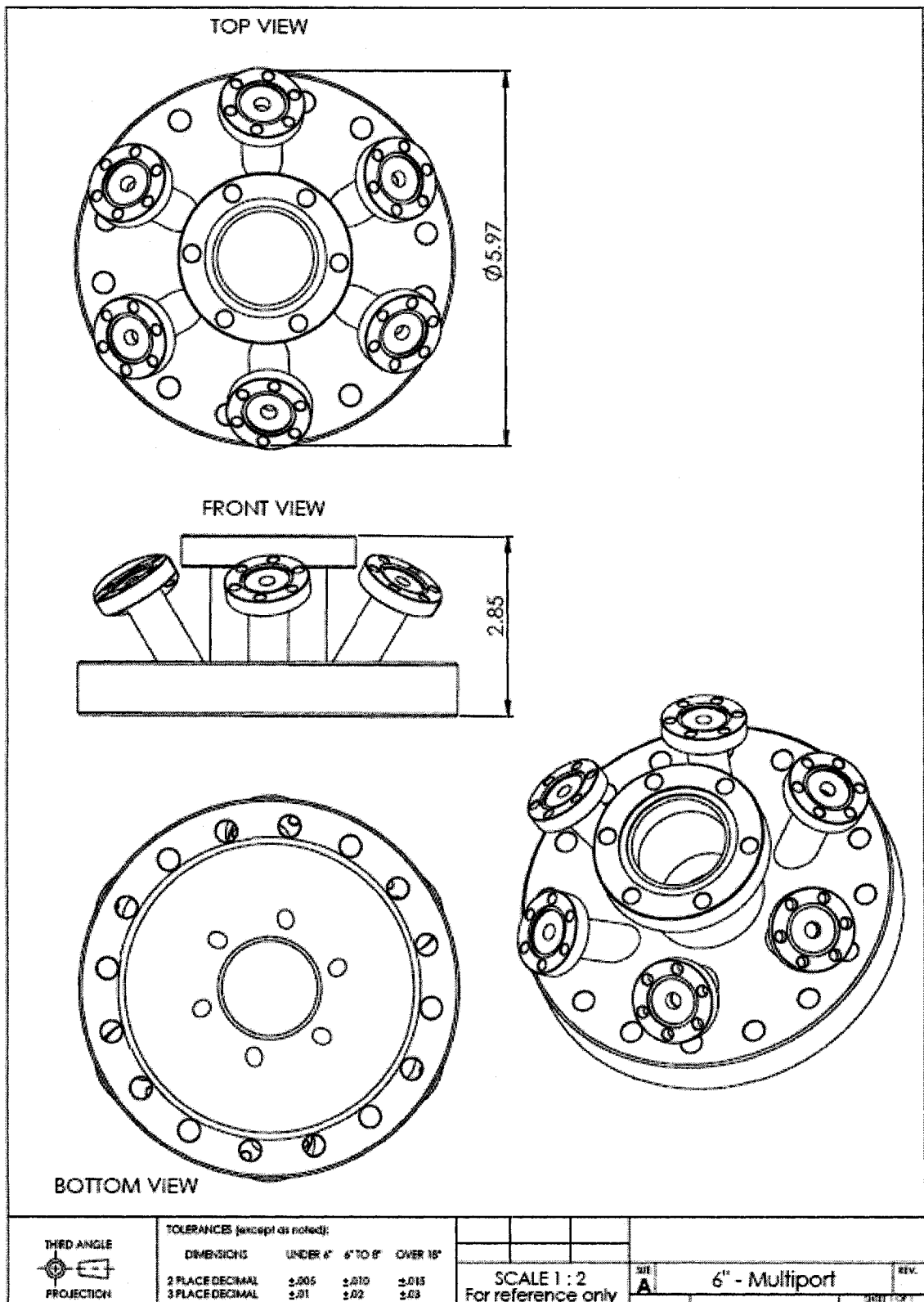


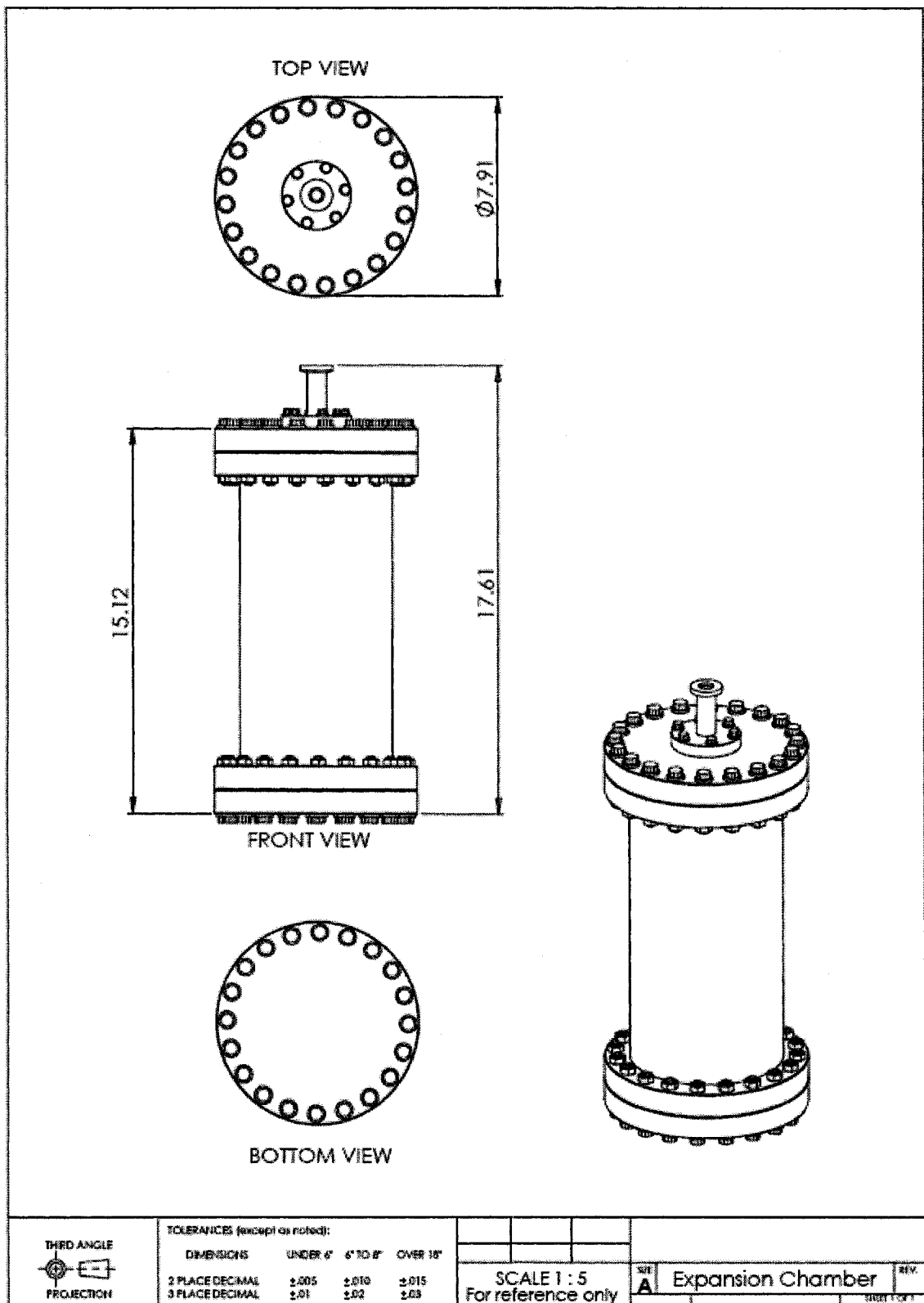
SCALE 1:10

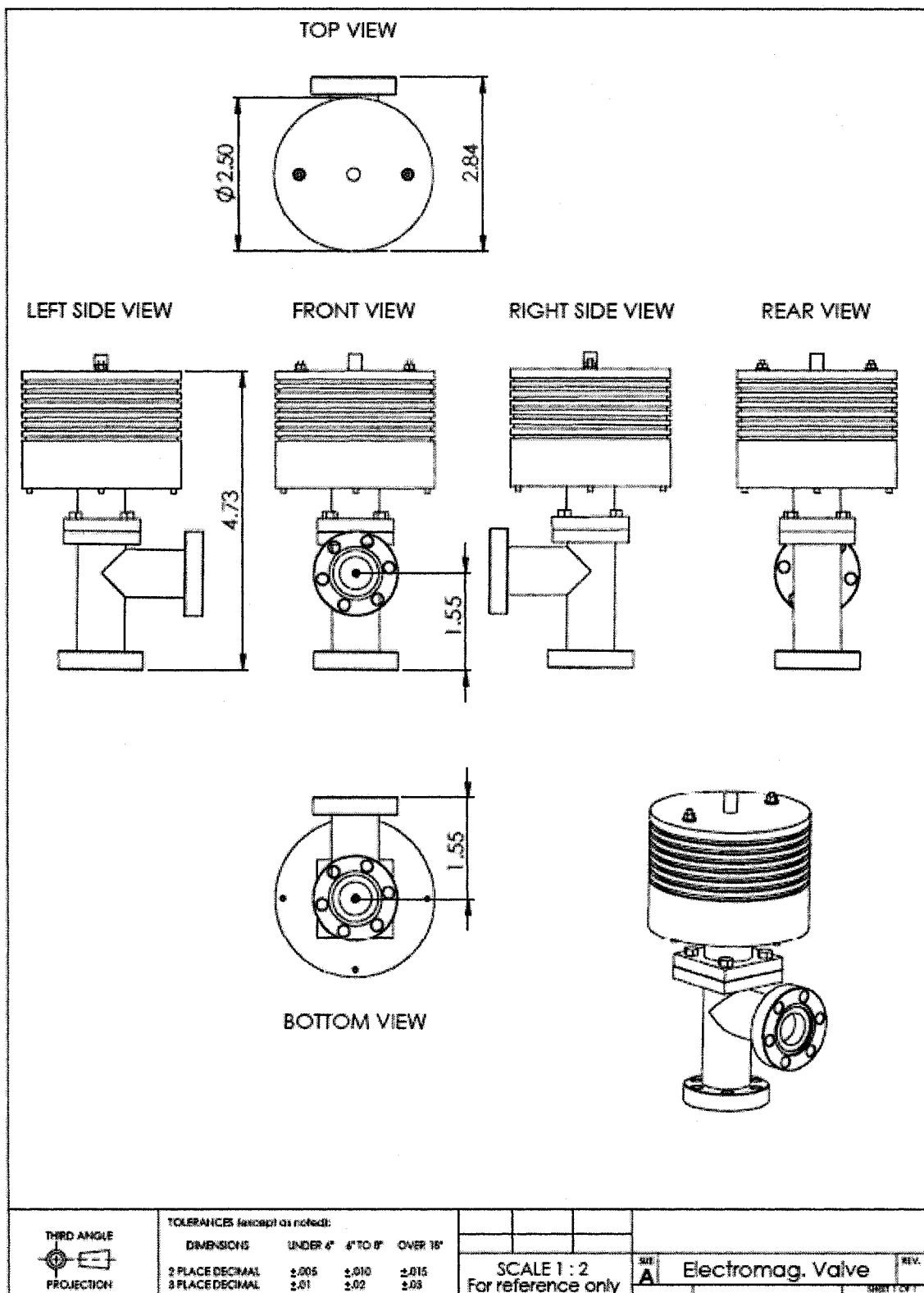
<div>THIRD ANGLE  PROJECTION</div>	TOLERANCES (except as noted):																																																																																																																																																																																																																																																																																																																																																																																																																																																																																																																																																																																																																																																																																																																																																																																																																																																																																																																																																																																																																																																																																																																																																																																																																																																																																																																																																																																																																																																																																																																																																																																																																																																																																																																																																																																																																																																																																																																									</
---	-------------------------------	--	--	--	--	--	--	--	--	--	--	--	--	--	--	--	--	--	--	--	--	--	--	--	--	--	--	--	--	--	--	--	--	--	--	--	--	--	--	--	--	--	--	--	--	--	--	--	--	--	--	--	--	--	--	--	--	--	--	--	--	--	--	--	--	--	--	--	--	--	--	--	--	--	--	--	--	--	--	--	--	--	--	--	--	--	--	--	--	--	--	--	--	--	--	--	--	--	--	--	--	--	--	--	--	--	--	--	--	--	--	--	--	--	--	--	--	--	--	--	--	--	--	--	--	--	--	--	--	--	--	--	--	--	--	--	--	--	--	--	--	--	--	--	--	--	--	--	--	--	--	--	--	--	--	--	--	--	--	--	--	--	--	--	--	--	--	--	--	--	--	--	--	--	--	--	--	--	--	--	--	--	--	--	--	--	--	--	--	--	--	--	--	--	--	--	--	--	--	--	--	--	--	--	--	--	--	--	--	--	--	--	--	--	--	--	--	--	--	--	--	--	--	--	--	--	--	--	--	--	--	--	--	--	--	--	--	--	--	--	--	--	--	--	--	--	--	--	--	--	--	--	--	--	--	--	--	--	--	--	--	--	--	--	--	--	--	--	--	--	--	--	--	--	--	--	--	--	--	--	--	--	--	--	--	--	--	--	--	--	--	--	--	--	--	--	--	--	--	--	--	--	--	--	--	--	--	--	--	--	--	--	--	--	--	--	--	--	--	--	--	--	--	--	--	--	--	--	--	--	--	--	--	--	--	--	--	--	--	--	--	--	--	--	--	--	--	--	--	--	--	--	--	--	--	--	--	--	--	--	--	--	--	--	--	--	--	--	--	--	--	--	--	--	--	--	--	--	--	--	--	--	--	--	--	--	--	--	--	--	--	--	--	--	--	--	--	--	--	--	--	--	--	--	--	--	--	--	--	--	--	--	--	--	--	--	--	--	--	--	--	--	--	--	--	--	--	--	--	--	--	--	--	--	--	--	--	--	--	--	--	--	--	--	--	--	--	--	--	--	--	--	--	--	--	--	--	--	--	--	--	--	--	--	--	--	--	--	--	--	--	--	--	--	--	--	--	--	--	--	--	--	--	--	--	--	--	--	--	--	--	--	--	--	--	--	--	--	--	--	--	--	--	--	--	--	--	--	--	--	--	--	--	--	--	--	--	--	--	--	--	--	--	--	--	--	--	--	--	--	--	--	--	--	--	--	--	--	--	--	--	--	--	--	--	--	--	--	--	--	--	--	--	--	--	--	--	--	--	--	--	--	--	--	--	--	--	--	--	--	--	--	--	--	--	--	--	--	--	--	--	--	--	--	--	--	--	--	--	--	--	--	--	--	--	--	--	--	--	--	--	--	--	--	--	--	--	--	--	--	--	--	--	--	--	--	--	--	--	--	--	--	--	--	--	--	--	--	--	--	--	--	--	--	--	--	--	--	--	--	--	--	--	--	--	--	--	--	--	--	--	--	--	--	--	--	--	--	--	--	--	--	--	--	--	--	--	--	--	--	--	--	--	--	--	--	--	--	--	--	--	--	--	--	--	--	--	--	--	--	--	--	--	--	--	--	--	--	--	--	--	--	--	--	--	--	--	--	--	--	--	--	--	--	--	--	--	--	--	--	--	--	--	--	--	--	--	--	--	--	--	--	--	--	--	--	--	--	--	--	--	--	--	--	--	--	--	--	--	--	--	--	--	--	--	--	--	--	--	--	--	--	--	--	--	--	--	--	--	--	--	--	--	--	--	--	--	--	--	--	--	--	--	--	--	--	--	--	--	--	--	--	--	--	--	--	--	--	--	--	--	--	--	--	--	--	--	--	--	--	--	--	--	--	--	--	--	--	--	--	--	--	--	--	--	--	--	--	--	--	--	--	--	--	--	--	--	--	--	--	--	--	--	--	--	--	--	--	--	--	--	--	--	--	--	--	--	--	--	--	--	--	--	--	--	--	--	--	--	--	--	--	--	--	--	--	--	--	--	--	--	--	--	--	--	--	--	--	--	--	--	--	--	--	--	--	--	--	--	--	--	--	--	--	--	--	--	--	--	--	--	--	--	--	--	--	--	--	--	--	--	--	--	--	--	--	--	--	--	--	--	--	--	--	--	--	--	--	--	--	--	--	--	--	--	--	--	--	--	--	--	--	--	--	--	--	--	--	--	--	--	--	--	--	--	--	--	--	--	--	--	--	--	--	--	--	--	--	--	--	--	--	--	--	--	--	--	--	--	--	--	--	--	--	--	--	--	--	--	--	--	--	--	--	--	--	--	--	--	--	--	--	--	--	--	--	--	--	--	--	--	--	--	--	--	--	--	--	--	--	--	--	--	--	--	--	--	--	--	--	--	--	--	--	--	--	--	--	--	--	--	--	--	--	--	--	--	--	--	--	--	--	--	--	--	--	--	--	--	--	--	--	--	--	--	--	--	--	--	--	--	--	--	--	--	--	--	--	--	--	--	--	--	--	--	--	--	--	--	--	--	--	--	--	--	--	--	--	--	--	--	--	--	--	--	--	--	--	--	--	--	--	--	--	--	--	--	--	--	--	--	--	--	--	--	--	--	--	--	--	--	--	--	--	--	--	--	--	--	--	--	--	--	--	--	--	--	--	--	--	--	--	--	--	--	--	--	--	--	--	--	--	--	--	--	--	--	--	--	--	--	--	--	--	--	--	--	--	--	--	--	--	--	--	--	--	--	--	--	--	--	--	--	--	--	--	--	--	--	--	--	--	--	--	--	--	--	--	--	--	--	--	--	--	--	--	--	--	--	--	--	--	--	--	--	--	--	--	--	--	--	--	--	--	--	--	--	--	--	--	--	--	--	--	--	--	--	--	--	--	--	--	--	--	--	--	--	--	--	--	--	--	--	--	--	--	--	--	--	--	--	--	--	--	--	--	--	--	--	--	--	--	--	--	--	--	--	--	--	--	--	--	--	--	--	--	--	--	--	--	--	--	--	--	--	--	--	--	--	--	--	--	--	--	--	--	--	--	--	--	--	--	--	--	--	--	--	--	--	--	--	--	--	--	--	--	--	--	--	--	--	--	--	--	--	--	--	--	--	--	--	--	--	--	--	--	--	--	--	--	--	--	--	--	--	--	--	--	--	--	--	--	--	--	--	--	--	--	--	--	--	--	--	--	--	--	--	--	--	--	--	--	--	--	--	--	--	--	--	--	--	--	--	--	--	--	--	--	--	--	--	--	--	--	--	--	--	--	--	--	--	--	--	--	--	--	--	--	--	--	--	--	--	--	--	--	--	--	--	--	--	--	--	--	--	--	--	--	--	--	--	--	--	--	--	--	--	--	--	--	--	--	--	--	--	--	--	--	--	--	--	--	--	--	--	--	--	--	--	--	--	--	--	--	--	--	--	--	--	--	--	--	--	--	--	--	--	--	--	--	--	--	--	--	--	--	--	--	--	--	--	--	--	--	--	--	--	--	--	--	--	--	--	--	--	--	--	--	--	--	--	--	--	--	--	--	--	--	--	--	--	--	--	--	--	--	--	--	--	--	--	--	--	--	--	--	--	--	--	--	--	--	--	--	--	--	--	--	--	--	--	--	--	--	--	--	--	--	--	--	--	--	--	--	--	--	--	--	--	--	--	--	--	--	--	--	--	--	--	--	--	--	--	--	--	--	--	--	--	--	--	--	--	--	--	--	--	--	--	--	--	--	--	--	--	--	--	--	--	--	--	--	--	--	--	--	--	--	--	--	--	--	--	--	--	--	--	--	--	--	--	--	--	--	--	--	--	--	--	--	--	--	--	--	--	--	--	--	--	--	--	--	--	--	--	--	--	--	--	--	--	--	--	--	--	--	--	--	--	--	--	--	--	--	--	--	--	--	--	--	--	--	--	--	--	--	--	--	--	--	--	--	--	--	--	--	--	--	--	--	--	--	--	--	--	--	--	--	--	--	--	--	--	--	--	--	--	--	--	--	--	--	--	--	--	--	--	--	--	--	--	--	--	--	--	--	--	--	--	--	--	--	--	--	--	--	--	--	--	--	--	--	--	--	--	--	--	--	--	--	--	--	--	--	--	--	--	--	--	--	--	--	--	--	--	--	--	--	--	--	--	--	--	--	--	--	--	--	--	--	--	--	--	--	--	--	--	--	--	--	--	--	--	--	--	--	--	--	--	--	--	--	--	--	--	--	--	--	--	----

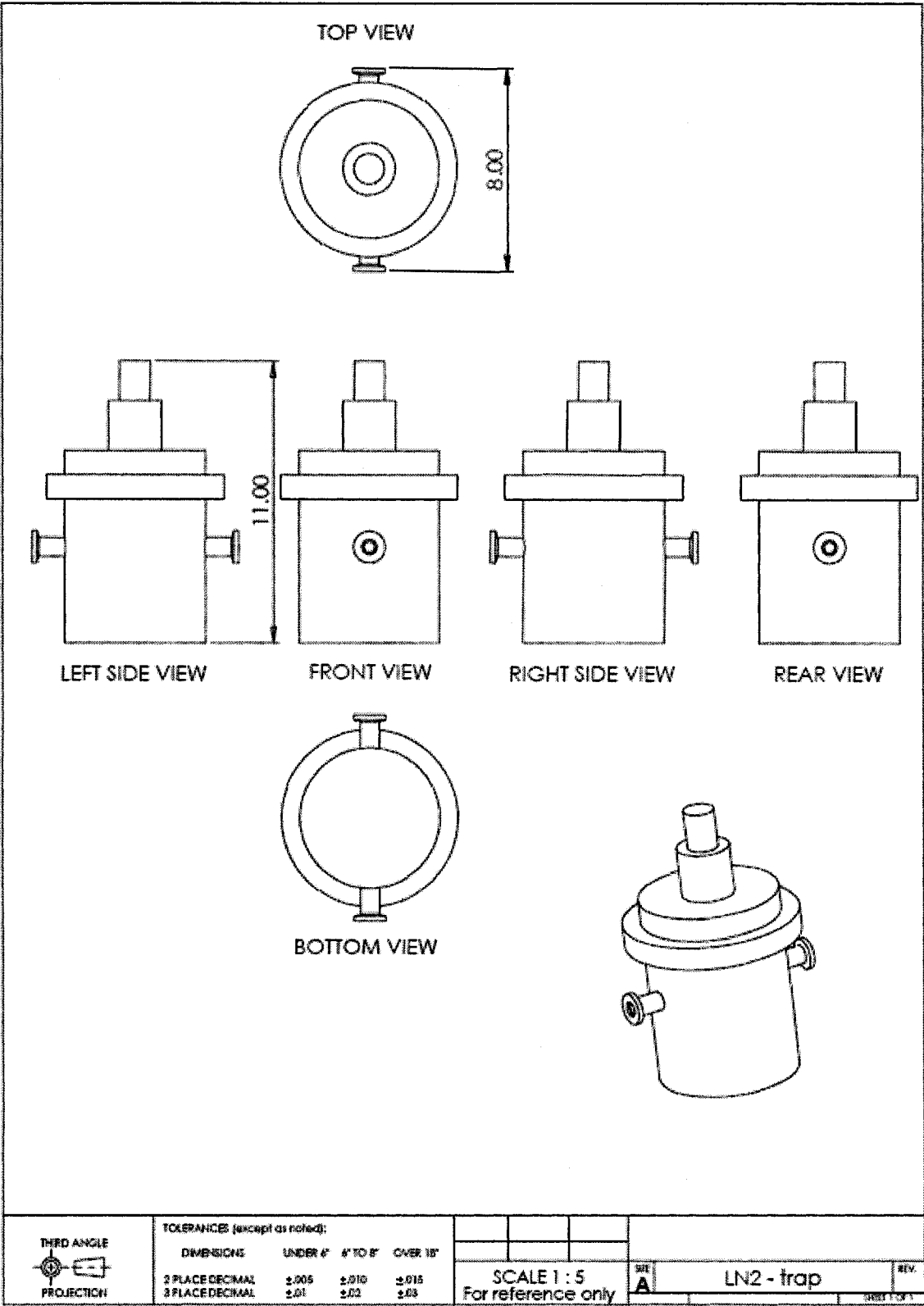


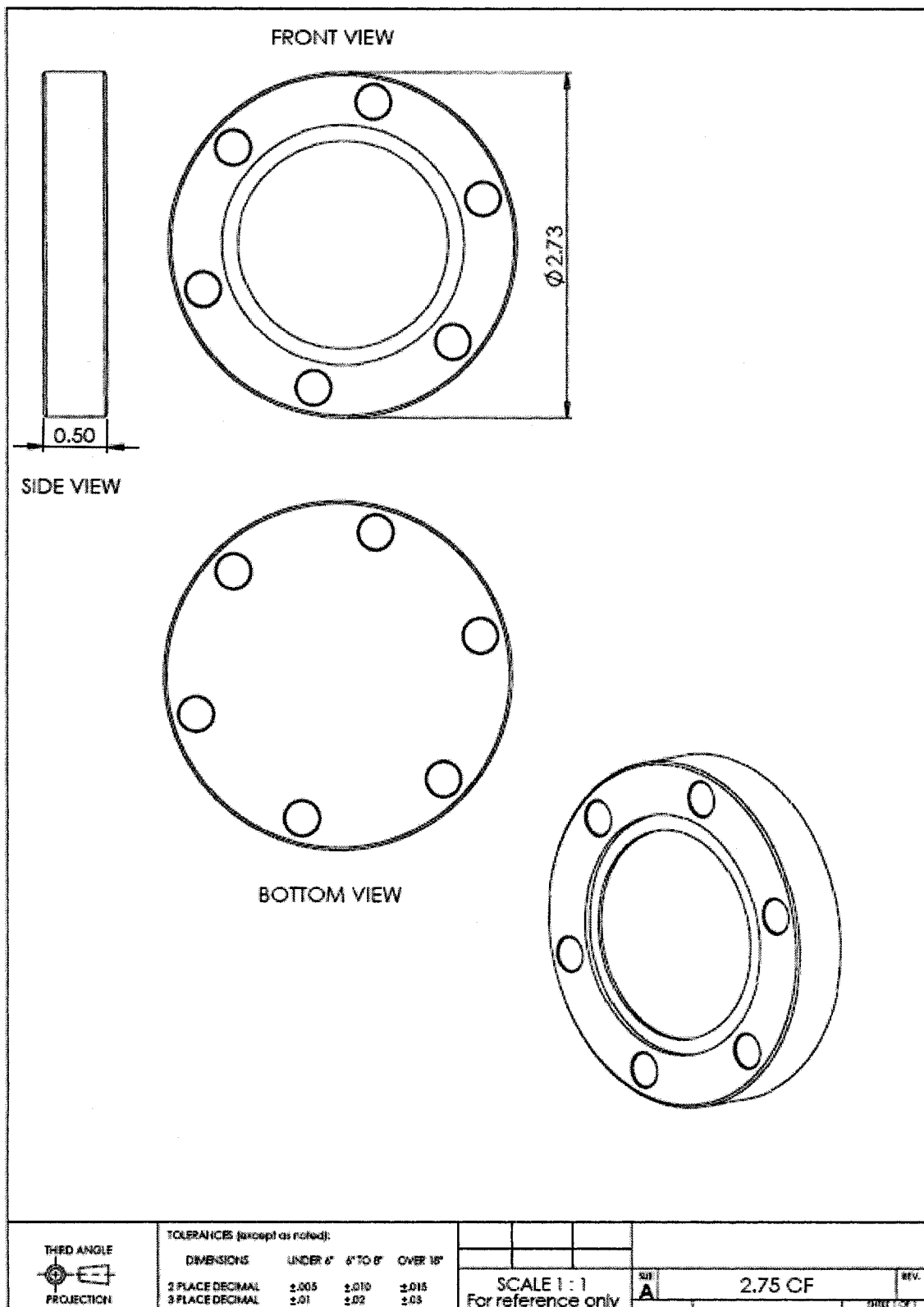


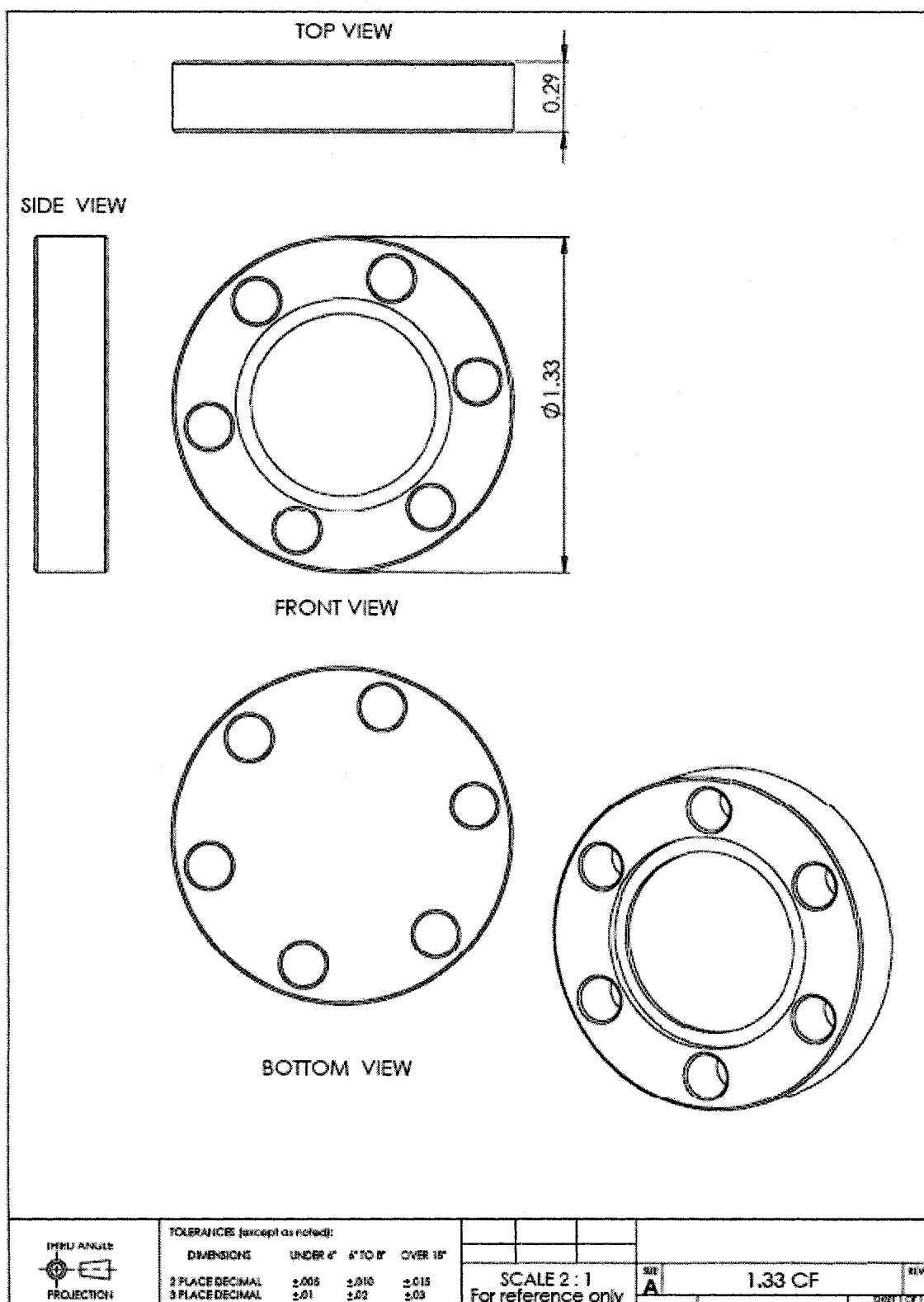


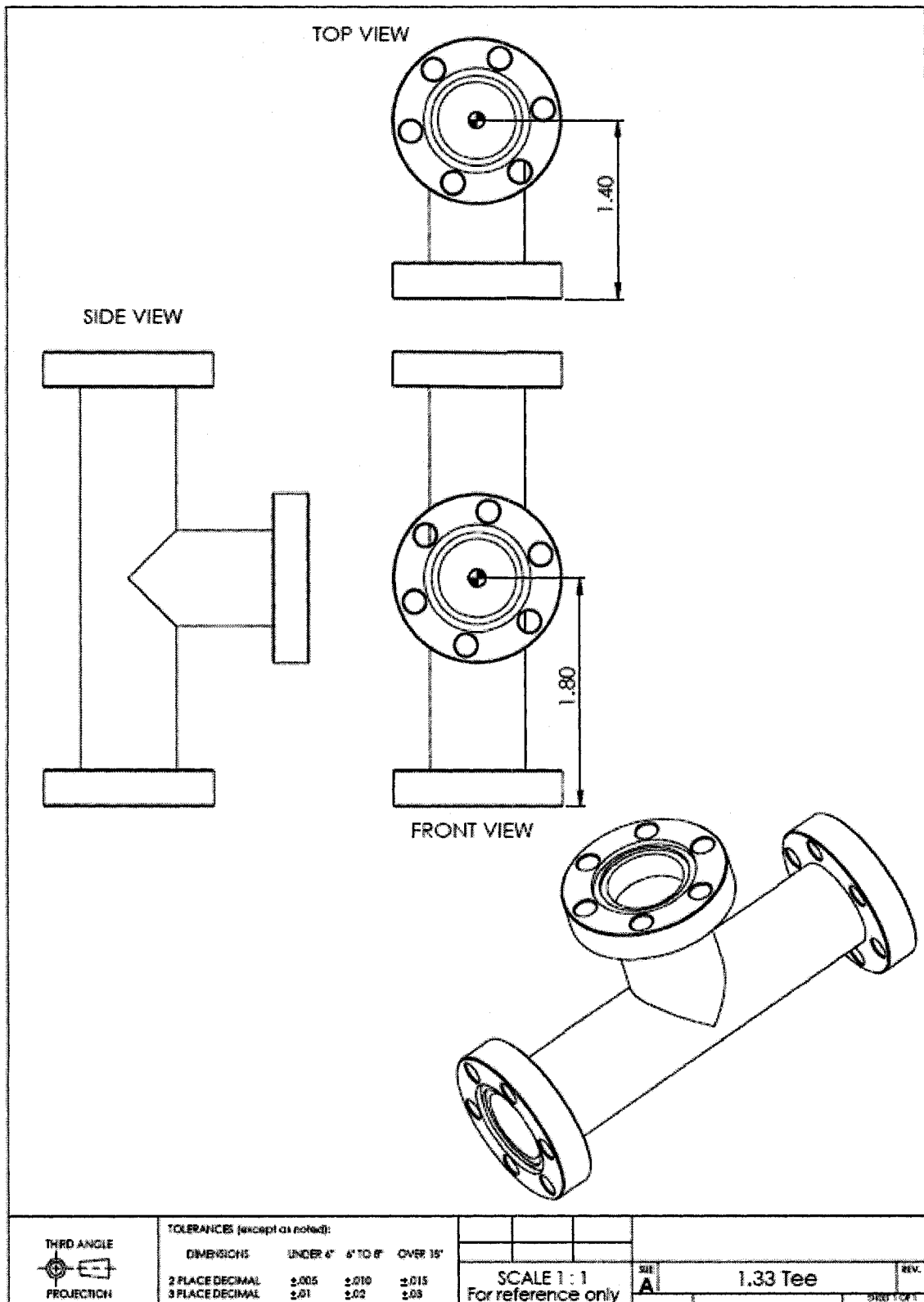














## APPENDIX B

### MATLAB CODE FOR SQUARE OPENING

```

clear;
clc;
format long;
R = 0.082057; %(L*atm)/(K*mol)
T = 300; %[K]
W_size = 2500*2500; %[square microns]
V_ech = 2.75; %[L]
Na = 6.02205*10^23; %[atoms/mol]
ML = 6.783*10^6; %[atoms/square microns]
Ratio = (5.42/4)*10^-4; %[microns]
=====
DP=[0.169
0.098
0.116
0.125
0.189
0.136
0.114
0.163
0.097
0.155
0.127
0.182
0.179
0.094
0.090
0.133
0.103
0.097
0.156
0.090
0.130
0.121

```

```

0.154
0.157
0.146];

for k = 1:size(DP,1);
    Delta_P(k) = (DP(k))*0.001315789;
    n(k) = (Delta_P(k)*V_ech)/(R*T);
    N(k) = Na*n(k);
end

for h=1
    Ar(1,h) = W_size;
    p(h) = N(1)/(ML*Ar(1,h));

    for m = 2:p(h);
        Delta_Area(m) = 4*sqrt(W_size)*Ratio+pi*((m*Ratio)^2-((m-1)*Ratio)^2);
        Ar(m,h) = Ar(m-1,h)+Delta_Area(m);
        N_remained(m)=N(h)-[sum(ML*Ar(:,1))+(Delta_Area(m)*ML)];
        if N_remained(m)< ML*Ar(m,h), break, end
    end

    Area(h) = Ar(m,:);
    ER(h) = size(Ar,1)*5.42/4*10^-4;

end

for h = 2:size(DP,1);
    p(h) = N(h)/(ML*Area(h-1));
    Ar1(1,h) = Area(h-1);

    for m = 2:p(h);
        Delta_Area(m) = 4*sqrt(W_size)*Ratio+pi*((m*Ratio)^2-((m-1)*Ratio)^2);
        Ar1(m,h) = Ar1(m-1,h)+Delta_Area(m);

```

```

        N_remaining(m)=N(h)-[sum(ML*Ar1(:,1))+(Delta_Area(m)*ML)];
        if N_remaining(m)< ML*Ar1(m,h), break, end
    end

    Area(h) = Ar1(m,h);
    ER(h) = m*5.42/4*10^-4
end

s = sqrt(W_size)/2;

% Contour of the MASK - TOP VIEW
for h = 1;
    x = [-s s s -s -s];
    y = [s s -s -s s];
    subplot(2,1,1),line(x,y,'Color','r','LineWidth',5)
    axis equal square
    xlabel('\bf Underetch in X Direction [um]\rm')
    ylabel('\bf Underetch in Y Direction [um]\rm')
    title('\bf TOP View \rm');
    grid on
    hold on
end

% Plot of the mask SIDE VIEW
X0 = [-s -(sum(ER(1:end))+2*s)];
Y0 = [0 0];
subplot(2,1,2),line(X0,Y0,'Color','b','LineWidth',8)
grid on
hold on
X00 = [s (sum(ER(1:end))+2*s)];
Y00 = [0 0];
subplot(2,1,2),line(X00,Y00,'Color','b','LineWidth',8)
hold on
XM = [-s s];
YM = [0 0];

```

```

subplot(2,1,2),line(XM,YM,'Color','r','LineWidth',5)
axis([- (2*s+sum(ER(1:h))) (2*s+sum(ER(1:h))) - (2*s+sum(ER(1:h)))
(2*s+sum(ER(1:h)))])
title('\bf Cross Section A - A \rm');
hold on

% Top and Side views of etching profiles starting with the second
pulse
for h = 5:5:size(DP,1);
    X1 = [-s s];
    Y1 = [s+sum(ER(1:h)) s+sum(ER(1:h))];
    subplot(2,1,1),line(X1,Y1,'Color','b','LineWidth',2)
    axis([- (2*s+sum(ER(1:h))) (2*s+sum(ER(1:h))) - (2*s+sum(ER(1:h)))
(2*s+sum(ER(1:h)))])
    ARC1 = [-s s sum(ER(1:h)) pi/2 pi];
    circularc(ARC1,'Color','b','LineWidth',2);
    grid on
    hold on

    X2 = [s+sum(ER(1:h)) s+sum(ER(1:h))];
    Y2 = [s -s];
    line(X2,Y2,'Color','b','LineWidth',2)
    ARC2 = [s s sum(ER(1:h)) 0 pi/2];
    circularc(ARC2,'Color','b','LineWidth',2);
    hold on

    X3 = [s -s ];
    Y3 = [-(s+sum(ER(1:h))) -(s+sum(ER(1:h)))];
    line(X3,Y3,'Color','b','LineWidth',2)
    ARC3 = [s -s sum(ER(1:h)) 3*pi/2 0];
    circularc(ARC3,'Color','b','LineWidth',2);
    hold on

    X4 = [-(s+sum(ER(1:h))) -(s+sum(ER(1:h)))];
    Y4 = [-s s];

```

```

line(X4,Y4,'Color','b','LineWidth',2)
ARC4 = [-s -s sum(ER(1:h)) pi 3*pi/2];
circularc(ARC4,'Color','b','LineWidth',2);
hold on

X11 = [-s s];
Y11 = [-sum(ER(1:h)) -sum(ER(1:h))];
subplot(2,1,2),line(X11,Y11,'Color','b','LineWidth',2)
axis([- (2*s+sum(ER(1:h))) (2*s+sum(ER(1:h))) -(s/2+sum(ER(1:h)))
0])

hold on
ARC11 = [-s 0 sum(ER(1:h)) pi 3*pi/2];
circularc(ARC11,'Color','b','LineWidth',2);
hold on
ARC1_1 = [s 0 sum(ER(1:h)) 3*pi/2 2*pi];
circularc(ARC1_1,'Color','b','LineWidth',2);
hold on
xlabel('\bf Underetch [um]\rm')
ylabel('\bf Etch Depth [um]\rm')

axis manual square equal

end

for q = 1;
    ED(q) = ER(q);
    EV(q) = Area(q)*ED(q);
end

for q = 2:30;
    ED(q) = ED(q-1) + ER(q);
    EV(q) = Area(q)*ED(q);
end

```

## APPENDIX C

### MATLAB CODE FOR CIRCULAR OPENING

```
clear;
clc;
format long;
R = 0.082057; %[L*atm)/(K*mol)
T = 300; % [K]
Phi = 5000; %[circle diameter in microns]
W_size = pi*(Phi^2)/4; %[square microns]
V_etch = 2.75; %[volume of the etch. chamber in liters]
Na = 6.02205*10^23; %[atoms/mol]
ML = 6.783*10^6; %[atoms/square microns]- Si(100) surface density
Ratio = (5.42/4)*10^-4; %[microns]
```

```
=====
DP=[0.321
```

```
0.347
```

```
0.284
```

```
0.270
```

```
0.269
```

```
0.216
```

```
0.266
```

```
0.249
```

```
0.262
```

```
0.251
```

```
0.270
```

```
0.252
```

```
0.234
```

```
0.252
```

```
0.245
```

```
0.265
```

```
0.250
```

```
0.261
```

```
0.249
```

```
0.259
```

```
0.275
```

```

0.253
0.234
0.256
0.242];

for k = 1:size(DP,1);
    Delta_P(k) = (DP(k))*0.001315789;
    n(k) = (Delta_P(k)*V_ech)/(R*T);
    N(k) = Na*n(k);
end

for h=1
    Ar(1,h) = W_size;
    p(h) = N(1)/(ML*Ar(1,h));

    for m = 2:p(h);
        Delta_Area(m) = pi*((Phi/2+Ratio)^2-((Phi^2)/4));
        Ar(m,h) = Ar(m-1,h)+Delta_Area(m);
        N_remained(m)=N(h)-[sum(ML*Ar(:,1))+(Delta_Area(m)*ML)];
        if N_remained(m)< ML*Ar(m,h), break, end
    end

    Area(h) = Ar(m,:);
    ER(h) = size(Ar,1)*5.42/4*10^-4;

end

for h = 2:size(DP,1);
    p(h) = N(h)/(ML*Area(h-1));
    Ar1(1,h) = Area(h-1);

    for m = 2:p(h);
        Delta_Area(m) = pi*((Phi/2+Ratio)^2-((Phi^2)/4));
        Ar1(m,h) = Ar1(m-1,h)+Delta_Area(m);
        N_remained(m)=N(h)-[sum(ML*Ar1(:,1))+(Delta_Area(m)*ML)];

```

```

        if N_remained(m)< ML*Ar1(m,h), break, end
    end

    Area(h) = Ar1(m,h);
    ER(h) = m*5.42/4*10^-4

end

% Contour of the MASK - TOP VIEW
for h = 1;
    subplot(2,1,1)
    ARC1 = [0 0 Phi/2 pi/2 pi];
    circularc(ARC1,'Color','r','LineWidth',5);
    grid on
    hold on
    ARC2 = [0 0 Phi/2 pi 3*pi/2];
    circularc(ARC2,'Color','r','LineWidth',5);
    grid on
    hold on
    ARC3 = [0 0 Phi/2 3*pi/2 2*pi];
    circularc(ARC3,'Color','r','LineWidth',5);
    grid on
    hold on
    ARC4 = [0 0 Phi/2 2*pi pi/2];
    circularc(ARC4,'Color','r','LineWidth',5);
    grid on
    hold on
    axis equal square
    xlabel('\bf Underetch in X Direction [um]\rm')
    ylabel('\bf Underetch in Y Direction [um]\rm')
    title('\bf TOP View \rm');
    grid on
    hold on
end

```



```

% Plot of the mask SIDE VIEW
X0 = [-Phi/2 -(sum(ER(1:end))+2*Phi/2)];
Y0 = [0 0];
subplot(2,1,2),line(X0,Y0,'Color','b','LineWidth',8)
grid on
hold on
X00 = [Phi/2 (sum(ER(1:end))+2*Phi/2)];
Y00 = [0 0];
subplot(2,1,2),line(X00,Y00,'Color','b','LineWidth',8)
hold on
XM = [-Phi/2 Phi/2];
YM = [0 0];
subplot(2,1,2),line(XM,YM,'Color','r','LineWidth',5)
axis([- (2*Phi/2+sum(ER(1:h))) (2*Phi/2+sum(ER(1:h))) -
(2*Phi/2+sum(ER(1:h))) (2*Phi/2+sum(ER(1:h)))])
title('\bf Cross Section A - A \rm');
hold on

% Top and Side views of etching profiles starting with the second
pulse
for h = 5:5:size(DP,1);
    subplot(2,1,1)
    ARC1 = [0 0 Phi/2+sum(ER(1:h)) pi/2 pi];
    circularc(ARC1,'Color','b','LineWidth',2);
    grid on
    hold on

    ARC2 = [0 0 Phi/2+sum(ER(1:h)) 0 pi/2];
    circularc(ARC2,'Color','b','LineWidth',2);
    hold on

    ARC3 = [0 0 Phi/2+sum(ER(1:h)) 3*pi/2 0];
    circularc(ARC3,'Color','b','LineWidth',2);
    hold on

```

```

ARC4 = [0 0 Phi/2+sum(ER(1:h)) pi 3*pi/2];
circularc(ARC4,'Color','b','LineWidth',2);
hold on

X11 = [-Phi/2 Phi/2];
Y11 = [-sum(ER(1:h)) -sum(ER(1:h))];
subplot(2,1,2),line(X11,Y11,'Color','b','LineWidth',2)
axis([- (2*Phi/2+sum(ER(1:h))) (2*Phi/2+sum(ER(1:h))) -
(Phi/2/2+sum(ER(1:h))) 0])
hold on
ARC11 = [-Phi/2 0 sum(ER(1:h)) pi 3*pi/2];
circularc(ARC11,'Color','b','LineWidth',2);
hold on
ARC1_1 = [Phi/2 0 sum(ER(1:h)) 3*pi/2 2*pi];
circularc(ARC1_1,'Color','b','LineWidth',2);
hold on
xlabel('\bf Underetch [um]\rm')
ylabel('\bf Etch Depth [um]\rm')
axis manual square equal

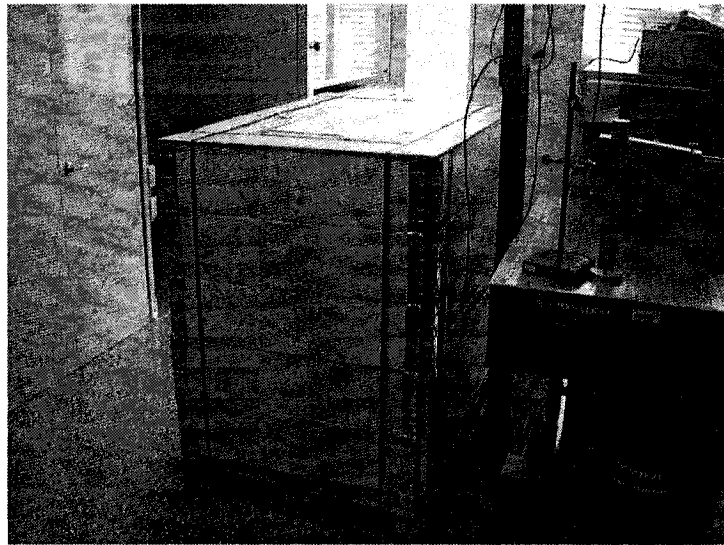
end

for q = 1;
    ED(q) = ER(q);
    EV(q) = Area(q)*ED(q);
end

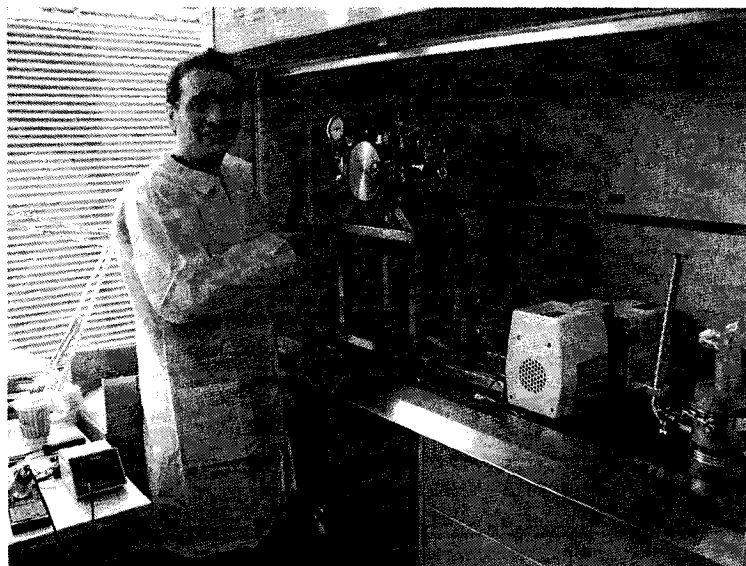
for q = 2:size(DP,1);
    ED(q) = ED(q-1) + ER(q);
    EV(q) = Area(q)*ED(q);
end

```

**APPENDIX D**  
**PICTURES TAKEN DURING ASSEMBLING OF EQUIPMENT**



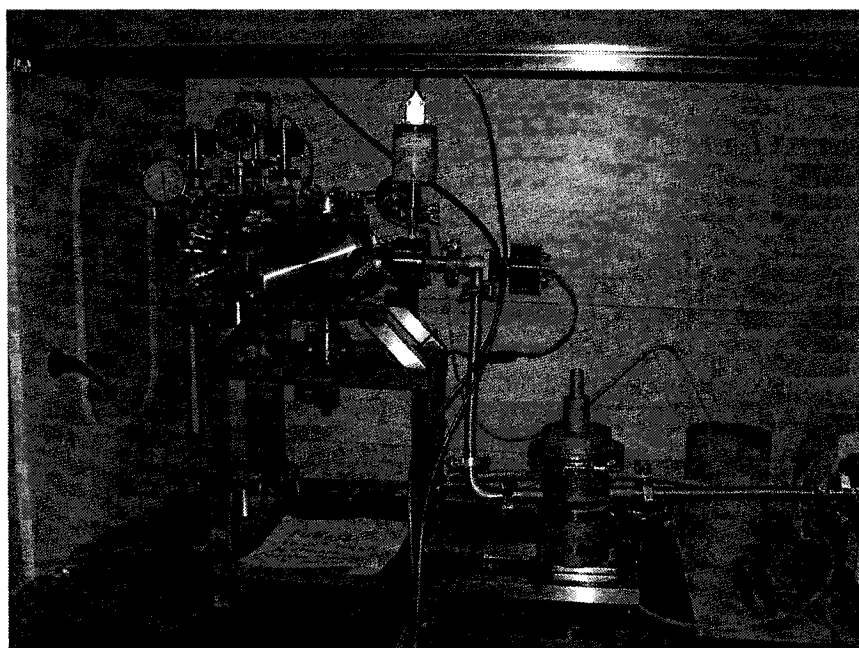
**Figure D-1** Equipment parts in the FedEx shipping box.



**Figure D-2** Author while wiring the electromagnetic valves.



**Figure D-3** Working Place while wiring electrical connection.



**Figure D-4** The developed etching setup during pressure leak testing.